State of New Jersey

New Jersey Board of Public Utilities (NJBPU)

Bureau of Conservation and Renewable Energy & Office of Clean Energy

"An Advanced Atmospheric/Ocean Assessment Program Designed to Reduce the Risks Associated with Offshore Wind Energy Development Defined by the NJ Energy Master Plan and the NJ Offshore Wind Energy Economic Development Act"

School of Environmental and Biological Sciences

Rutgers University

71 Dudley Road

New Brunswick, NJ 08901

848-932-6555

Principal Investigators

PI: Scott Glenn, Sc.D. and Co PI: Rich Dunk, Ph.D.,CCM

glenn@marine.rutgers.edu / dunk@marine.rutgers.edu

Final Report for the Period of Performance

14 Apr 2011-13 Apr 2013

30 Apr 2013

Contents

Data and Images can be found on the following website:
http://rucool.marine.rutgers.edu/bpu

RUTGERS
Coastal Ocean Observation Lab

Rutgers/BPU Advanced Offshore Wind Resource Monitoring/Modeling Analysis Program

RU Grant #: BPU-069G

Period of Performance: 14 Apr 2011-13 Apr 2013.

Abstract

Once proposed offshore wind systems become operational, substantial wind energy penetrations into the power grid can be expected for densely populated coastal areas (e.g., NJ) where energy demand is high. The variability in the wind resource at atmospheric heights representative of offshore wind turbine dimensions in conjunction with varying energy demand must be taken into account to ensure economical and reliable electrical grid management. Therefore, the "risks" and associated costs resulting from the variability of wind power production and uncertain demand requirements can be significantly reduced with a representative analytical/predictive program designed specifically for each offshore wind energy site, transmission/distribution hubs, and affected adjacent coastal/inland areas. Therefore, the Rutgers Coastal Ocean Observation Laboratory (RU-COOL), which is a research division of the Rutgers University Institute of Marine and Coastal Sciences (IMCS), developed an innovative monitoring/modeling program that is designed specifically for analyzing and predicting the wind resource properties that are associated with the offshore area that is adjacent to NJ's coast. The advanced and adaptive coastal/offshore analytical/predictive programs developed by RU-COOL have been extensively applied to determine the climatology and associated variability of both the mesoscale and microscale wind resource encompassed by NJ's offshore area that is designated for wind energy development (Glenn and Dunk, 2010). These programs include high-resolution sea surface current monitoring along with representative surface wind field estimations determined by coastal radar (CODAR), which is used to detect sea breeze development and evaluate model performance over the spatial area designated for offshore wind energy development. Also, RU-COOL has developed a unique product for determining realistic sea surface temperatures (SSTs) detected by infrared (IR) satellite remote sensing. This product enables high-resolution SST detection during both clear and cloudy atmospheric conditions. The spatial and temporal resolution of SSTs derived allows identification of coastal upwelling centers that affect the duration and extent of the sea breeze circulation. Furthermore, it has been demonstrated by scientific literature that SST is one of the most significant model inputs for determining the dynamics of the offshore wind resource. Therefore, the RU-COOL monitoring/modeling program should prove to be the most accurate and representative methodology for analyzing and predicting the wind characteristics that are specific for NJ's coastal and adjacent offshore areas.

Note: Data and resources associated with this project can be accessed at:
http://rucool.marine.rutgers.edu/bpu

1. Introduction

The climatology and variability of the wind resource associated with the area designated for NJ's offshore wind development endeavors was determined by RU-COOL during an extensive innovative monitoring/modeling effort that was conducted over the two year period 14 Apr 2011-13 Apr 2013 with funding provided by the NJ Board of Public Utilities (NJBPU). The offshore area designated for wind energy development, which is defined in the following map (Figure 1, red boundary line), coincides with the area covered by the NJ Department of Environmental Protection (NJDEP) Ecological Baseline Study and also encompasses the area being used for our high-resolution wind resource modeling assessments. This map defines the demarcation between State waters (coast to 3nm) and Federal waters (>3nm to 200 nm) along with the DOE Bureau of Ocean Energy Management (BOEM) lease block locations.

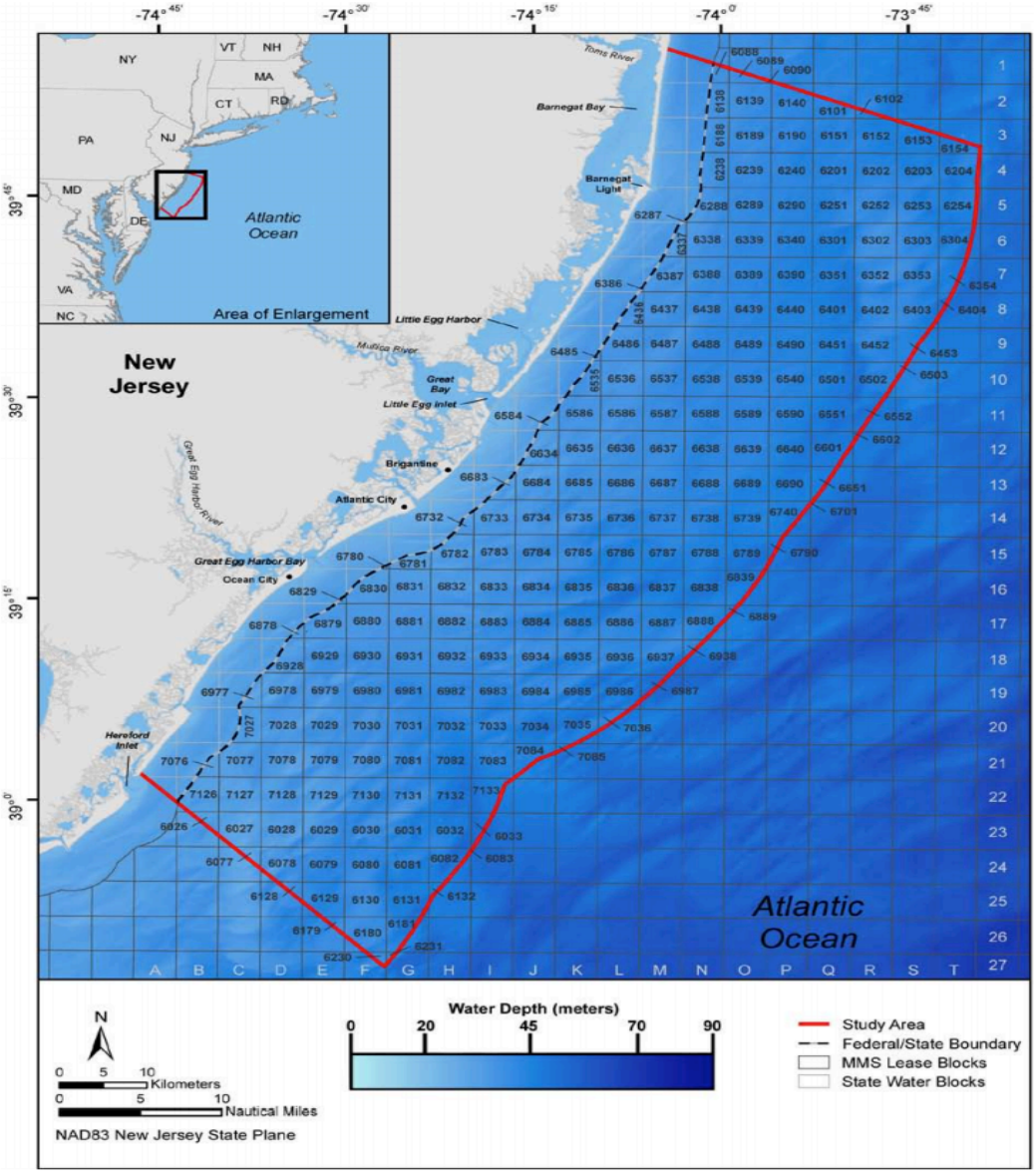

Figure 1. NJ Area Defined for Offshore Wind Development, Federal Lease Blocks, and the NJ/Fed Boundary.

2. Project Objectives

- Determine the impact of the sea breeze circulation on the offshore wind resource and evaluate what areas within the study domain would be enhanced by the sea breeze and where the sea breeze would produce adverse conditions for wind power production. (Sec. 4.7)

- Determine the diurnal, monthly, and seasonal temporal variability of the offshore wind resource. (Sec. 4.4, website)

- Determine the vertical and horizontal spatial variability of the offshore wind resource and validate with observations provided by offshore atmospheric/oceanic monitoring systems (vertical) and shore based surface current mapping radars (horizontal). (Sec. 4.4, 4.2)

- Determine optimum offshore wind resource areas where wind power production would be enhanced and ecological impacts along with logistical constraints including existing vessel traffic would be minimal. Develop and implement an operational area-specific weather forecast model to support met tower and WTG construction activities, provide site-specific wind resource predictions pertinent to wind power production penetration into the electrical grid along with its influence on load management, energy distribution, and the energy market. (Sec. 4.4, 4.5, 4.6, website)

- Determine sea surface conditions for the entire study domain to support both wind resource analyses and ecological studies associated with offshore wind development. (Sec 4.1, Appendix 2)

- Determine where NJ's offshore wind resource along with possible impacts on the marine and atmospheric environments can potentially support additional capacity above the currently proposed 1100 MW offshore wind energy generating capacity. (Sec. 4.5, 4.6, 4.7)

3. Methodology

3.1 Ocean Monitoring

3.1.1 Sea Surface Currents. Sea surface conditions are continually being monitored using Coastal Ocean Dynamics Applications RADAR (CODAR) systems. These high-frequency (HF) coastal RADARs that detect currents, waves, and derived surface winds associated with extreme weather (e.g., nor'easters and hurricanes) along with upwelling and sea breeze events were used to determine the impact of these wind perturbations on the offshore wind resource. CODAR data were used to determine the spatial differences in the offshore wind resource resulting from the sea breeze circulation, weather system frontal passages, coastal storms, and other potential wind resource perturbations. All four BPU 13 MHz CODAR systems along with the supporting CODAR network collected ocean surface data for the designated offshore wind energy development area over the study period. The details of the HF radar network operations are presented in Appendix 1 of this report. Surface current maps from this network are posted in

real-time on the web at http://marine.rutgers.edu/cool/maracoos/imagery/. The designated monitoring area, individual CODAR locations, and a recently produced sea surface current image are respectively shown in Figure 2.

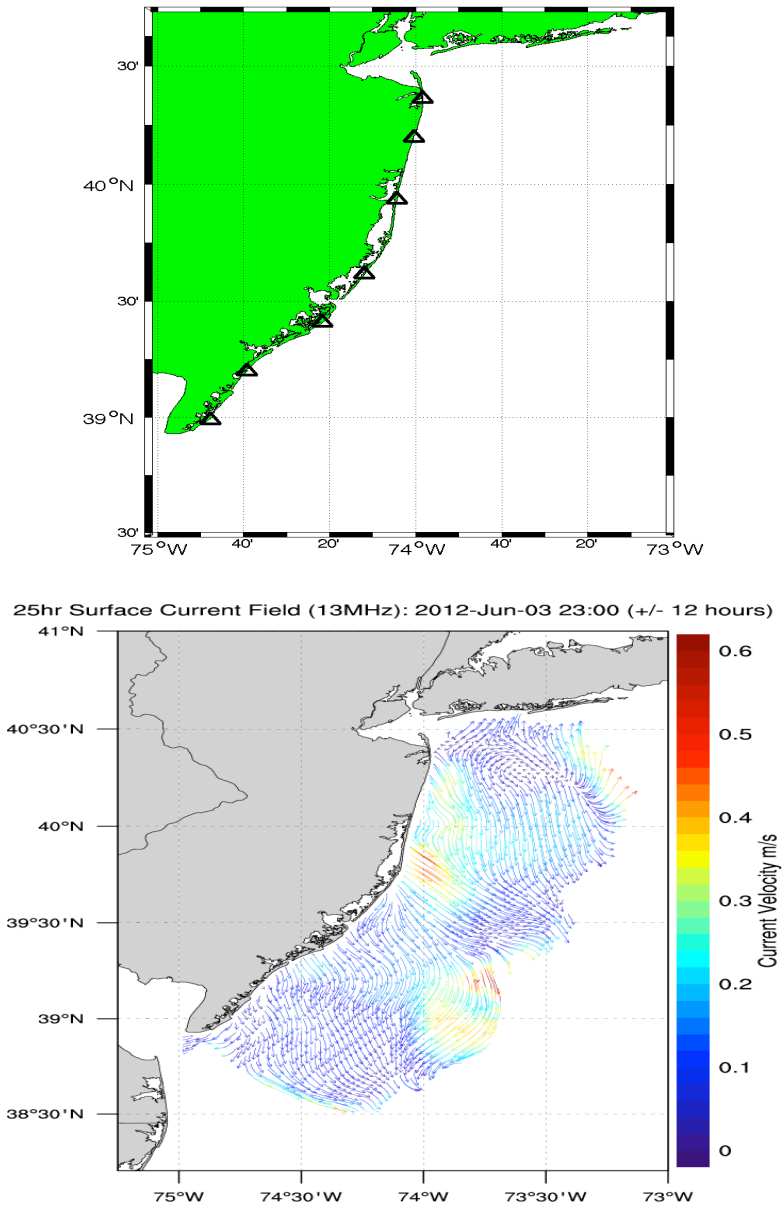

Figure 2: Map indicating CODAR Site Locations along the New Jersey Coast (top) and a High-Resolution Sea Surface Current Map Indicating the Footprint and Resolution of the Data (bottom).

The HF radar network along the New Jersey coast provided hourly surface current maps from January through December 2012. The coverage varied over that time as described in this report. In Appendix 2 we present the surface current data as monthly mean and standard deviation fields across the study domain. Only data with 50% coverage over both the entire year and over the specific time period for each figure are shown. The hourly currents were used to

map the surface ocean response to local wind forcing over each month of the year by using a least squares method (Kohut et al. 2004) to extract the tides. For each month we provide:

1.) The mean surface velocity field.
2.) The variability of the currents reported as a map of standard deviation.
3.) Wind rose representing the wind forcing observed over that month at the Tuckerton WeatherFlow station.
4.) Conditional mean surface current fields based on wind direction.

The conditional mean fields average the detided currents observed for all times in that month in which the winds originated from the northeast, southeast, southwest and northwest quadrants. All images are included as Appendix 2 to this report. The maps show that for 2012 there was a significant influence of the offshore winds from the northwest. This typical wind direction observed during the winter months extended into the spring. This drove a mean offshore flow in the surface current fields for much of the year. This annual mean offshore flow is consistent with the annual mean observed in 2004 (NJDEP, 2010). It was not until later in the summer that the winds became more alongshore from either the northeast or southwest. Under these conditions the surface currents moved predominately alongshore toward the northeast (southwest) with a slight offshore (onshore) component when the winds were upwelling favorable from the southwest (downwelling favorable from the northeast). Section 4.2.2 of this report will discuss the spatial variability observed in these fields and how it informed the evaluation of the spatial patterns predicted by the Rutgers University Weather Research and Forecasting (RU-WRF) offshore winds. In the fall the influence of Superstorm Sandy is seen in the reduction of coverage to only those stations south of the storm's eye reporting after the storm. This resulted in most monthly mean fields moving offshore toward the southeast.

3.1.2 Sea Surface Temperature. Sea Surface Temperature (SST) is the primary indicator for energy exchange between the ocean and overlying atmosphere. Accurate SST measurements are important because temperature differences across a geographical area will produce a temperature gradient that will cause the overlying air to be set into motion. The intensity of this air movement (i.e., wind) is directly proportional to the temperature difference and resultant temperature gradient intensity. Consequently, differences between the air and sea temperatures along with adjacent coastal terrestrial temperatures and resultant gradients will significantly influence the dynamics of the offshore wind resource. Therefore, representative SSTs are considered to be a critical model input parameter for both diagnostic and predictive applications.

Since IR satellite signals associated with cloud cover are usually colder than actual SSTs, warmest pixel composites of several satellite scans are frequently used to remove any data contaminated by clouds or cloudy edges. However, this technique is prone to eliminating storm mixing processes that produce colder SSTs and coastal upwelling occurrences (i.e., deeper colder water brought to the surface by persistent strong southerly winds). To rectify this problem in representative SST detection, RU-COOL has developed a new algorithm that realistically resolves SSTs during cloudy conditions. The algorithm includes a visible reflectivity routine that differentiates between partly cloudy pixels and upwelling pixels associated with infrared (IR) satellite detection. This product “de-clouds” satellite SST data obtained from the Advanced Very High Resolution Radiometer (AVHRR) aboard various satellite platforms. The radiometer determines sea surface temperature by using various visible and near IR thresholds, which are

empirically derived for each season and location. Then a 3-day *coldest* pixel composite of the de-clouded 1-km resolution AVHRR data is performed, which preserves and resolves coastal upwelling and storm mixing conditions. Next, a coldest pixel composite is again performed using the 3-day AVHRR data and NASA's Short-term Prediction Research and Transition Center (SPoRT) SST composite product to fill in any remaining gaps due to persistent clouds. The SPoRT's SST product is a 2-km, 7-day weighted composite of data obtained from the Moderate-Resolution Imaging Spectroradiometer (MODIS) and National Environmental Satellite Data and Information Service (NESDIS).

The innovative RU-COOL "de-clouding" product, which has never been used by any other institution or organization, is unique to our offshore wind analysis project. This technology enables us to realistically resolve area-specific SSTs and associated upwelling/non-upwelling events. The new de-clouded product, which has been tested and verified, has been automated for atmospheric model input and appears to enhance model accuracy and overall performance. This enhanced performance will ensure that simulations of the offshore wind resource are the most realistic that can be achieved by the "best" state-of-the-science modeling methods.

The following images show recent IR Satellite SSTs that were resolved using respectively: only the SPoRT composite (i.e., a standard technique for SST detection, Figure 3), and a combination of the RU-COOL de-clouded product and SPoRT composite that provide us with the SST values being used for our model input (Figure 4). These images, obtained during a sea breeze/upwelling event in September 2012, highlight the detail captured in the combined Rutgers/SPoRT observations of the Upwelling centers. The more detailed maps were made available to the atmospheric forecast (RU-WRF) as a bottom boundary condition.

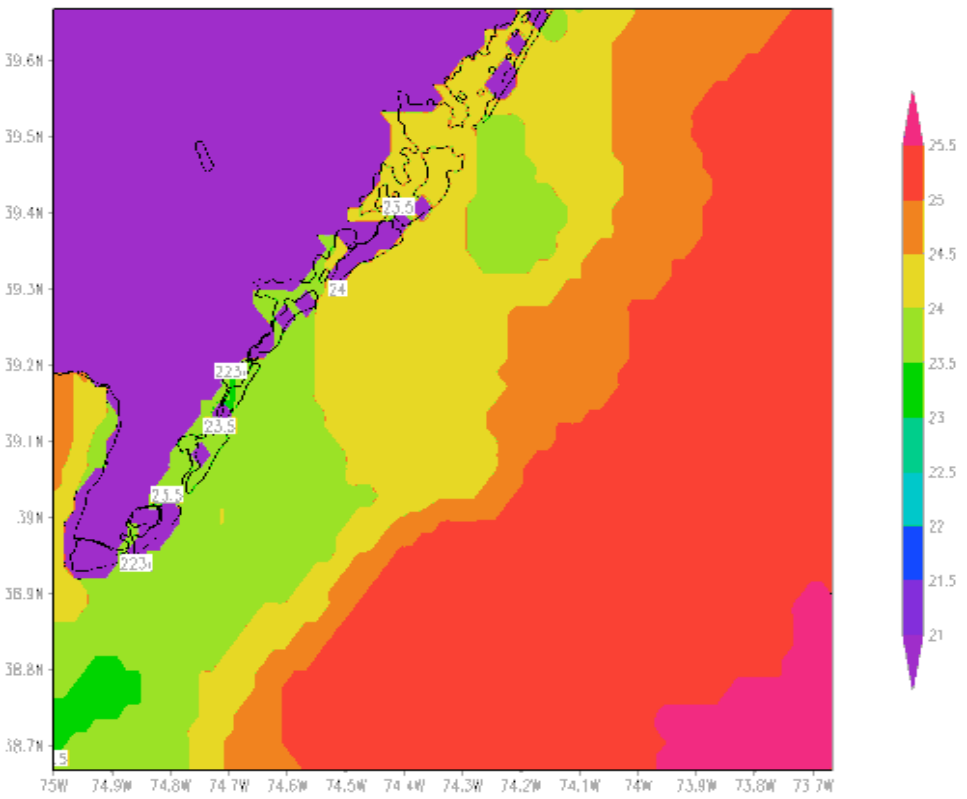

Figure 3: IR Satellite SSTs determined only by the "Standard" SPoRT Composite Technique.

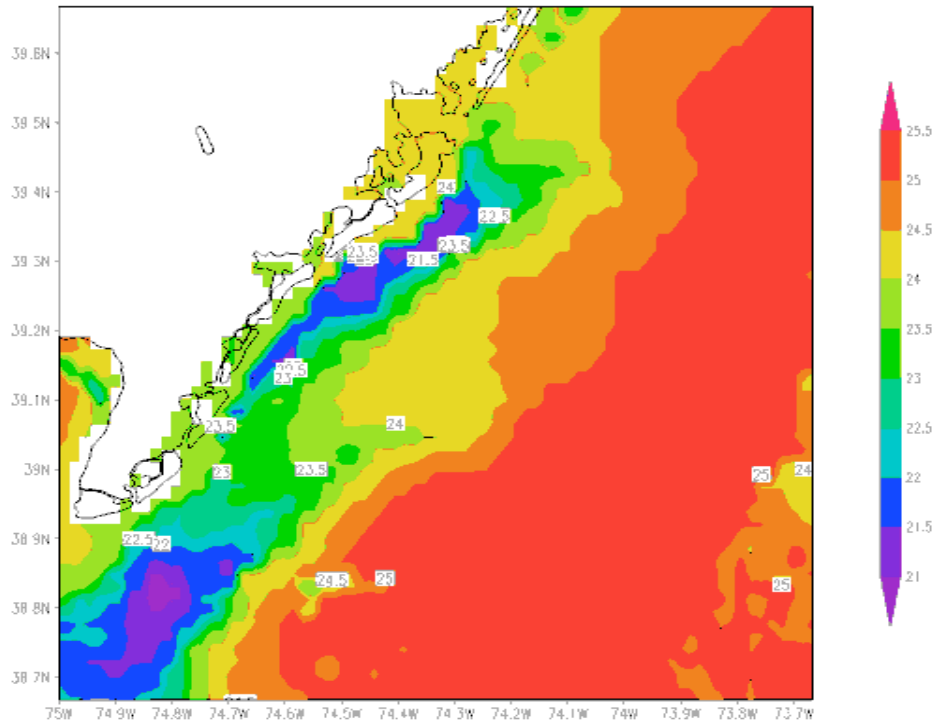

Figure 4: IR Satellite Detected SSTs using the Rutgers "De-Clouded" Product

The preceding IR satellite images of SSTs indicate that the RU-COOL de-clouded product detected upwelling centers along the coast and provided significantly higher resolution SSTs when compared to the "standard" technique for measuring sea surface temperatures. Three interesting observations associated with NJ's upwelling occurrences are:

1) Upwelling cores occur near the boundary line that separates state and federal waters.

2) The spatial scale of upwelling occurrences are similar to the spatial scales associated with proposed for offshore wind park dimensions.

3) As a result of enhanced temperature gradients between the upwelling areas and adjacent areas, onshore flow (e.g., winds associated with the sea breeze circulation) intensities will tend to increase downwind from the upwelling areas (i.e., generally, along the coast and inland) and may decrease from farther offshore areas toward the coast, which will be dependent on offshore SST values.

The following figure shows the most prominent upwelling locations. Note that the majority of upwelling centers occur within the area designated for NJ's offshore wind energy development endeavors.

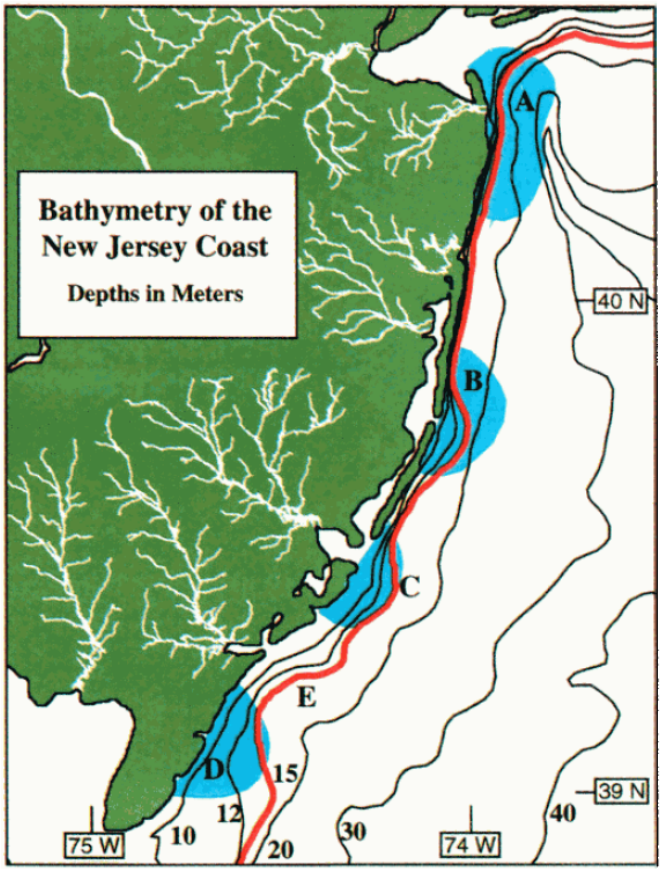

Figure 5: NJ Coastal Upwelling Centers

3.2 Atmospheric Monitoring

RU-COOL is conducting our own "internal" model performance evaluation using available temporal and spatial data acquired from coastal/offshore monitoring systems. Model results are continuously being compared with monitoring data using criteria accepted by the wind energy industry. Monitoring systems being used for our validation procedure include:

- The 120m Exelon Oyster Creek Nuclear Plant coastal meteorological tower located in Forked River adjacent to the Barnegat Bay.

- The Ship John Shoal (SJSN4) and Brandywine Shoal Offshore Coast Guard (BRND1) meteorological monitoring platforms located in the DE Bay. Anemometer heights are at ~ 20m above msl.

- The Chesapeake Light (CHLV2) monitoring station located offshore from Virginia Beach, VA. Anemometer height is ~ 43m above msl.

- The Buzzards Bay (BUZM3) monitoring station located offshore between New Bedford, MA and Newport, MA. Anemometer height is ~ 25m above msl.

- The Delaware Bay (44009) NOAA monitoring buoy located 26 nm southeast of Cape May, NJ. Anemometer height is 5m above the sea surface.

Figure 6: **Meteorological observation points utilized for RU-WRF model validation. Points in red are near surface locations with 10m anemometer heights (NWS/FAA Airports and WeatherFlow) and buoys with 5m anemometer heights (NDBC); points in orange are lighthouse/offshore platform sites with 19 to 45m anemometer heights (NDBC); points in yellow indicate tall tower data at Salem and Oyster Creek Nuclear Plants, and the point in magenta indicates the location of a Scanning LIDAR in Margate, NJ. The acronyms NWS, FAA, and NDBC are abbreviations for the respective agencies: Federal Aviation Agency, Federal Aviation Agency, and the National Data Buoy Center.**

Examples of the monitoring systems being used for RU-WRF model validation program are shown in the figures portrayed below:

Figure 7: 120m Above Sfc Coastal Met Tower

Figure 8: DE Bay Monitoring Station (20m Above MSL Meteorological Tower)

Figure 9: Chesapeake Light Offshore Monitoring Station (43m Above MSL Meteorological Tower)

Figure 10: NOAA Monitoring Buoy (Anemometer Height at 5m Above MSL)

Figure 11: Meteorological observation points in relation to the 45 Virtual Met Tower locations.

3.3 Atmospheric Modeling

3.3.1 Synopsis. The current offshore wind assessment study encompasses the offshore area adjacent to NJ that is defined for wind energy development and will produce representative offshore wind resource assessments including local wind pattern simulations, such as the sea breeze circulation, that will impact wind power production. It should be noted that winds generally increase in intensity from the coast to areas farther offshore. Furthermore, offshore winds tend to be more consistent with less variability when compared to winds over land. However, during "typical" NJ sea breeze events, wind intensities tend to decrease offshore and become very variable, especially over the area defined for NJ's offshore wind energy development applications. During well-developed sea breeze events, maximum wind speeds

tend to occur near the coast, decrease offshore where proposed wind parks are to be installed, and increase much farther offshore.

The Weather Research and Forecasting (WRF) model, which is accepted by most government agencies, the military, and academic institutions, is used as the basis for the unique RU-COOL micro/mesoscale modeling system (RU-WRF) that is designed primarily for analyzing and forecasting NJ's coastal/offshore wind resource and associated atmospheric parameters. The horizontal grid resolutions for the micro and meso scales for atmospheric motion (i.e., wind and turbulence) are respectively defined as: <2 km (microscale) and ≥2 km to <2000 km (mesoscale). Model performance is regularly evaluated using accepted validated monitoring data acquired from representative coastal meteorological towers and meteorological systems installed on offshore platforms that were described in the previous section (i.e., **3.2 Atmospheric Monitoring**).

The RU-WRF model was used for the current study to determine offshore wind characteristics during diurnal, monthly, seasonal, and annual periods. The model was also used to analyze specific sea breeze occurrences and "extreme" weather events (e.g., Hurricanes "Irene" and "Sandy") that impact the offshore wind resource. As previously discussed, a significant parameter that is being incorporated into the RU-WRF model is sea surface temperature (SST), which is essential for enhancing model accuracy associated with offshore wind analyses. The model is also programmed to account for the unique microphysics that controls the wind dynamics that are specific to NJ's offshore areas. The RU-WRF model is therefore configured to be used specifically for the analysis and forecasting of NJ's offshore wind resource and associated weather phenomena.

3.3.2 RU-WRF Model Configuration. Temporal and spatial resolutions of the study area along with the external modeling domain dimensions have been established to determine optimal model run times without sacrificing model reliability and accuracy. New computer modules with several additional processors have been dedicated to our offshore wind resource modeling programs. This enhanced computing system has substantially increased our computing efficiency, which will ensure that we achieve maximum computational capability for both analytical and predictive applications.

The current model configuration is based on the following conditions:

- Initial conditions at a 13.0 km grid resolution were determined from results obtained from the National Centers for Environmental Prediction (NCEP) Rapid Refresh (RAP) assimilation/modeling system.

- The initial boundary and surface conditions that define the *external modeling domain* were utilized to initialize the WRF-ARW (Weather Research and Forecasting-Advanced Research WRF) model, which is the most current version accepted by both government organizations and academic institutions.

- The RU-WRF model was run at a 3.0 km grid resolution for the *internal modeling domain* (i.e., offshore/inland regions adjacent to and within NJ's designated offshore wind energy development area). Lateral boundary conditions for the 3.0 km RU-WRF model runs were updated every hour utilizing the NCEP North American Mesoscale (NAM) modeling system at 12.0 km horizontal resolution.

- The results of the 3.0 km runs were then used to set boundary conditions for the high-resolution 0.75 km horizontal grid spacing configured specifically for the offshore areas selected by the *Wind Developers* for their wind energy development activities.

The 3.0 km and 0.75 km modeling domains are portrayed in the following figures:

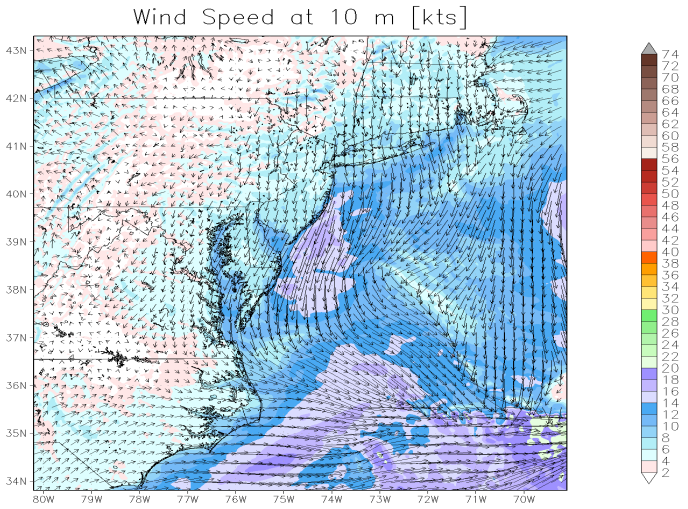

Figure 12: RU-WRF Model 3.0 km Grid Resolution Modeling Domain

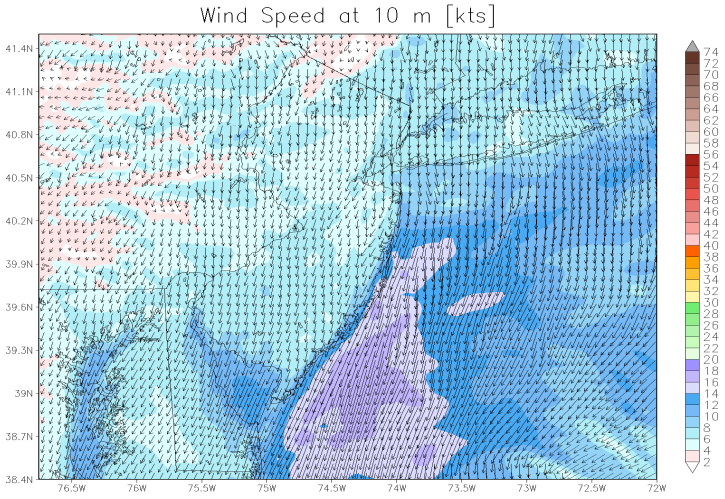

Figure 13: RU-WRF Model 0.75 km Grid Resolution Modeling Domain

The preceding modeling configuration conditions will enable us to respectively analyze the larger spatial characteristics of the offshore wind resource along with the smaller spatial scale relevant to the area size of "typical" offshore wind turbine arrays. RU-COOL will be using the results of the RU-WRF model as input to an analytical/empirical model with grid resolutions <0.75 km to determine turbulence and wind shear characteristics of selected "virtual" meteorological tower sites and proposed offshore locations that appear to be the most conducive for wind energy development. Current RU-WRF model forecasts and simulations can be reviewed on the following web site:

http://rucool.marine.rutgers.edu/index.php/COOL-Data/ru-cool-weather.html

3.3.3 Virtual Meteorological Towers. High-resolution atmospheric modeling (described above) was conducted for an array of locations contained within the project region, creating "Virtual Meteorological Towers." This area encompasses the region established for offshore wind energy development. The virtual meteorological tower array is depicted in the following image (Figure 14) and defined in Table 1.

Figure 14: Offshore "Virtual Meteorological Towers" Locations

Table 1: "Virtual Meteorological Tower" Site Coordinates

Virtual Met Tower ID	Latitude	Longitude	Virtual Met Tower ID	Latitude	Longitude	Virtual Met Tower ID	Latitude	Longitude
A1	38.939	-74.769	D1	39.477	-74.244	G1	40.015	-73.945
A2	38.938	-74.654	D2	39.476	-74.128	G2	40.014	-73.828
A3	38.938	-74.538	D3	39.475	-74.012	G3	40.013	-73.711
A4	38.938	-74.423	D4	39.474	-73.895	G4	40.012	-73.594
A5	38.937	-74.308	D5	39.473	-73.779	G5	40.010	-73.477
B1	39.119	-74.653	E1	39.657	-74.126	H1	40.196	-73.943
B2	39.118	-74.537	E2	39.656	-74.009	H2	40.194	-73.825
B3	39.118	-74.422	E3	39.655	-73.893	H3	40.193	-73.708
B4	39.117	-74.306	E4	39.653	-73.776	H4	40.192	-73.590
B5	39.116	-74.190	E5	39.652	-73.660	H5	40.190	-73.473
C1	39.298	-74.478	F1	39.836	-74.007	I1	40.375	-73.881
C2	39.298	-74.362	F2	39.835	-73.890	I2	40.374	-73.763
C3	39.297	-74.246	F3	39.834	-73.773	I3	40.373	-73.645
C4	39.296	-74.130	F4	39.832	-73.656	I4	40.371	-73.528
C5	39.295	-74.014	F5	39.831	-73.539	I5	40.370	-73.410

3.3.4 Model Validation Protocol. RU-WRF model performance was evaluated on a regular basis using data acquired from validated coastal and offshore monitoring systems that include both in-situ and remote sensing technology (*Refer to pages 11-13*). These monitoring systems provided data, where available, at heights compatible with offshore wind turbine (WTG) dimensions. Model results were compared to representative monitoring results and evaluated according to criteria accepted by the wind energy industry and NREL's National Wind Technology Center (NWTC) for determining model performance (Dvorak et al., 2012). The RU-WRF model validation protocol includes the following criteria:

1) The first validation criterion validates the ability of the RU-WRF model to accurately capture the overall variability in the wind characteristics of the monitoring location using raw model output. The standard deviation of the model results ($\boldsymbol{\sigma_{RUWRF}}$) was compared to the standard deviation of the selected monitoring site meteorological observations ($\boldsymbol{\sigma_{Obs}}$). If $\boldsymbol{\sigma_{RUWRF} \sim= \sigma_{Obs}}$, the model validated according to this criterion.

2) The second validation criterion proves that the variability of the raw model output error as compared to observations is within the variability of the observations. Consequently, if the Root Mean Squared Error (**RMSE**) of the model results was less than the natural wind variability of the site ($\boldsymbol{\sigma_{Obs}}$), the model error was within the bounds of the normal deviation of the wind at the site. Therefore, if $\boldsymbol{RMSE<\sigma_{Obs}}$, the model validated according to this criterion.

3) The third validation criterion proves that when model results are statistically adjusted to account for any bias when compared to the monitored parameter (e.g., wind speed (**WS**)), the unbiased (**ub**) model output will accurately simulate meteorological observations (**WS**) at the selected monitoring site. For this validation criterion, the **RMSE** was calculated using the following equation to remove the overall model bias: $\boldsymbol{[(WS_{RUWRFi} - WS_{RUWRFo}) - (WS_{Obsi} - WS_{Obso})]}$, where (**i**) connotates individual values for model results and coinciding monitor observations; (**o**) connotates the mean values for model results and corresponding monitor observations. If $\boldsymbol{RMSE_{ub}<\sigma_{Obs}}$, the statistically adjusted model results were within the bounds of the normal deviation of the **WS** at the site and the model was considered to be valid. This third validation criterion was expected to reduce the overall **RMSE** in the final wind resource analysis.

If the preceding criteria were satisfied, the model was considered to be valid at the measurement location. It should be noted that the validation criteria account for *Systematic Errors* in both the model program and monitoring instrumentation. *Systematic Errors* can be defined as accountable biases in modeling programs or instrument error attributed to mechanical properties that are inherit to that particular instrument.

Observed deviations from the standard or "normal" variation in monitoring data are caused by anomalies in the monitored parameters and are considered *Random Errors*, which can be considered as statistical “outliers” and cannot be predicted and were therefore eliminated from

the validation procedure. The model evaluation/verification program was automated to continuously conduct model performance analyses for our wind resource assessment and prediction procedures. This process enabled the model configuration to constantly be refined to ensure resultant model values were accurate and precise.

4. Results

4.1 Seasonal SST Analysis

One objective of our study was to determine sea surface conditions for the entire study domain that will support both wind resource analyses and ecological studies associated with offshore wind development. The two key aspects to our analysis of sea surface conditions over the study period include surface ocean currents via our 13 MHz CODAR system and SSTs via our regional-specific, upwelling- and storm mixing-resolving satellite SST composite. The de-clouded, coldest-pixel SST composites that were developed for this study were ingested daily as bottom boundary conditions for real-time RU-WRF model runs.

In addition, a seasonal SST analysis was performed using these daily data for direct comparison to the NJDEP Offshore/Wind Power Ecological Baseline Study (OSWEBS). The dates used for each season, which most closely matched the dates used for each season defined in the NJDEP OSWEBS (NJDEP, 2010), are:

- **Winter:** 01 January 2012 to 09 April 2012
- **Spring:** 10 April 2012 to 21 June 2012
- **Summer:** 22 June 2012 to 27 September 2012
- **Fall:** 28 September 2012 to 17 December 2012

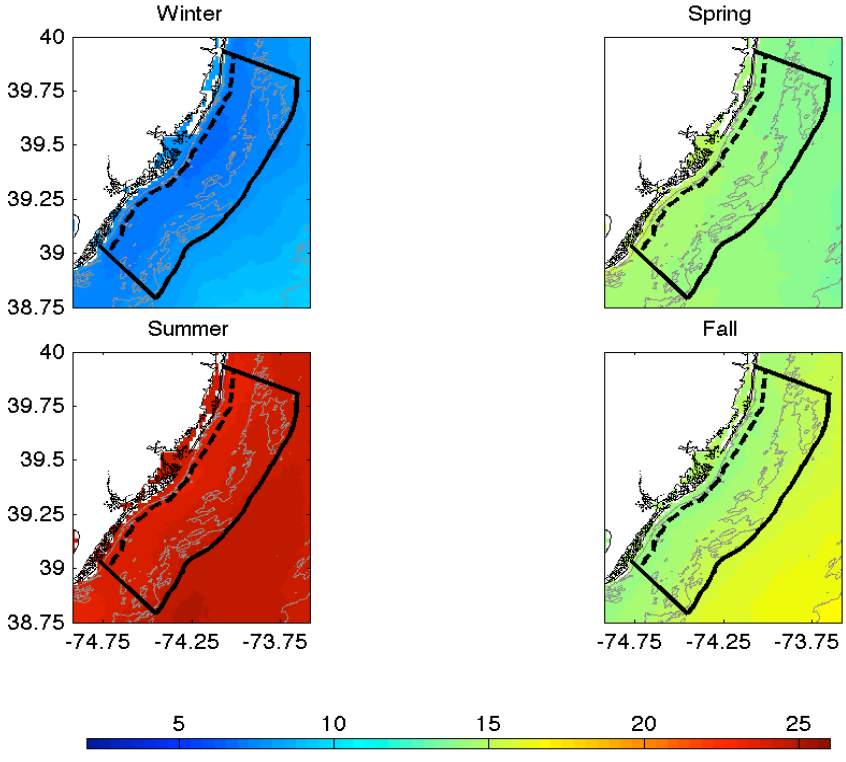

Figure 15: Seasonal SSTs (°C) in the study area from 01 January 2012 through 17 December 2012. Data are displayed using a single scale from 2°C to 26°C to provide an overview of the SSTs in relation to season.

Referring to the preceding images, it appears that mean winter SSTs were about 6-7°C inshore, increasing to about 8-9°C farther offshore. Mean spring SSTs were uniformly 14-15°C across the study domain. Fall SSTs ranged from approximately 13-15°C. The SSTs observed for the winter, spring, and fall seasons closely match the patterns observed during the NJDEP OSWEBS. However, mean summer SST values were significantly higher in 2012 (SSTs were 24°C+) than those observed during the NJDEP OSWEBS that was conducted during the period 2007-2009 (SSTs were ~ 18-20°C). Assuming that water temperatures near the sea floor (~9-10°C during the summer season) remain relatively constant from year to year, it is very probable that warmer SSTs will cause increased stratification throughout the water column (Houghton et al. 1982). This increased stratification will produce stronger temperature gradients in the upper ocean along with an enhancement in the energy exchange from the sea surface to the overlying atmosphere. This increase in energy imparted to the atmosphere could potentially alter the intensity of the offshore wind resource.

The following SST images (Figure 16) are similar to Figure 15 except the temperature scales are set to coincide with the minimum and maximum SST values of each season, which provides greater resolution of the indicated SST values. A similar procedure was conducted to resolve SST values during the NJDEP OSWEBS.

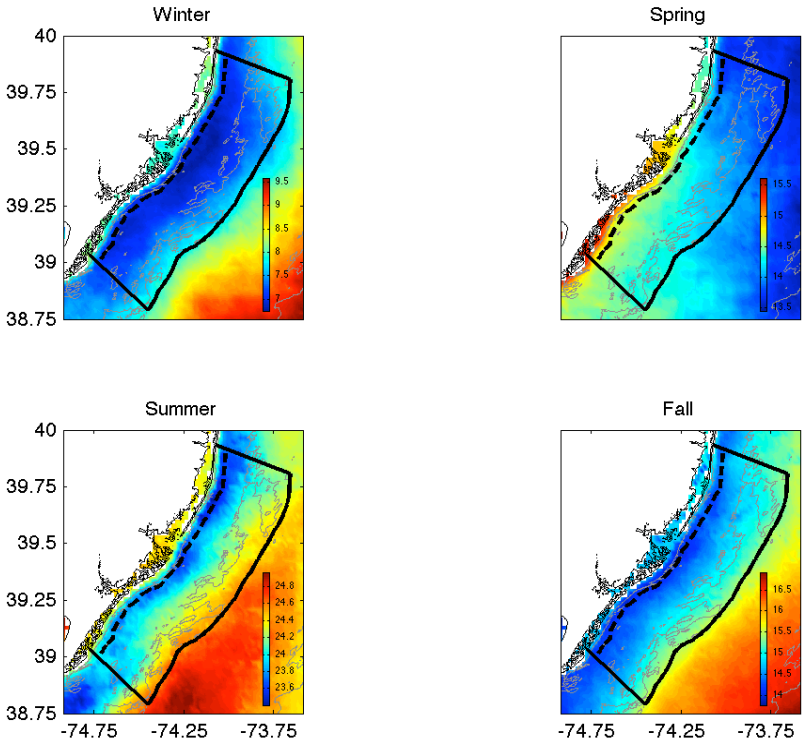

Figure 16: Similar to Figure 9; however, data are displayed using scales that coincide with the minimum and maximum temperatures for each season to provide a greater resolution for the indicated SST values.

Referring to the preceding images (Figure 16), mean winter SSTs are lower near shore (~7°C) and higher farther offshore (~ 9°C). Mean spring SSTs provide an interesting reverse pattern when compared to winter SSTs. Spring SSTs are warmer near shore, approaching 16°C farther south toward Cape May. At greater distances offshore, observed SSTs are colder (~13°C). The SST observations for the winter and spring seasons are consistent with the SST patterns presented in the NJDEP OSWEBS. However, detailed SST patterns detected during the

summer and fall show that there are significant coastal upwelling centers of colder SSTs along the coast and warmer SSTs offshore. Detected SSTs along the coast for the respective summer and fall seasons were approximately 23 and 14°C with farther offshore SSTs being respectively 25 and 17°C. This upwelling pattern is not apparent in the referenced NJDEP OSWEBS SST evaluation. Therefore, the RU-COOL de-clouded SPoRT composite provides a product that can realistically detect actual SSTs during unique physical phenomena, such as upwelling events, that would otherwise go unnoticed when using "standard" IR satellite detection procedures.

4.2 Model Validation Results

4.2.1 Vertical Model Validation (5m to 120m atmospheric heights). The results of the model validation evaluation show that RU-WRF validated at all selected locations except for Delaware Bay Buoy. A potential reason that could explain the failure of the model at this point is that the Delaware Bay Buoy has a measurement height of 5 m, which is well below all those involved in the validation, while the data extracted from the model are at a measurement height of 10 m, and the wind shear between 10 m and the buoy anemometer height can be impacted by the proximity to the surface. Otherwise, RU-WRF performed very well with a RMSE ranging from 2.06 – 2.76 m/s. The results of the vertical model validation are summarized in Table 2. ***"These results verify that the RU-WRF model is validated and can thus be used to accurately and realistically analyze and predict the various parameters associated with NJ's coastal/offshore wind resource at heights representative of offshore WTG dimensions."***

Table 2: Vertical Model Validation Results (5m to 120m Atmospheric Heights).

Site	Delaware Bay Buoy	Buzzards Bay	Chesapeake Light	Brandywine Light	Ship John's Shoal	Oyster Creek
	44009	BUZM3	CHLV2	BRND1	SJSN4	OYC
Observation Height (m)	5	24.8	43.3	19.3	20.4	115
Observed Average Wind Speed (m/s)	5.70	7.59	7.54	6.07	5.60	6.41
Observed Standard Deviation (m/s)	3.24	3.91	3.79	3.00	3.02	2.80
RU-WRF Average Wind Speed (m/s)	5.75	7.30	7.72	6.59	5.51	6.49
RU-WRF Standard Deviation (m/s)	2.89	3.53	3.42	3.26	2.85	2.98
Model Bias (m/s)	0.04	-0.29	0.18	0.52	-0.09	0.09
RMSE (m/s)	3.46	2.42	2.77	2.27	2.14	2.06
RMSE unbiased (m/s)	3.46	2.43	2.76	2.35	2.13	2.06
Criterion 1 (% diff between $\sigma_{RU\text{-}WRF}$ and σ_{Obs})	10.66%	9.78%	9.82%	-8.62%	5.53%	-6.40%
Validated	No	**Yes**	**Yes**	**Yes**	**Yes**	**Yes**
Criterion 2 (RMSE/ $\boldsymbol{\sigma_{Obs}} * 100$)	107.0%	61.9%	73.1%	75.7%	70.9%	73.6%
Validated	No	**Yes**	**Yes**	**Yes**	**Yes**	**Yes**
Criterion 3 ($RMSE_{ub}$/ $\boldsymbol{\sigma_{Obs}} * 100$)	107.0%	62.1%	72.9%	78.3%	70.6%	73.6%
Validated	No	**Yes**	**Yes**	**Yes**	**Yes**	**Yes**

4.2.2 Horizontal Model Performance Evaluation (Spatial dimensions that define the offshore area defined for NJ offshore wind energy development).

Synopsis: The temporal and spatial variability in the NJ offshore wind resource has large implications on the energy production for proposed offshore wind parks. The RU-WRF modeling system (i.e., RU-WRF model) that we have developed for the current project can begin to diagnose as well as predict key sources of variability both in space and time, including sea and land breezes and frontal passages within and beyond the study area.

It is critical to evaluate the performance of the RU-WRF model not only in the vertical but also over the spatial horizontal study domain to identify areas for improvement and subsequently, if necessary, refine the model. An objective of the study states that the vertical and horizontal spatial variability of the offshore wind resource will be determined and validated with existing observational systems. Although vertical validation of winds can be performed with meteorological towers and approved remote sensing systems, horizontal spatial evaluation of winds, especially for offshore areas, can be difficult with pre-existing observational systems. Satellite-based scatterometers (e.g. QuikSCAT; Shirtliffe, 1999) have historically provided wind measurements over the ocean. However, their relatively low spatial resolution of 25 km is not adequate for wind resource assessments associated with the spatial scale for most offshore wind turbine arrays.

RU-COOL has applied high-resolution surface current mapping capabilities of the high frequency (HF) coastal RADAR (CODAR) to resolve wind fields over the offshore RU-WRF atmospheric modeling domain. The surface currents sampled by the shore-based CODAR system are forced by a combination of processes. In our study region the surface currents are largely driven by tides, buoyancy, and local winds (Beardsley et al., 1976, Beardsley & Haidvogel, 1981). The tides were extracted from the raw observed currents using standard least squares approaches (Kohut et al., 2004). We have found that in our region the relative importance of local winds in driving detided surface currents depends largely on stratification. During the winter season when the water column is mixed, bottom friction and pressure gradients drive the flow. During the summer, strong stratification isolates the slippery surface layer from the bottom leading to a surface current more dependent on the local wind forcing. Here we apply a regression model to estimate the offshore surface wind fields during this summer-stratified season at a resolution of 2 km across the designated study area.

We identified two sea breeze events during the summer-stratified season on which to focus our CODAR surface current-based wind model: one without coastal upwelling (30 Aug-6 Sep 2012) and one with coastal upwelling (8-15 Sep 2012). We trained the model on one month of data spanning both events, 25 Aug to 25 Sep, while the water column was still stratified. We used measured wind from the Ocean City WeatherFlow site, which is on the coast centered on the study region and has good coverage over this time period. Wind observations were 75-minute center averaged to be consistent with the CODAR processing (Figure 17).

The wind model is based on the correlation between the local wind observation in Ocean City, NJ and the surface current observations at each grid point in the survey region (Kohut et al., 2004). For each grid point we calculated complex correlation between the local wind observation and the observed detided surface current. The magnitude across the field had a mean of 0.56 and a maximum of 0.73, and most of the region had a correlation higher than 0.4. The phase indicates that the highest correlated current was shifted to the right of the wind with an angle that ranged from about 0 to 60° across the field. These values are based on a zero time lag between the wind and current. Three points in regions of high correlation were used to determine

the time lag that yielded the highest correlation between surface winds and currents. For each of these points we lagged the currents by 0 to 12 hours and recalculated the complex correlation. For each point, the highest correlation between wind and current peaked with a lag of 3 hours. This indicates that the surface currents lag the wind forcing by approximately three hours (Figure 18).

The complex correlation was then recalculated with this lag across all grid points. The majority of the study region now has a mean correlation of 0.62 and a maximum of 0.92, with over 50% of the region at a correlation above 0.6. The new correlation values increased with lowest values near the edges and the highest values again near the center of the HF radar coverage (Figure 19). Surface currents were rotated based on the angles shown in the right panel of Figure 19 and a best-fit line applied to the rotated surface u (v) current and measured u (v) wind three hours previous as in Kohut et al. (2004). Estimated wind maps were then generated by rotating HF radar-measured surface currents and applying the best-fit equations to the rotated currents. The resulting surface current-based wind estimates were the basis for the spatial evaluation of the offshore wind fields predicted by the RU-WRF model. An example of the final suite of imagery that was used to spatially evaluate RU-WRF offshore winds is presented in Figure 20, which includes CODAR detided currents, surface winds, and RU-WRF modeled 10m winds.

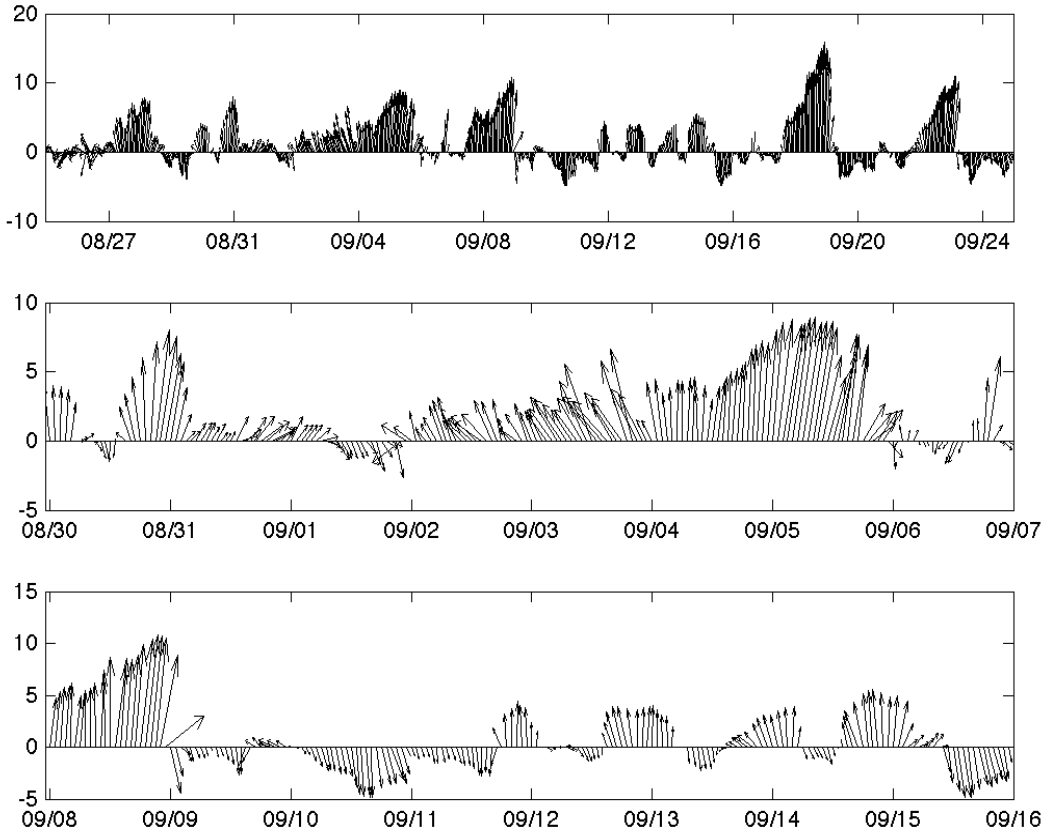

Figure 17: Hourly 75-minute averaged wind measurements at the Ocean City WeatherFlow site for the time period used to train the surface current-based wind model. Top panel shows winds for the entire time period, middle panel shows the early September sea breeze case, and the bottom panel shows the mid-September sea breeze case. Tick marks are at 00:00 GMT for day noted.

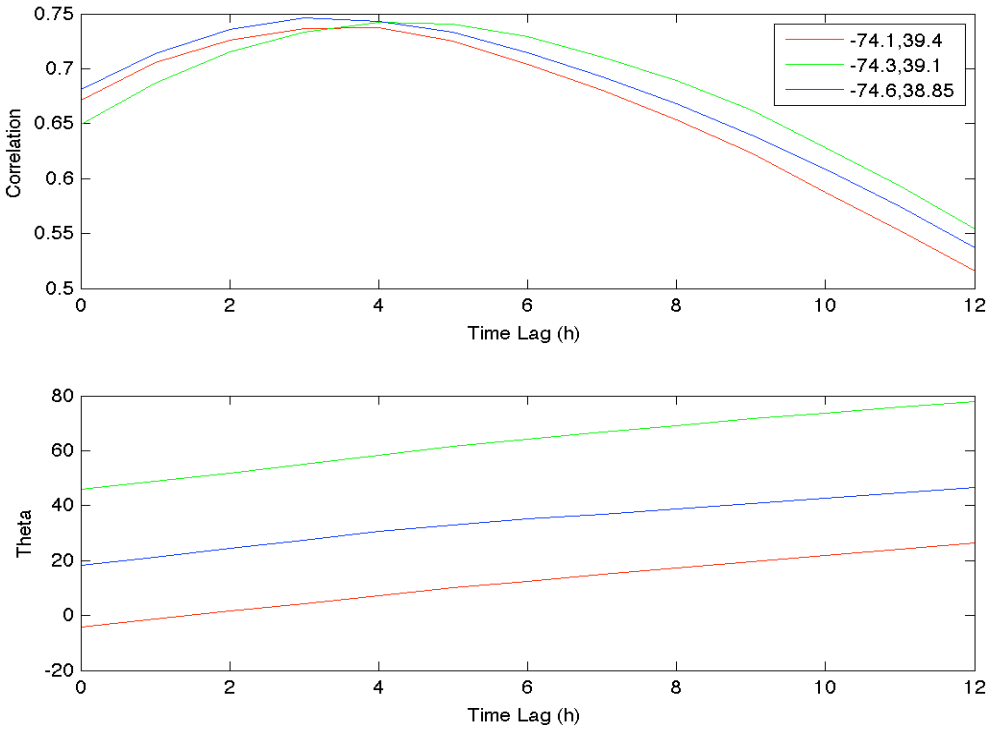

Figure 18: Time-lag dependent complex correlation magnitude (top) and angle offset between highest correlated components of wind and surface current (bottom) for three points in regions of high correlation (red: northernmost, green: central, blue: southernmost). The correlation peaks at a time lag of around three hours, and offset angle steadily increases with increasing time lag.

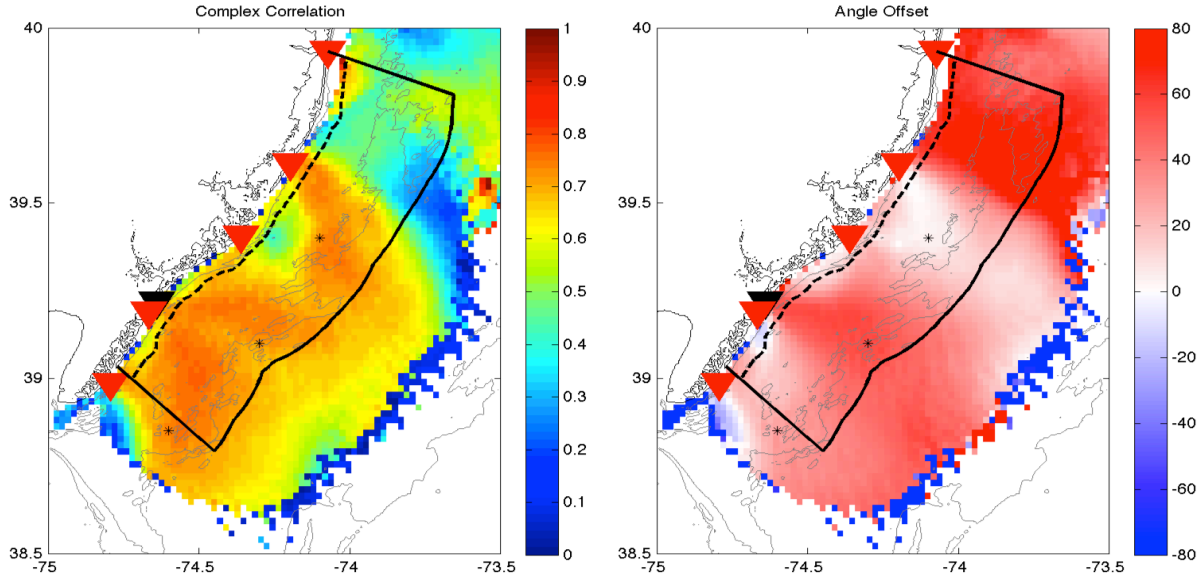

Figure 19: Magnitude of complex correlation and angle offset between the highest correlated components of the wind and surface currents with a three-hour lag. Black triangle: location of the Ocean City WeatherFlow site, red triangles: 13 MHz CODAR sites, solid line: study area coinciding with the NJDEP OSWEBS area for offshore wind (extending 20 nm offshore), dashed line: boundary between federal and state waters (3 nm offshore), asterisks: test locations for time lags.

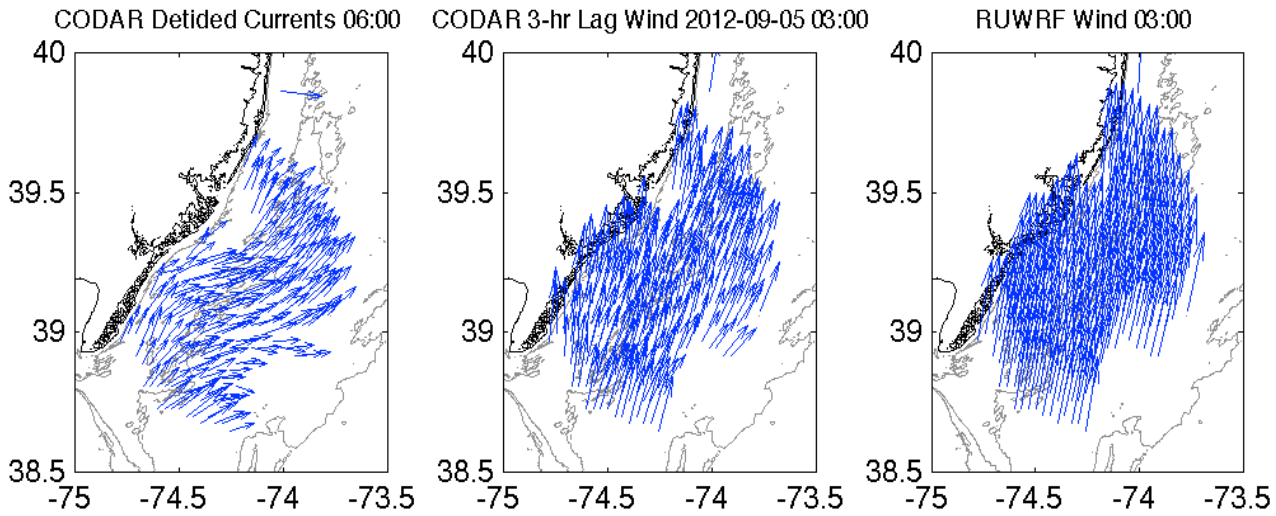

Figure 20: Detided surface currents on 5 Sep 2012, 06:00 GMT (left), wind predicted for 03:00 based on those currents (center), and RU-WRF model 10m wind at 03:00 (right).

RU-WRF Model Performance Evaluation Case Studies: For the upwelling and non-upwelling case studies, we used the CODAR surface wind estimate to evaluate RUWRF performance offshore throughout the study region. Figure 21 depicts the complex correlation magnitude and angle offset between CODAR-derived surface winds and RU-WRF model 10m winds.

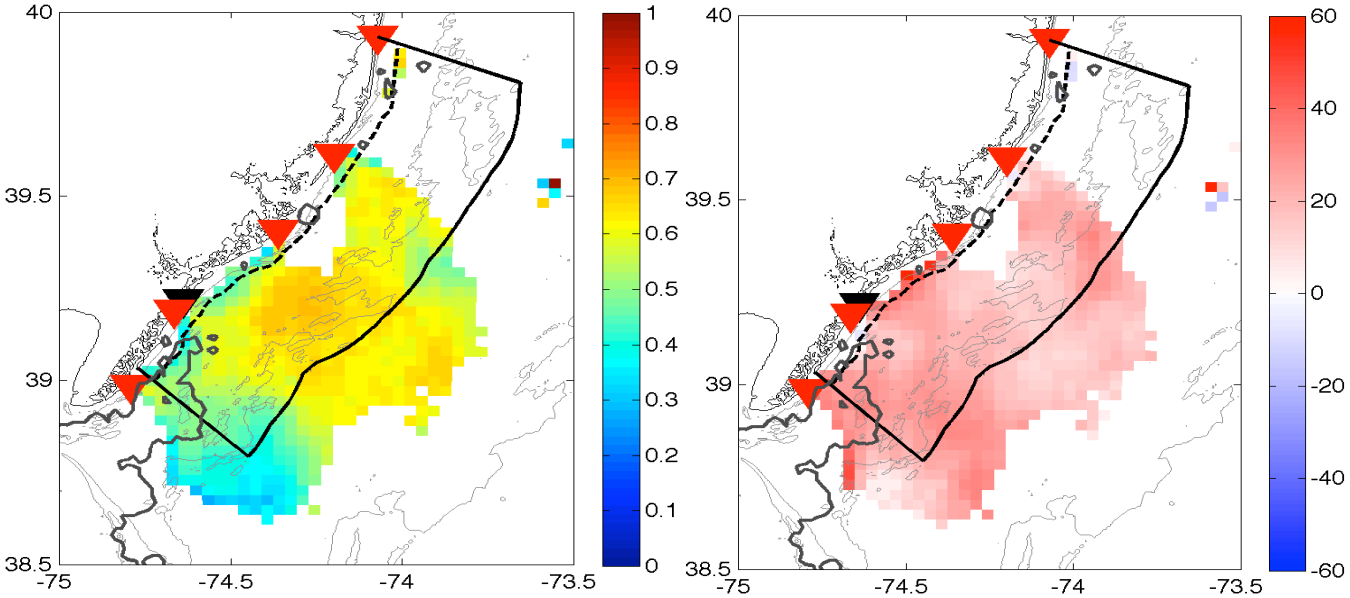

Figure 21: Magnitude of complex correlation (left) and angle offset (right) between the CODAR-predicted surface wind (e.g. Figure 20, center) and RUWRF modeled 10m wind (e.g. Figure 20, right), for the *non-upwelling* case (30 Aug 2012-6 Sep 2012). Black triangle: location of the Ocean City WeatherFlow site, red triangles: 13 MHz CODAR sites, black solid line: study area coinciding with the NJDEP OSWEBS area for offshore wind (extending 20 nm offshore), dashed line: boundary between federal and state waters (3 nm offshore), dark gray solid contour: 24°C isotherm of SST, showing minimal to no coastal upwelling occurring in the study area.

In this evaluation, we limited the comparison between CODAR derived winds and RU-WRF model winds to those grid points in which the correlation between the CODAR currents and Ocean City winds was at least 0.6. For these grid points, the comparison between HF radar winds and RU-WRF model winds were determined for the upwelling and non-upwelling cases. For the non-upwelling case between 30 Aug 2012 and 6 Sep 2012, the correlation coefficient was at least 0.5 across the study region, with a large area of 0.65 correlation near the center of the field. Angle offset values were consistently between 0° and about 20° across the study region indicating that the most correlated RU-WRF model wind vector is shifted to the right of the CODAR wind estimate.

The upwelling case, between 8 Sep 2012 and 15 Sep 2012, had a very different spatial pattern in the comparison between CODAR wind estimates and RU-WRF model simulated offshore winds. For the upwelling case there was a cross and along-shelf gradient in the correlation with the lowest values near shore close to the center of the field. Farther offshore there is a banding pattern with the highest correlations centered on the middle of the field (Figure 22). The region of low correlation near shore with values less than about 0.3, coincides directly with the core of coastal upwelling that occurred for much of the time period. This zone of upwelling is depicted by the gray contour of 22°C SST along the coast of Atlantic City. Inside the upwelling center the water column is well mixed (Chant et al., 2004). Under these mixed conditions it has been shown the CODAR surface currents are less responsive to local winds. Therefore, the low correlation in this upwelling center is likely more a result of uncertain CODAR estimates of the winds rather than inaccuracies in the RU-WRF model winds.

The bands of lower correlation in the alongshore direction farther offshore are spaced approximately 30 km apart, matching the scale of the inshore upwelling center. It has been shown that these upwelling centers are characterized by an alongshore velocity jet running up the NJ coast along the offshore edge of the surface front (Chant et al., 2004). A closer examination of the surface currents over this upwelling case show that the surface currents offshore tend to follow the shape of the upwelling center with a general flow along the coast near the southern boundary of our survey region that turns sharply offshore just south of the upwelling center before turning alongshore farther north. This spatially dependent perturbation in the flow around the upwelling center could bias the wind estimates from the CODAR systems.

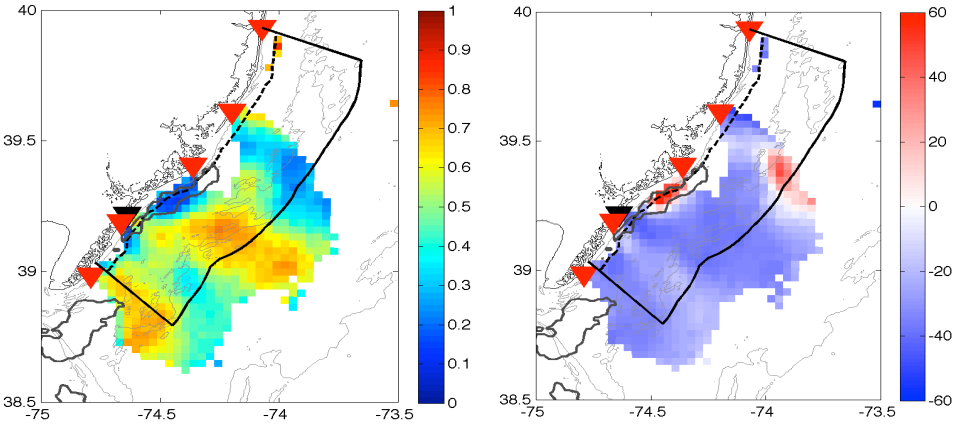

Figure 22: Magnitude of complex correlation (left) and angle offset (right) between the CODAR-predicted surface wind and RUWRF modeled 10m wind, for the upwelling case. Black triangle: location of the Ocean City WeatherFlow site; Red triangles: 13 MHz CODAR sites; Black solid line: study area coinciding with NJDEP OSWEBS area; Dashed line: boundary between federal and state waters: Gray solid contour: 22°C isotherm of SST, showing coastal upwelling in the study area.

CODAR derived wind field estimates were used to evaluate the RU-WRF model performance in resolving the spatial structure of the offshore wind field. Wind estimates derived from CODAR data appear to be influenced by the near-shore upwelling center. Therefore, we chose to concentrate this analysis on the non-upwelling case. During the non-upwelling case the CODAR estimated winds were more correlated with the RU-WRF model results over most of the study region.

Figure 23 depicts a subtle banding in convergence/divergence west to east in the RU-WRF modeled winds (Figure 23, right) as well as the CODAR-derived surface wind field (Figure 23, center) on 4 Sep 2012 at 19:00 GMT. A convergence band is evident on the southwestern edge of the study area in both the CODAR wind and RU-WRF wind fields. Just to the east, an area of lighter, more divergent winds is evident in both fields, and then farther east another area of higher, more convergent winds. In general, there is good overall correlation between wind direction in both the CODAR product and RU-WRF model (i.e. both from the south), while CODAR de-tided currents are more variable from the southwest, west, and south at that time as one moves north up the coast (Figure 23, left).

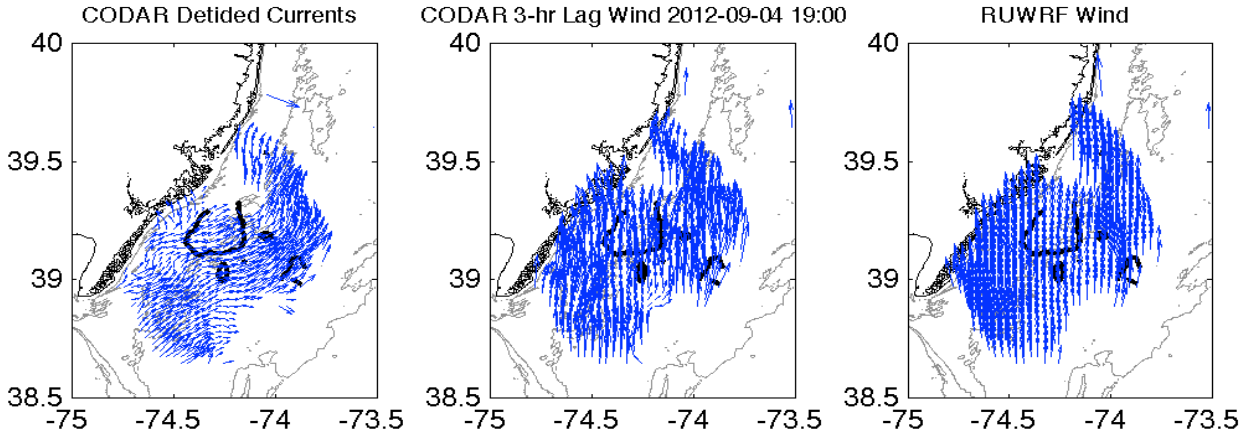

Figure 23: De-tided surface currents on 4 Sep 2012, 19:00 GMT (left), wind predicted for 19:00 based on the currents 3-hrs earlier (center), and RU-WRF modeled 10m wind at 19:00 (right). Black contour: greater than 0.65 correlation between CODAR-derived surface winds and RU-WRF modeled 10m winds during the entire non-upwelling case.

Throughout the model study the RU-WRF model winds showed significant spatial variability associated with local processes including fronts associated with the sea breeze and passing thunderstorms. To demonstrate the feature tracking of the CODAR and RU-WRF model simulated offshore winds, we focused on a passing cold front between about 18:00 GMT on 5 Sep 2012 and 06:00 GMT on 6 Sep 2012. A strong line of thunderstorms developed along the front; at 23:00 GMT, the line of storms was directly over the northern section of the study area. At the same time, the near-surface wind response to the thunderstorms was evident in our RU-WRF model run with a distinct area of surface divergence located in the northeastern section of the study area, offshore of Tuckerton, NJ (Figure 24, bottom left).

The surface divergence in the winds was likely caused by either a strong outflow boundary ahead of the thunderstorm front or directly from the cold downdraft in the core of the cold rain, which would reach the ocean's surface and diverge outwards. The forcing was so strong that the response was evident in both the CODAR de-tided ocean currents (Figure 24, top

left) that are directed offshore in the coincident area, and the CODAR-derived surface winds (Figure 24, top right) that are directed outward from the thunderstorm core and offshore of Tuckerton. This case warrants future analysis in surface ocean response to thunderstorm outflow boundaries and downdrafts.

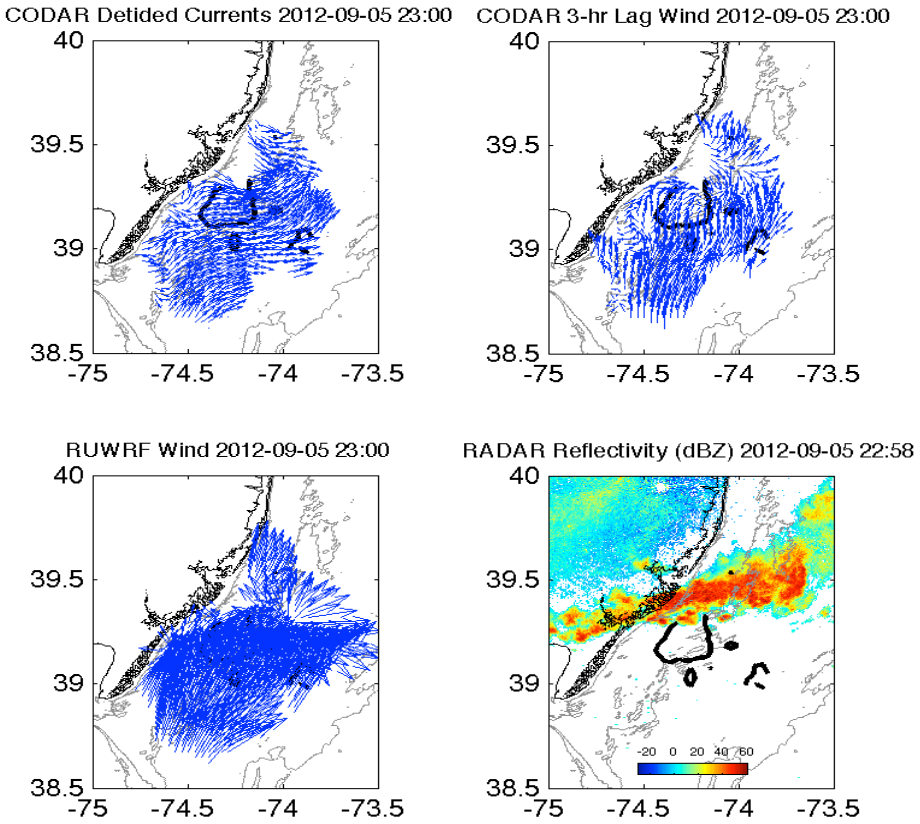

Figure 24: De-tided surface currents on 5 Sep 2012 23:00 GMT (top left), wind predicted for 23:00 GMT based on the currents 3-hrs earlier (top right), RU-WRF model 10m wind at 23:00 (bottom left), and weather radar reflectivity depicting a line of strong thunderstorms at 22:58 GMT (bottom right). Black contour: greater than 0.65 correlation between CODAR-derived surface winds and RU-WRF model 10m winds during the entire non-upwelling case.

"The preceding evaluation of CODAR detected surface currents and derived winds with RU-WRF model simulations provides evidence that the Model performance is representative of the spatial area designated for NJ's offshore wind energy development endeavors. Therefore, it can be assumed with a relatively high degree of confidence that the RU-WRF model is capable of producing accurate predictions of the spatial structure, size, and movement of some significant sources of variability in the NJ offshore wind resource."

4.3 RU-WRF Model Simulations vs. Climatology

The methodology used to develop the data set from RU-WRF model results that is representative of NJ's offshore wind resource climatology is described in the following discussion. The RU-COOL offshore wind resource study utilized daily RU-WRF model simulations to formulate a representative long-term wind resource data set for the offshore waters of New Jersey. The development of this extensive data set was accomplished by

extracting data from the daily model simulations for meteorological variables pertinent for the evaluation of an offshore wind project. These variables include wind speed and wind direction at elevations of 10m, 50m, 60m, 70m, 80m, 90m, 100m, 110m, and 120m, air temperature and relative humidity at 100 m, and sea-level pressure. In addition, the model output was averaged into monthly, seasonal, and annual values that were used to create the wind maps.

RU-WRF model data were extracted at each monitoring location in order to create an "8760" (i.e., hourly data for each hour of the year) data set that will determine and eliminate model bias as described in the model validation protocol. This unbiased model output is then used to compare to long-term datasets of measured wind speed in order to determine the long-term average at these monitoring sites. Data were extracted at each virtual met tower and are then unbiased using the bias corrections (monthly) determined from the model validation. The virtual met towers are unbiased using the bias correction found from the nearest observation point, and then in some cases averaged with the next nearest observation point. The model grids are unbiased using the overall average of bias correction of the observation points within the region bounded by latitude 38.5 N to 41.5 N and longitude 76.0 W to 73.0 W for each month. The overall model grid bias was determined to be +0.14 m/s.

4.3.1 Long-term (Climatological) Analysis. The unbiased virtual meteorological tower "8760" data set, as well as the model grids are then corrected to a long-term average utilizing observed monitoring data. As a result of non-existent offshore tall tower data, the long-term analysis has been done using the Long Island Buoy (44025) and Atlantic City airport (KACY). While the Oyster Creek meteorological dataset would be quite beneficial in the determination of above surface long-term wind speeds, the data made available consisted of only three years (2010-2012). The Delaware Bay buoy would have also been a beneficial data point; however the anemometer was damaged in Nov 2012 and unavailable until late Feb 2013. To properly assess the long-term wind speed, a data record of 5-years is necessary, with longer data sets preferred. An example of a long-term time series of wind speeds for one of the offshore virtual meteorological towers is shown in Figure 25.

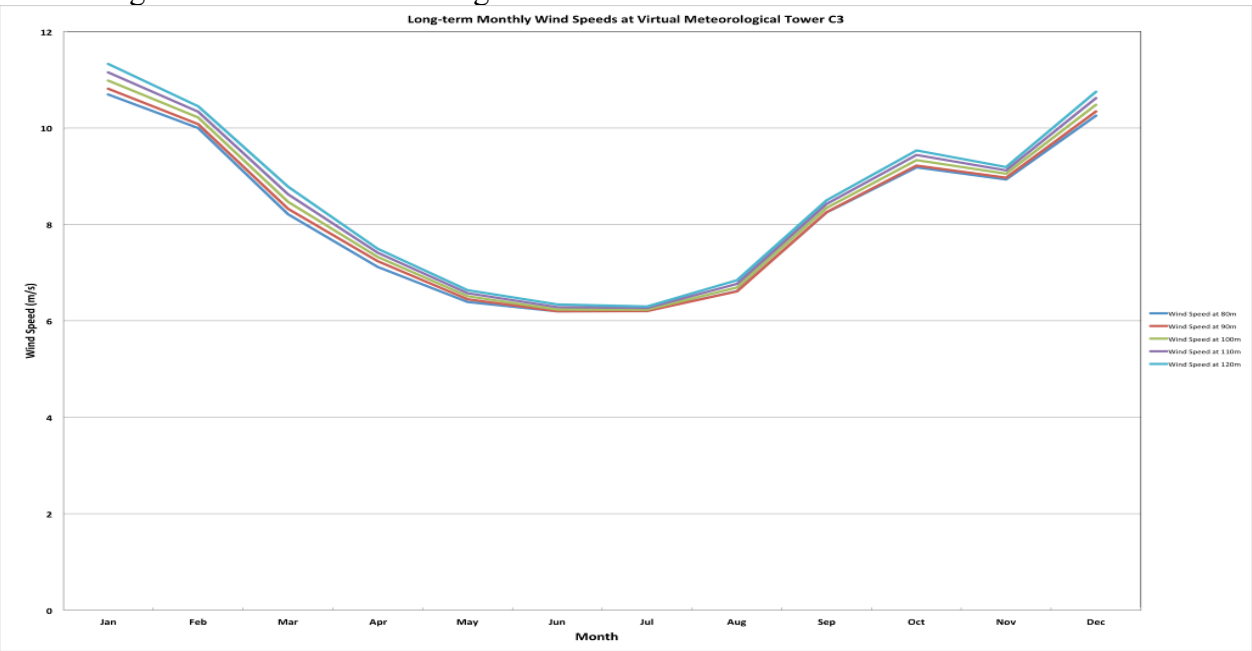

Figure 25: Long-term Monthly Wind Speeds at Virtual Meteorological Tower C3

The overlapping data between the model derived "8760" data and observations were correlated at a monthly level. The R-squared values between observed and modeled values on a monthly basis ranged from 0.8782 at 44025 (Figure 26) to 0.9378 at KACY (Figure 27). R-squared values greater than 0.8 on a monthly basis are generally considered acceptable for long-term corrections.

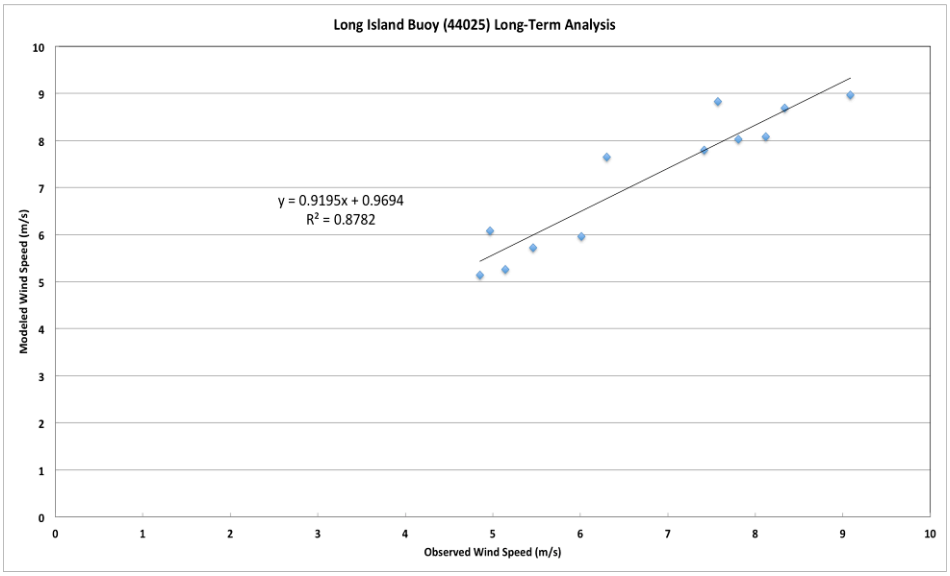

Figure 26: Long Island Buoy monthly correlation to Virtual Met Tower 44025

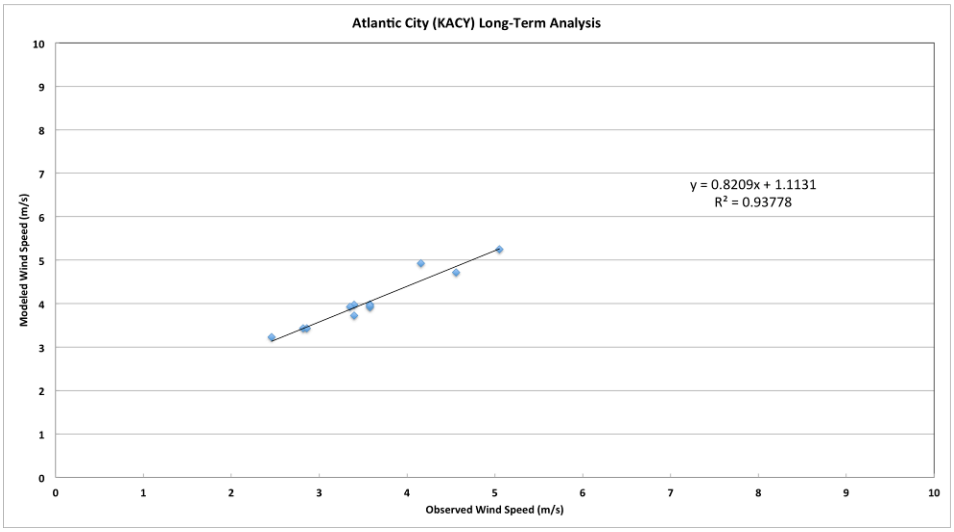

Figure 27: Atlantic City Airport (KACY) monthly correlation to Virtual Met Tower KACY

The RU-WRF model monthly averages at KACY and 44025 are then run through the monthly correlation equations to determine the long-term average wind speed of the virtual met tower. The ratio of the long-term average modeled wind speed and the modeled Apr 2012-Mar 2013 monthly values is the deviation from climatology for the month. During the study period, the annual deviation from climatology indicates that winds are 1.5% less intense when compared to average (climatological) annual wind speeds at KACY. In contrast, wind speeds at 44025 were found to be 0.5% more intense than the long-term average.

Table 3. Atlantic City Airport (KACY) long-term correction by month.

Atlantic City Airport (KACY)			
	Long-term Average 04/2008-03/2013	Observed Values 04/2012-03/2013	Deviation from Climatology
January	3.86	3.58	92.6%
February	4.51	4.56	101.2%
March	4.32	5.05	117.0%
April	4.20	4.16	98.9%
May	3.63	3.40	93.6%
June	3.10	3.40	109.5%
July	2.98	2.82	94.6%
August	2.73	2.46	90.2%
September	3.08	2.86	92.8%
October	3.42	3.35	98.2%
November	3.52	3.58	101.5%
December	4.05	3.58	88.3%
Overall	3.61	3.56	98.5%

Table 4. Long Island Buoy (44025) long-term correction by month.

Virtual Met Tower 44025 - Long Island Buoy			
	Long-term Average 04/2008-03/2013	Observed Values 04/2012-03/2013	Deviation from Climatology
January	8.29	7.81	94.2%
February	8.53	9.09	106.6%
March	7.19	8.34	116.0%
April	6.08	6.30	103.6%
May	5.12	4.97	97.0%
June	5.19	5.46	105.2%
July	5.02	5.14	102.4%
August	5.22	4.85	92.9%
September	6.44	6.01	93.3%
October	7.82	7.42	94.9%
November	7.54	8.12	107.7%
December	8.18	7.57	92.6%
Overall	6.71	6.74	100.5%

The conflicting values for the variation from climatology is interesting; however, a significant amount of this difference only occurs during the month of July. At the Long Island Buoy, July's wind speeds were 2.4% higher than normal, while at Atlantic City airport, roughly 8 miles inland, wind speeds during July were 5.4% lower than normal. Jul 2012 was found to have sea breeze development during 14 out of 31 days. A more active sea breeze month can result in lower than average wind speeds inland along with higher than average wind speeds offshore. As a result of these findings, an average of the monthly deviation of KACY and 44025 was calculated for the fall and winter months. The deviation from normal at 44025 was determined for the "sea breeze season" (i.e., spring through summer). The overall result is that the study period Apr 2012 – Mar 2013 exhibited 0.04% less intense wind speeds than normal. "***This deviation from climatology is insignificant. Therefore, the study period is considered to be representative of the offshore wind resource climatology (i.e., "normal" or long-term average values)".*** The deviation in climatology for each month that was analyzed for the study period is presented in Table 5.

Table 5. Monthly offshore wind resource deviations from the long-term average adjusted to coincide with climatology, which ensures that the resultant wind resource assessment is representative for the study area.

Month	Deviation from Climatology
January	93.41%
February	103.88%
March	116.50%
April	103.55%
May	97.04%
June	105.22%
July	102.40%
August	92.90%
September	93.03%
October	96.52%
November	104.59%
December	90.45%
Overall	**99.96%**

4.4 NJ Offshore Wind Resource Simulations

Virtual meteorological tower data are scaled using hourly monthly values adjusted for climatology, resulting in a long-term "8760" data set at each virtual meteorological tower site. Similarly, the gridded RU-WRF model data is scaled by these values to produce long-term spatial wind maps at 80m, 90m, 100m, 110m, and 120m. ***The resultant offshore wind resource assessment along with previous bathymetric and ecological studies provide sufficient evidence that NJ's offshore waters are very conducive for wind energy development***. The following offshore wind resource simulations ("maps") derived by RU-WRF

model results, which are adjusted for climatology, are provided respectively for annual, seasonal, and monthly periods. They are plotted with the boundary of the NJDEP OSWEBS (black line offshore) and the 3 nm state boundary (black line inshore).

4.4.1 Annual Coastal/Offshore Wind Resource Maps

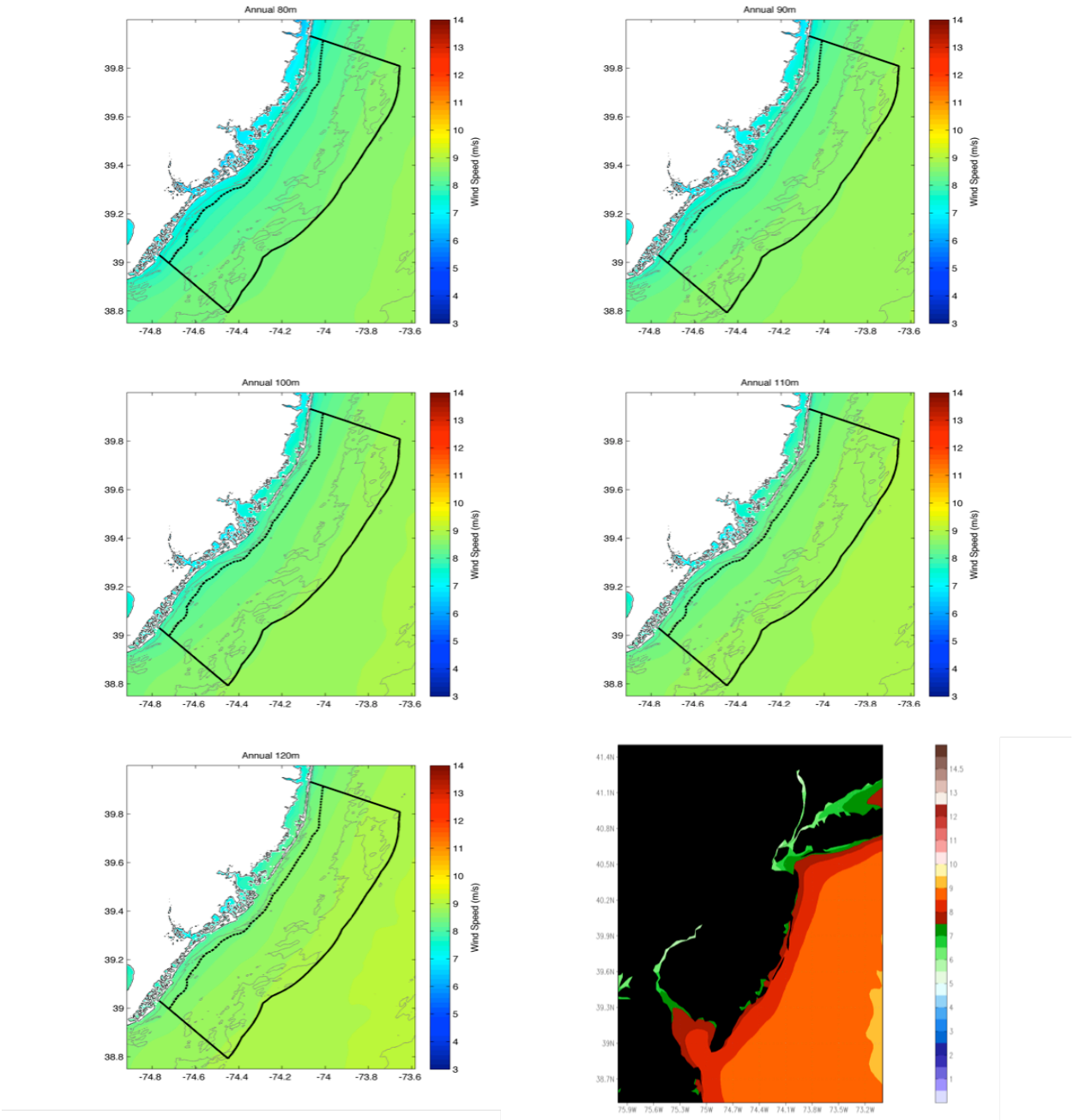

Figure 28: Annual average wind speed at (a) 80m, (b) 90m, (c) 100m, (d) 110m, (e) 120m, and (f) 100m (zoomed out)

4.4.2 Seasonal Coastal/Offshore Wind Resource Maps

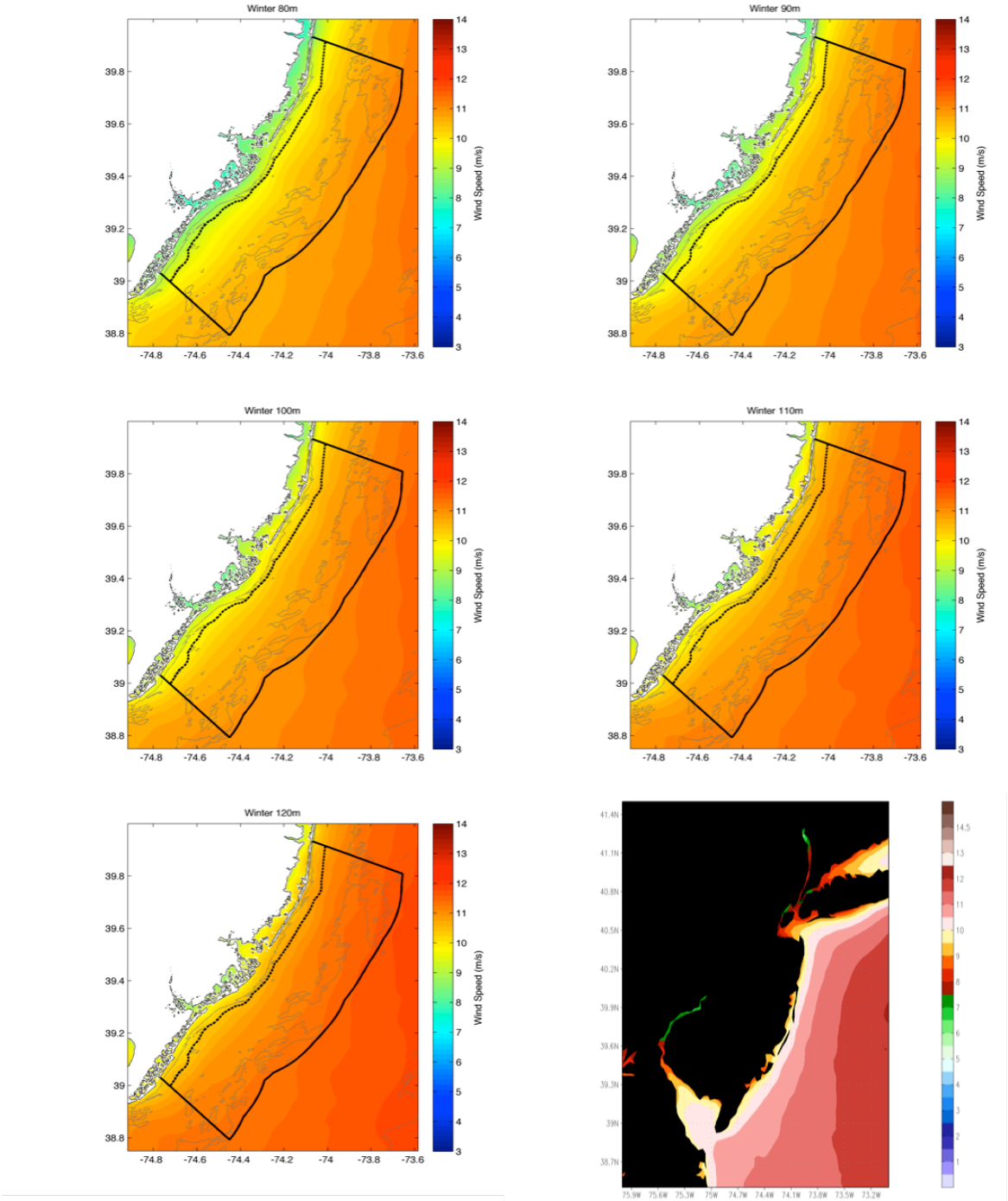

Figure 29: Winter average wind speed at (a) 80m, (b) 90m, (c) 100m, (d) 110m, (e) 120m, and (f) 100m (zoomed out).

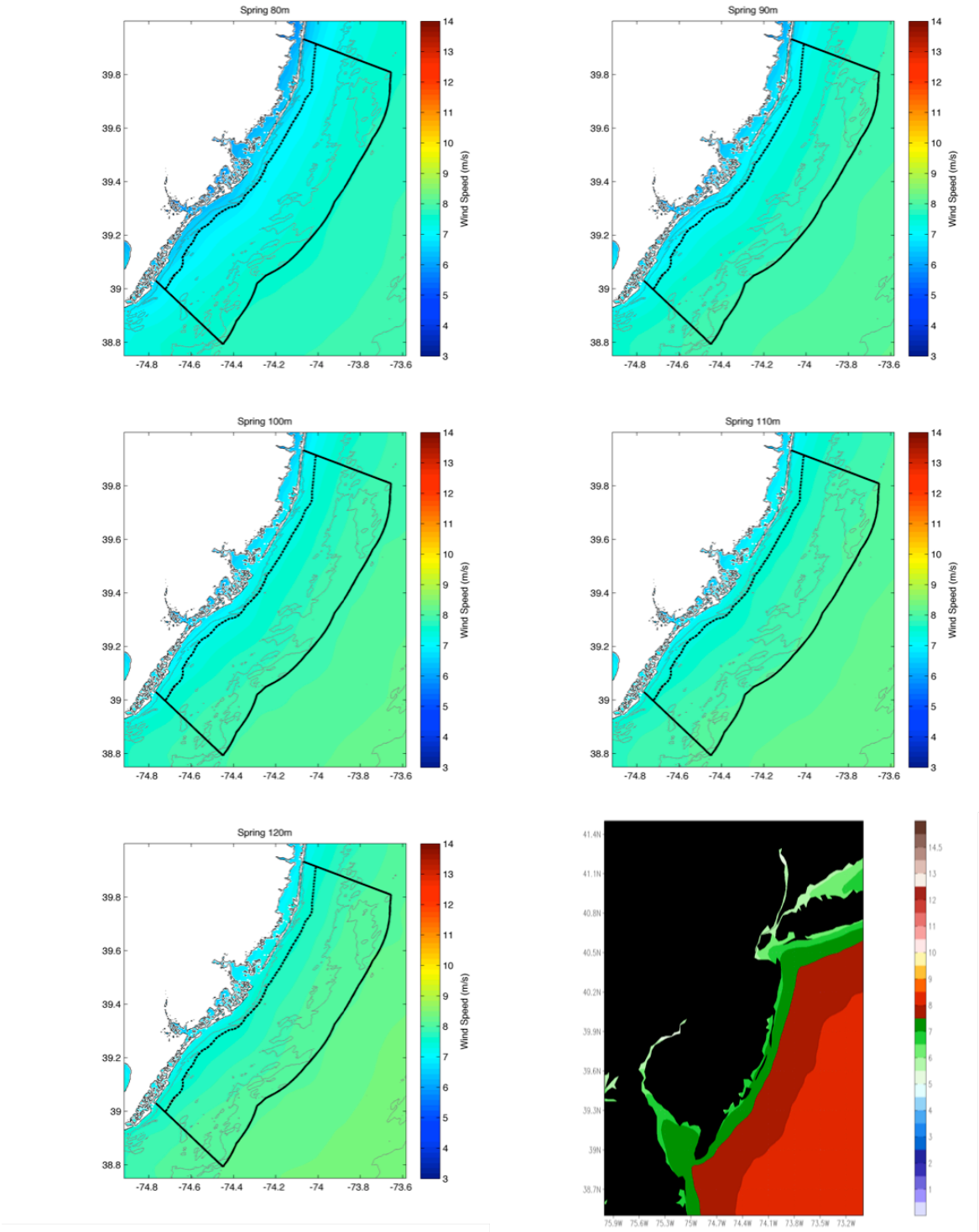

Figure 30: Spring average wind speed at (a) 80m, (b) 90m, (c) 100m, (d) 110m, (e) 120m, and (f) 100m (zoomed out).

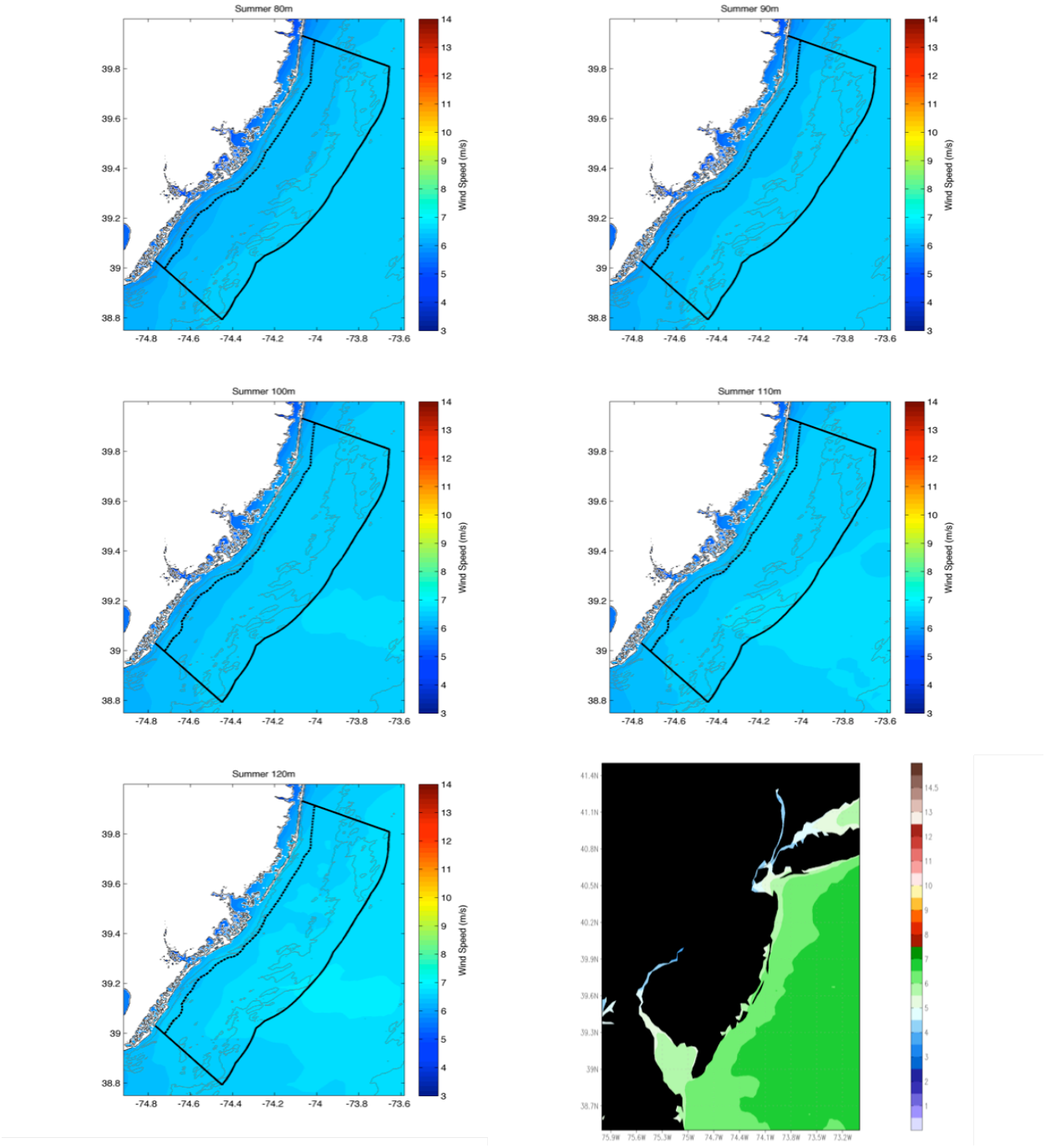

Figure 31: Summer average wind speed at (a) 80m, (b) 90m, (c) 100m, (d) 110m, (e) 120m, and (f) 100m (zoomed out).

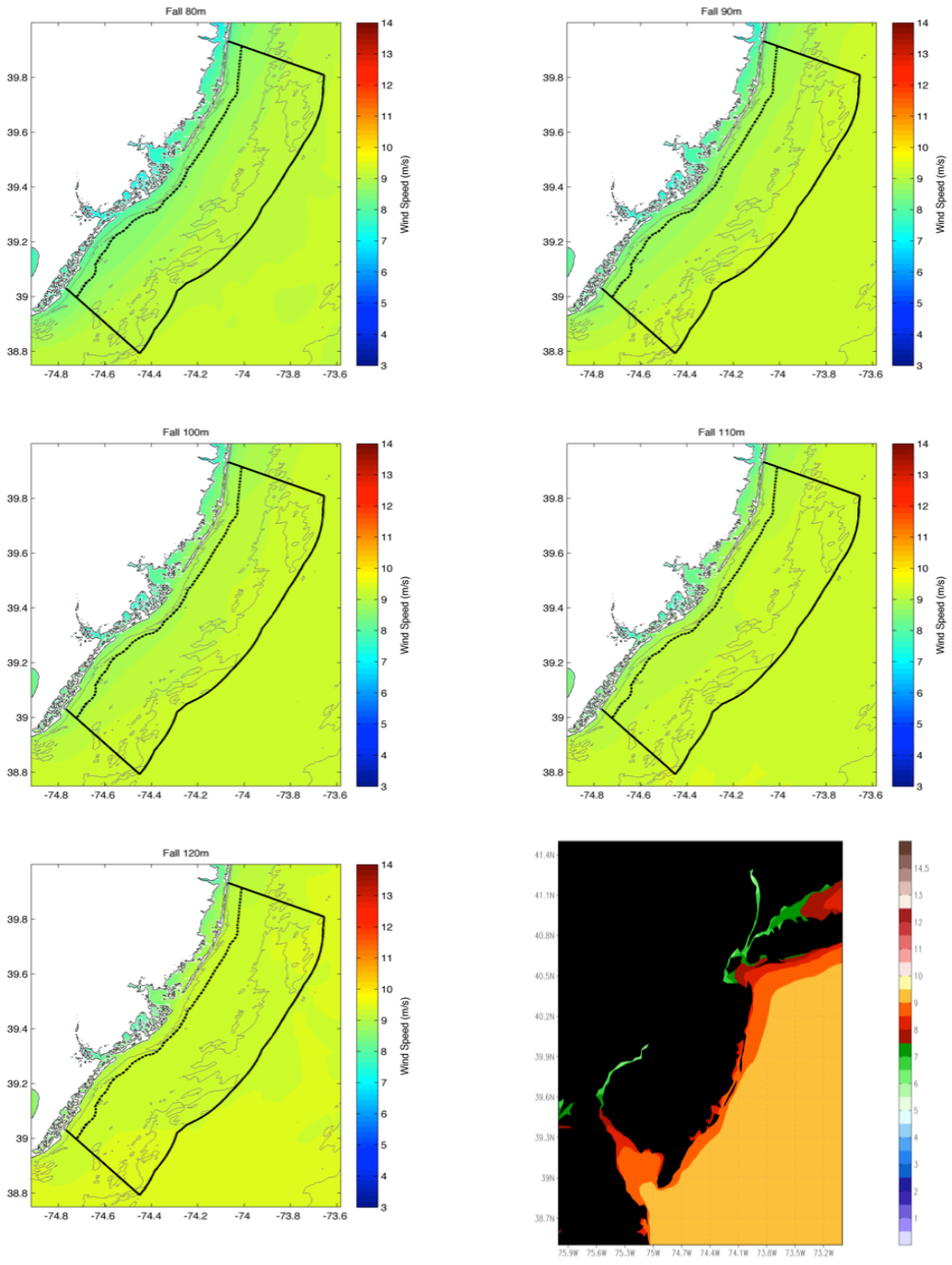

Figure 32: Fall average wind speed at (a) 80m, (b) 90m, (c) 100m, (d) 110m, (e) 120m, and (f) 100m (zoomed out).

4.4.3 Monthly Coastal/Offshore Wind Resource Maps

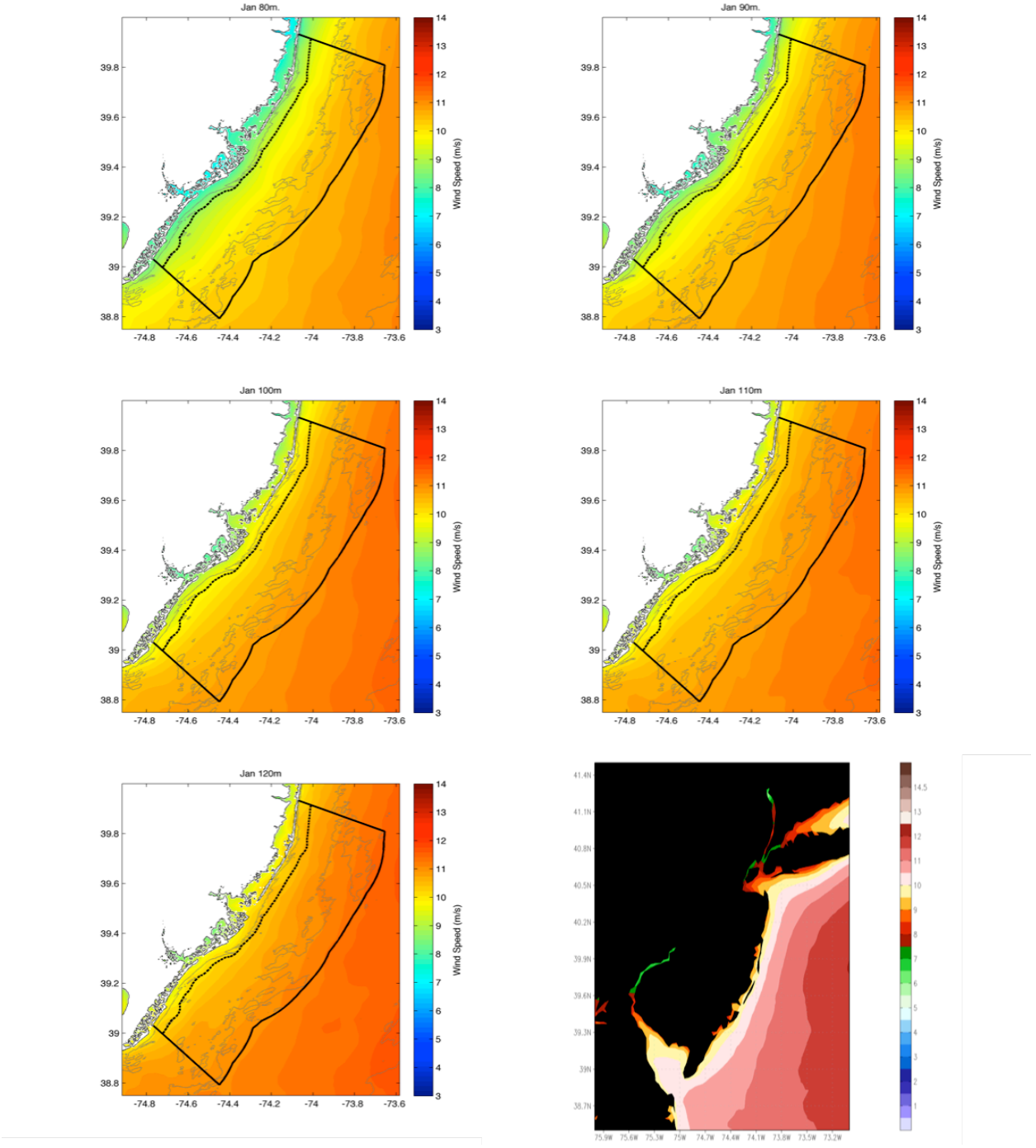

Figure 33: January average wind speed at (a) 80m, (b) 90m, (c) 100m, (d) 110m, (e) 120m, and (f) 100m (zoomed out).

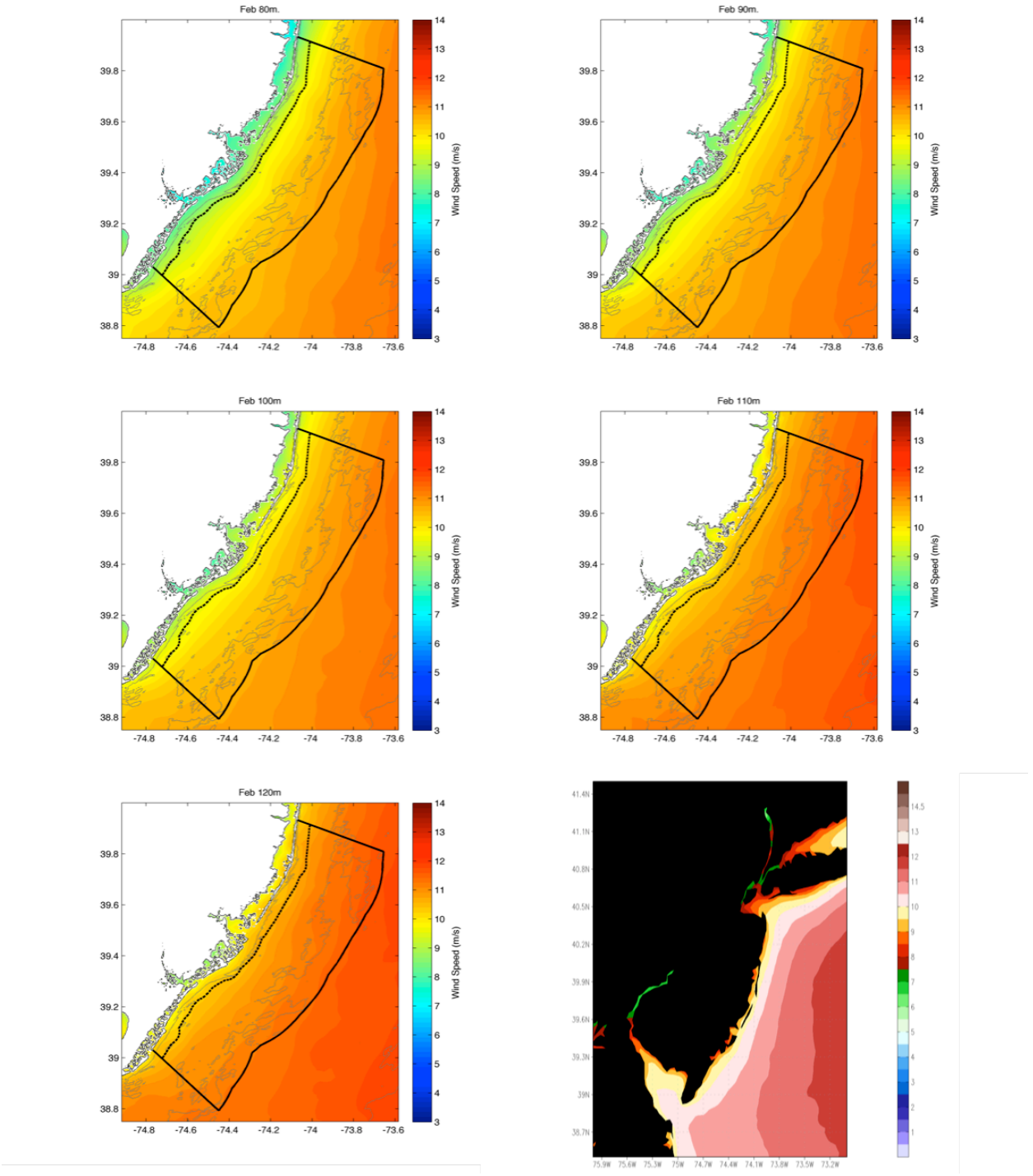

Figure 34: February average wind speed at (a) 80m, (b) 90m, (c) 100m, (d) 110m, (e) 120m, and (f) 100m (zoomed out).

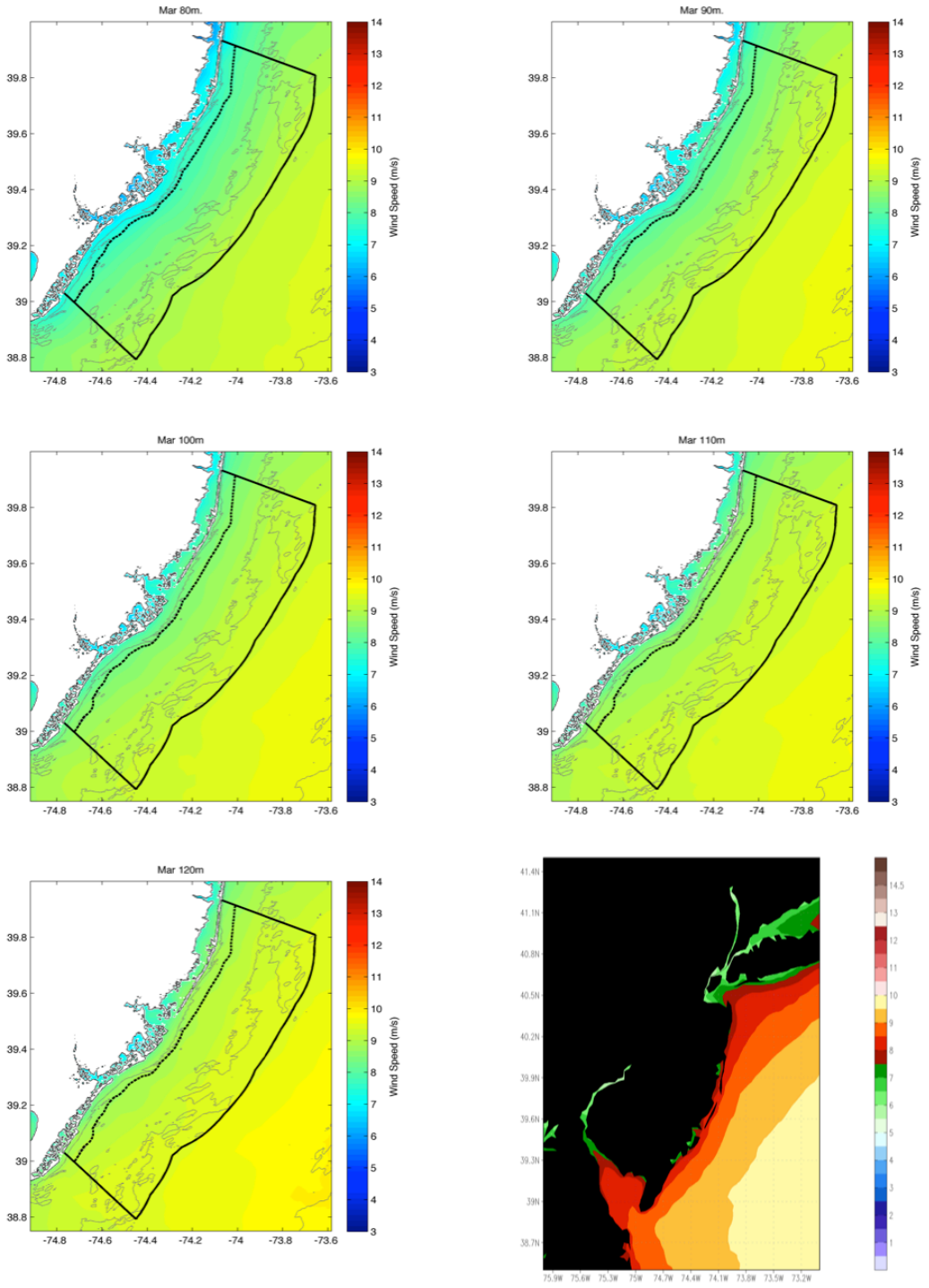

Figure 35: March average wind speed at (a) 80m, (b) 90m, (c) 100m, (d) 110m, (e) 120m, and (f) 100m (zoomed out).

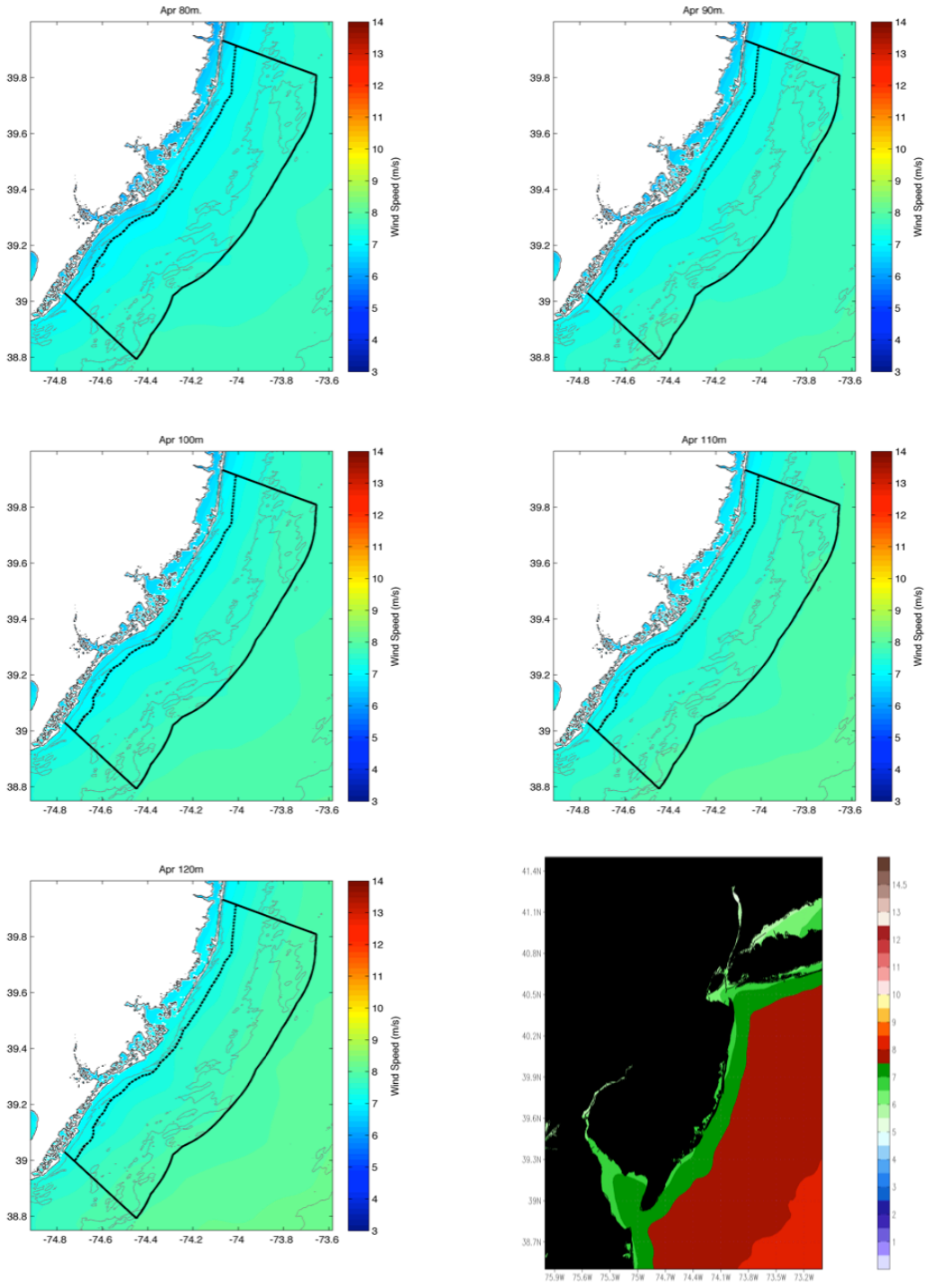

Figure 36: April average wind speed at (a) 80m, (b) 90m, (c) 100m, (d) 110m, (e) 120m, and (f) 100m (zoomed out).

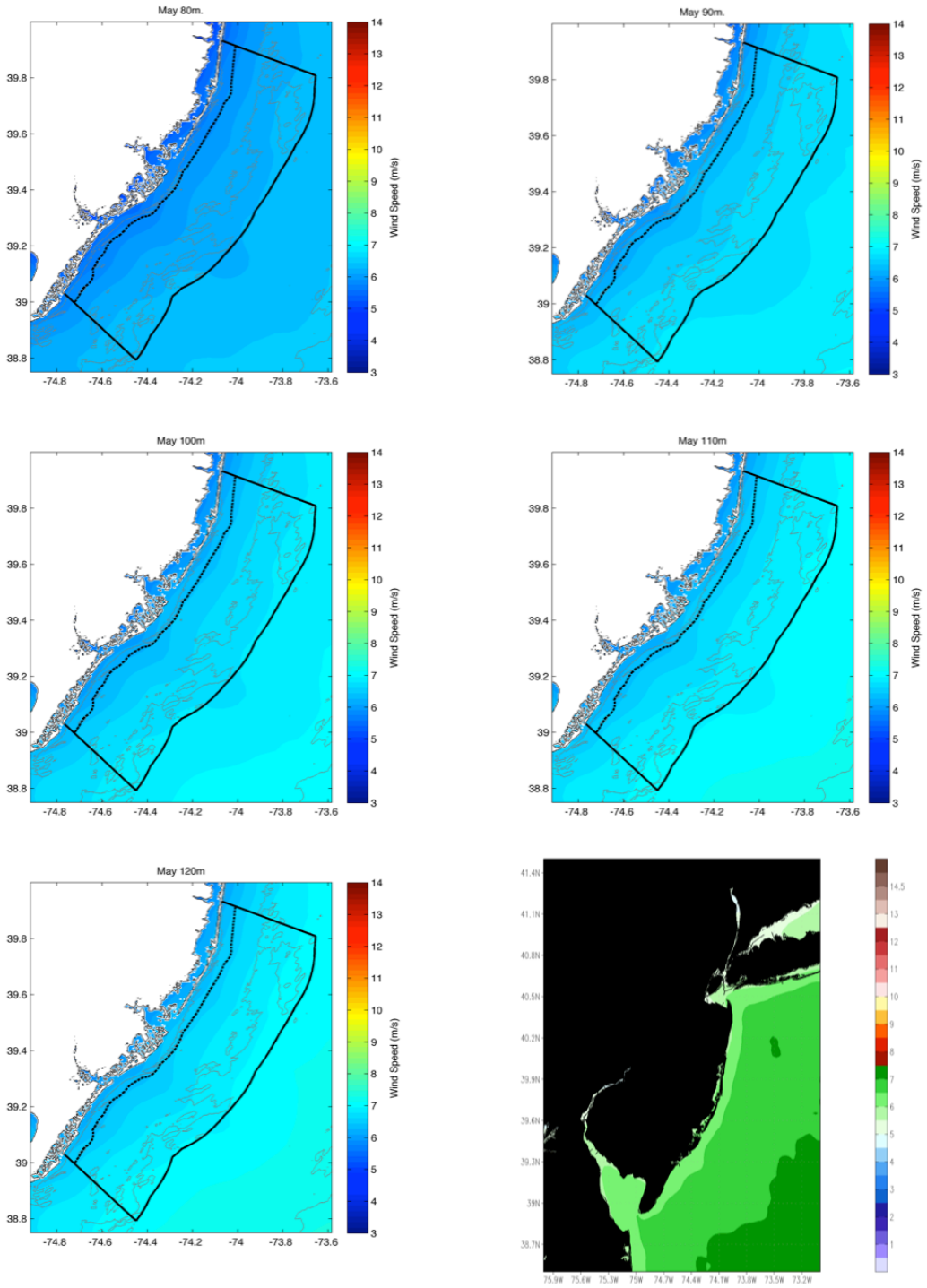

Figure 37: May average wind speed at (a) 80m, (b) 90m, (c) 100m, (d) 110m, (e) 120m, and (f) 100m (zoomed out).

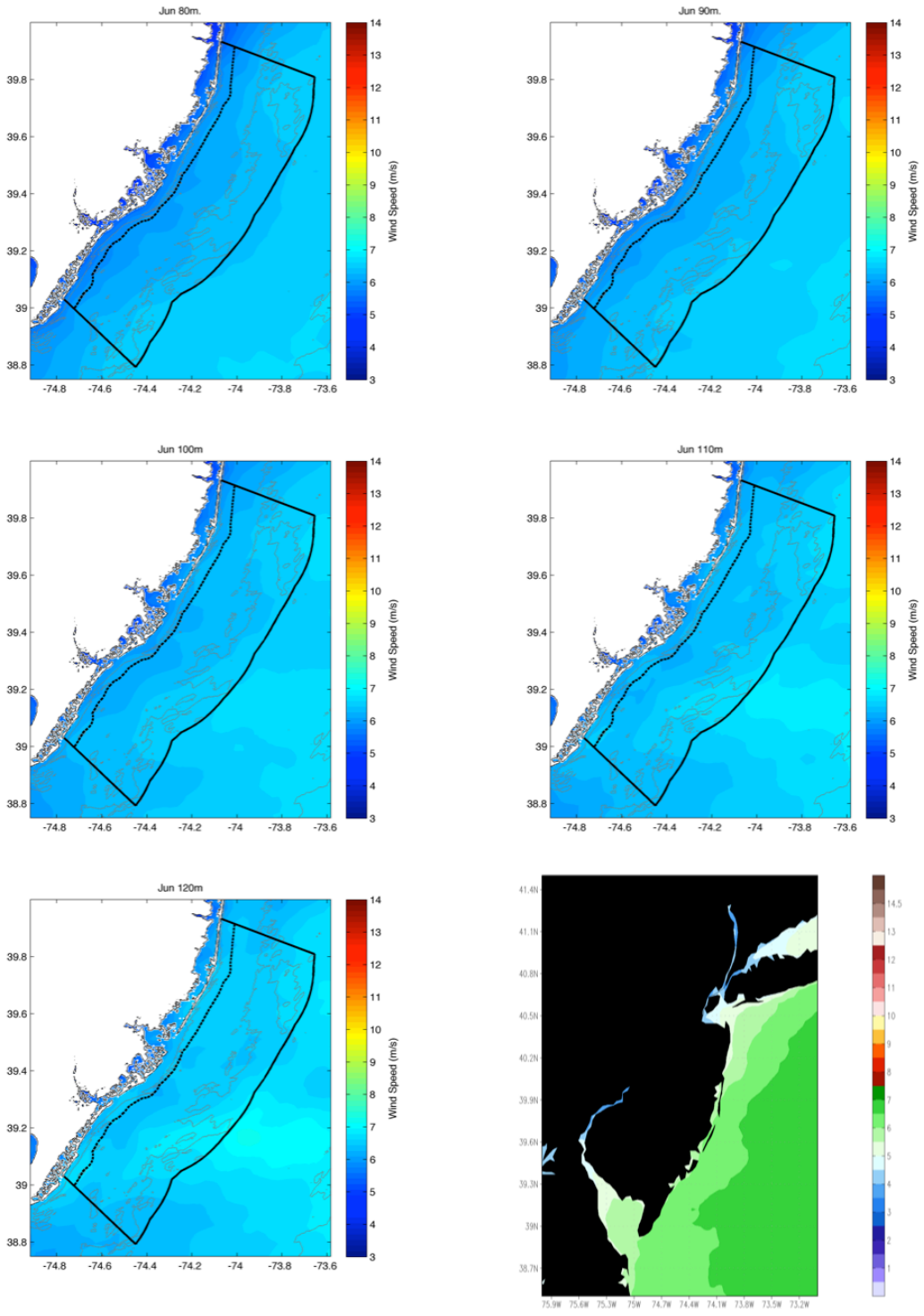

Figure 38: June average wind speed at (a) 80m, (b) 90m, (c) 100m, (d) 110m, (e) 120m, and (f) 100m (zoomed out).

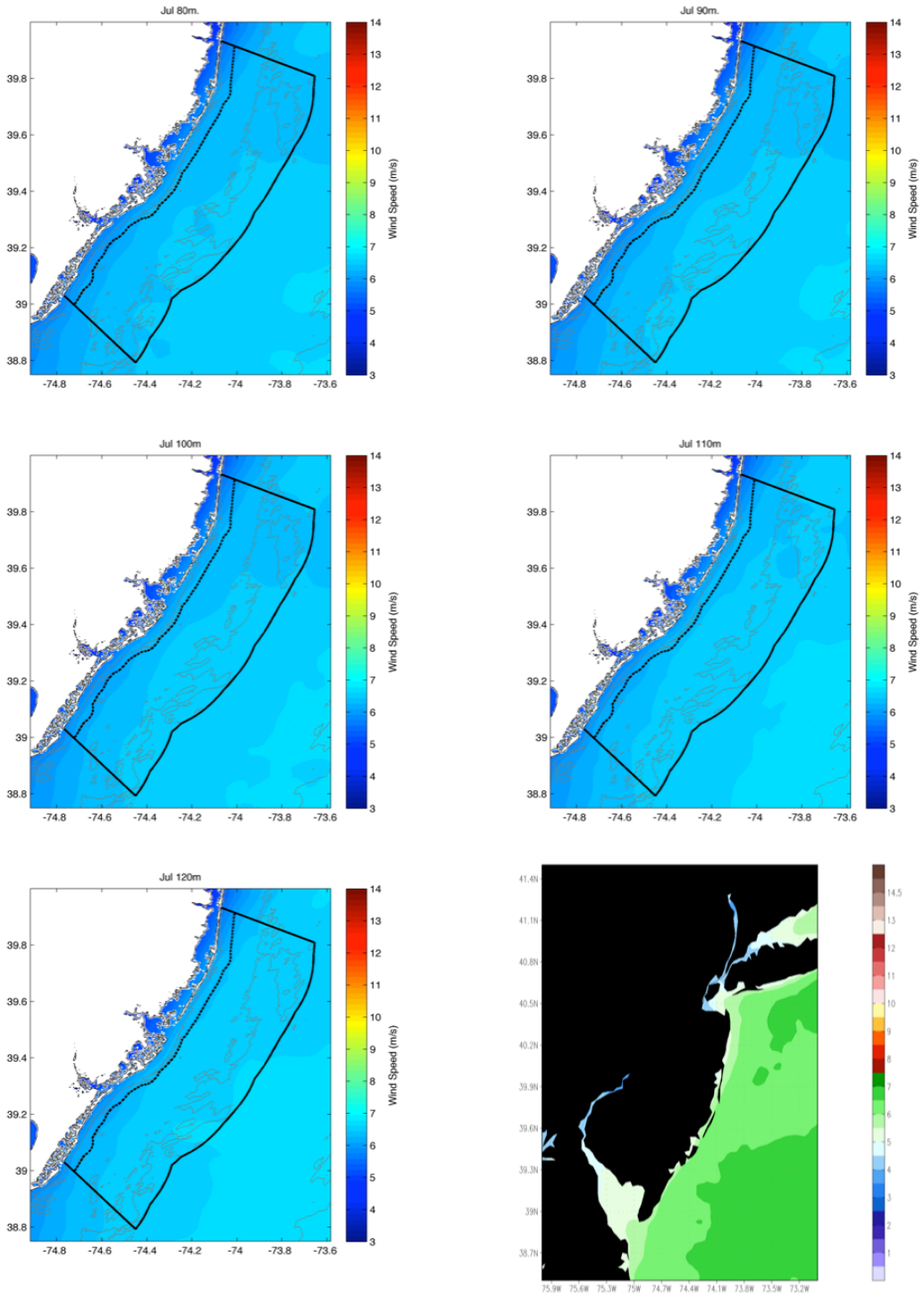

Figure 39: July average wind speed at (a) 80m, (b) 90m, (c) 100m, (d) 110m, (e) 120m, and (f) 100m (zoomed out).

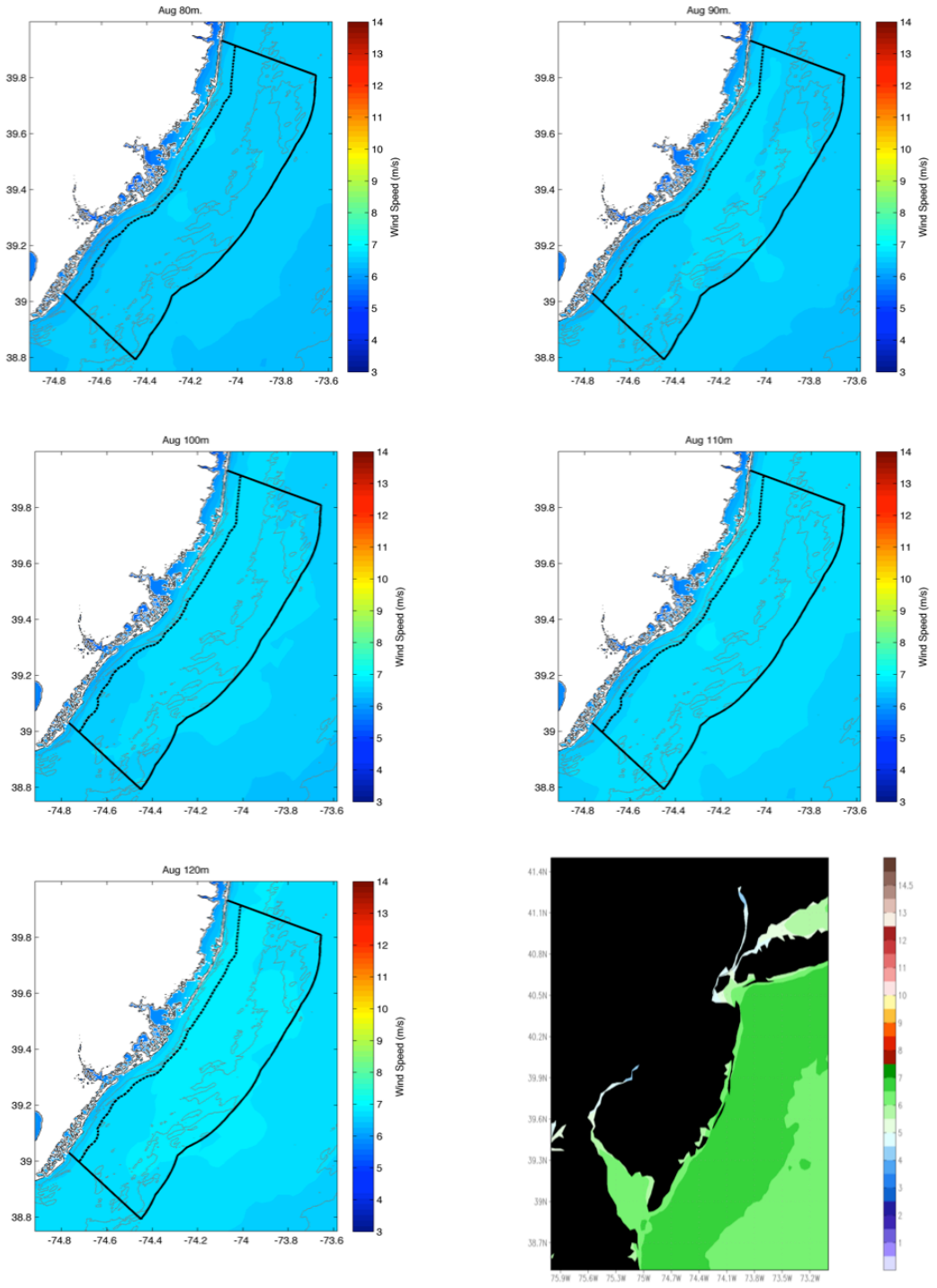

Figure 40: August average wind speed at (a) 80m, (b) 90m, (c) 100m, (d) 110m, (e) 120m, and (f) 100m (zoomed out).

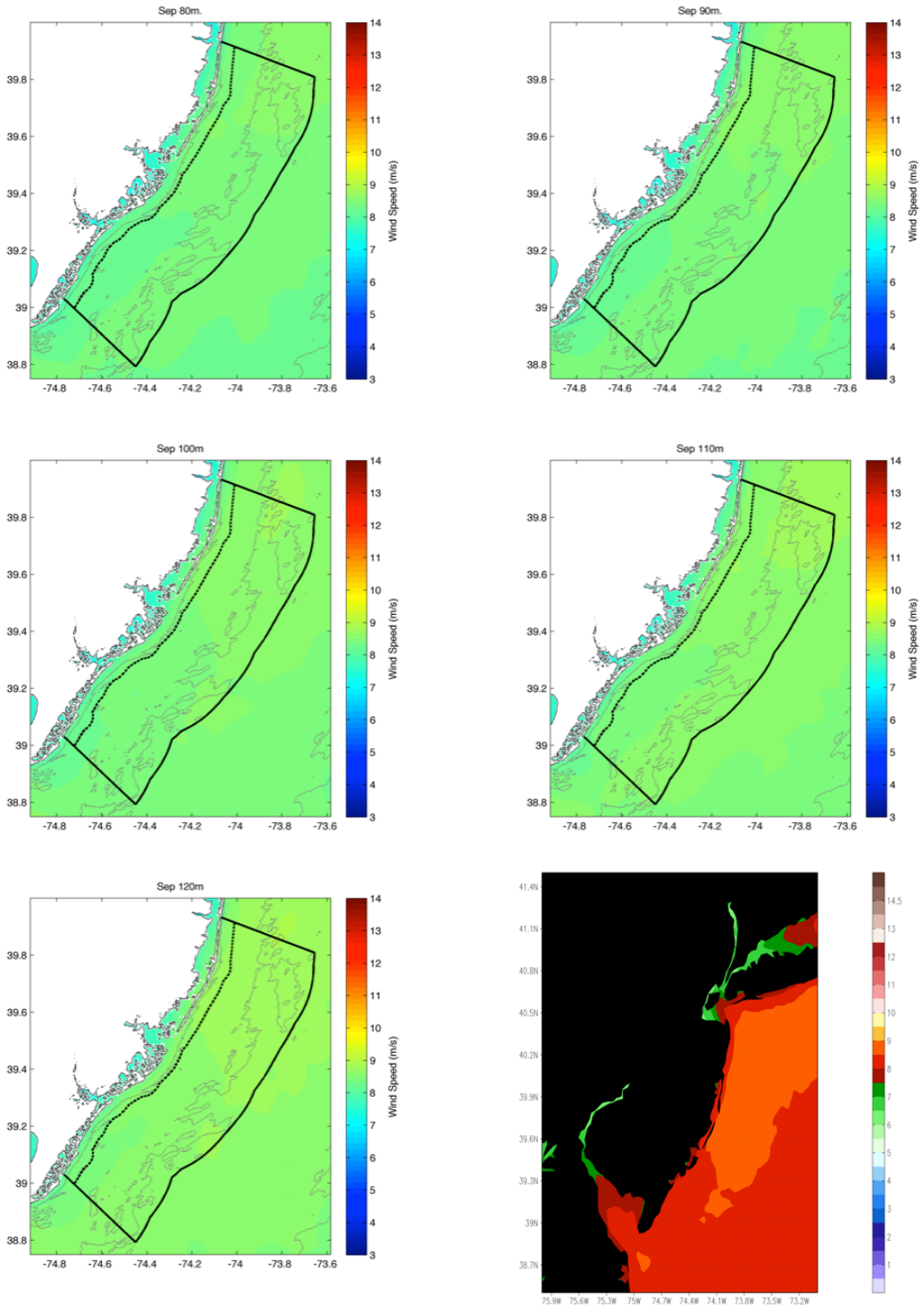

Figure 41: September average wind speed at (a) 80m, (b) 90m, (c) 100m, (d) 110m, (e) 120m, and (f) 100m (zoomed out).

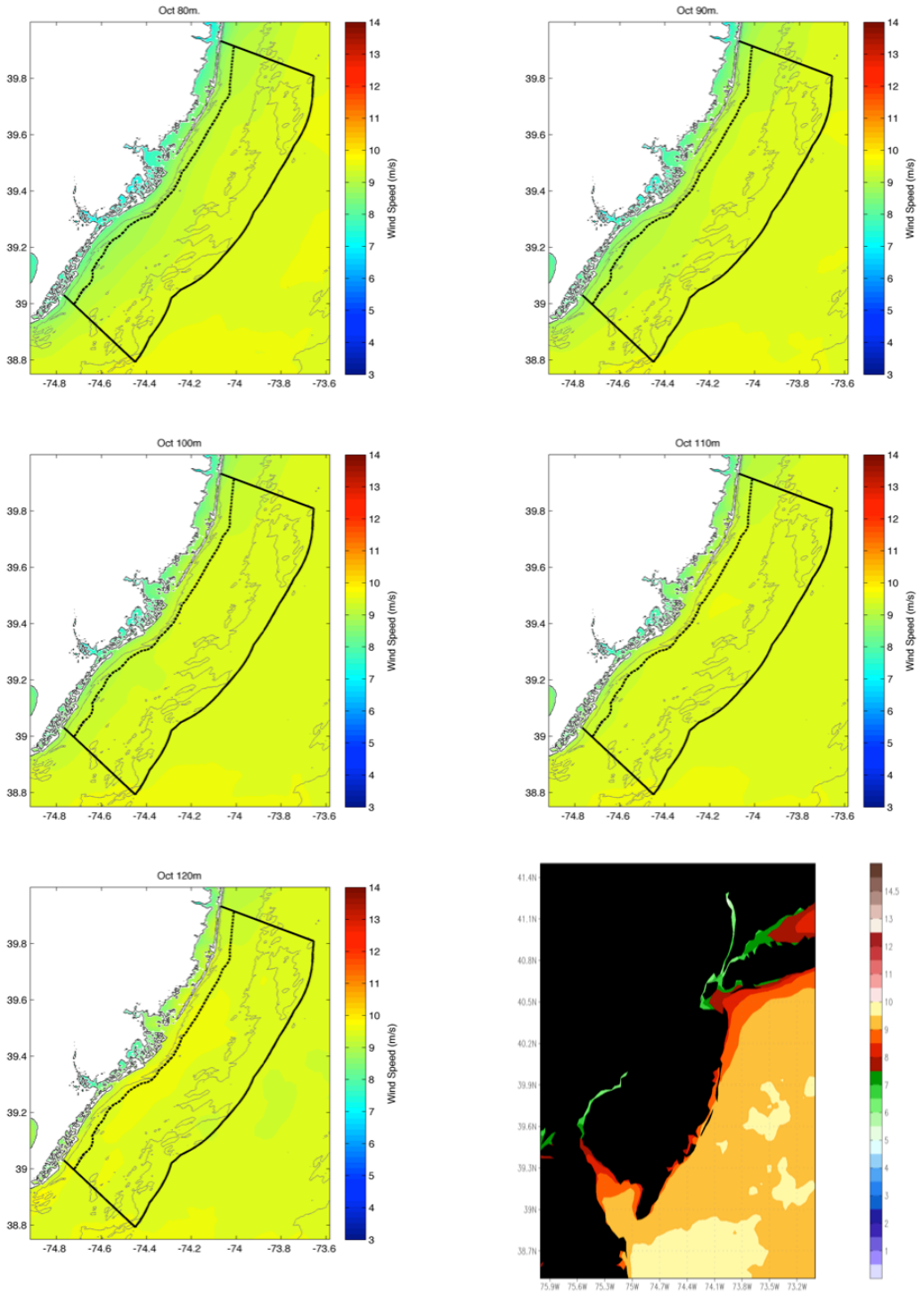

Figure 42: October average wind speed at (a) 80m, (b) 90m, (c) 100m, (d) 110m, (e) 120m, and (f) 100m (zoomed out).

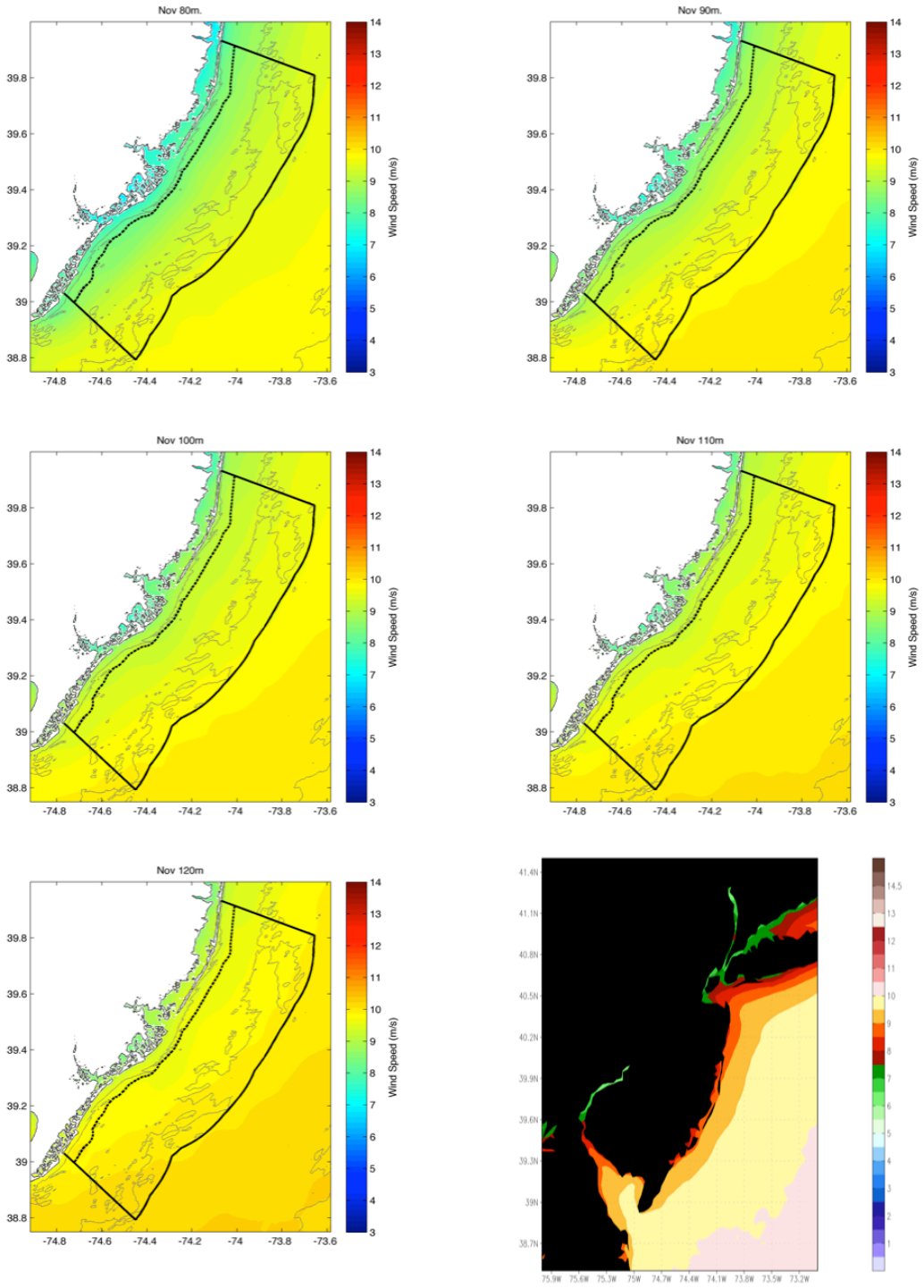

Figure 43: November average wind speed at (a) 80m, (b) 90m, (c) 100m, (d) 110m, (e) 120m, and (f) 100m (zoomed out).

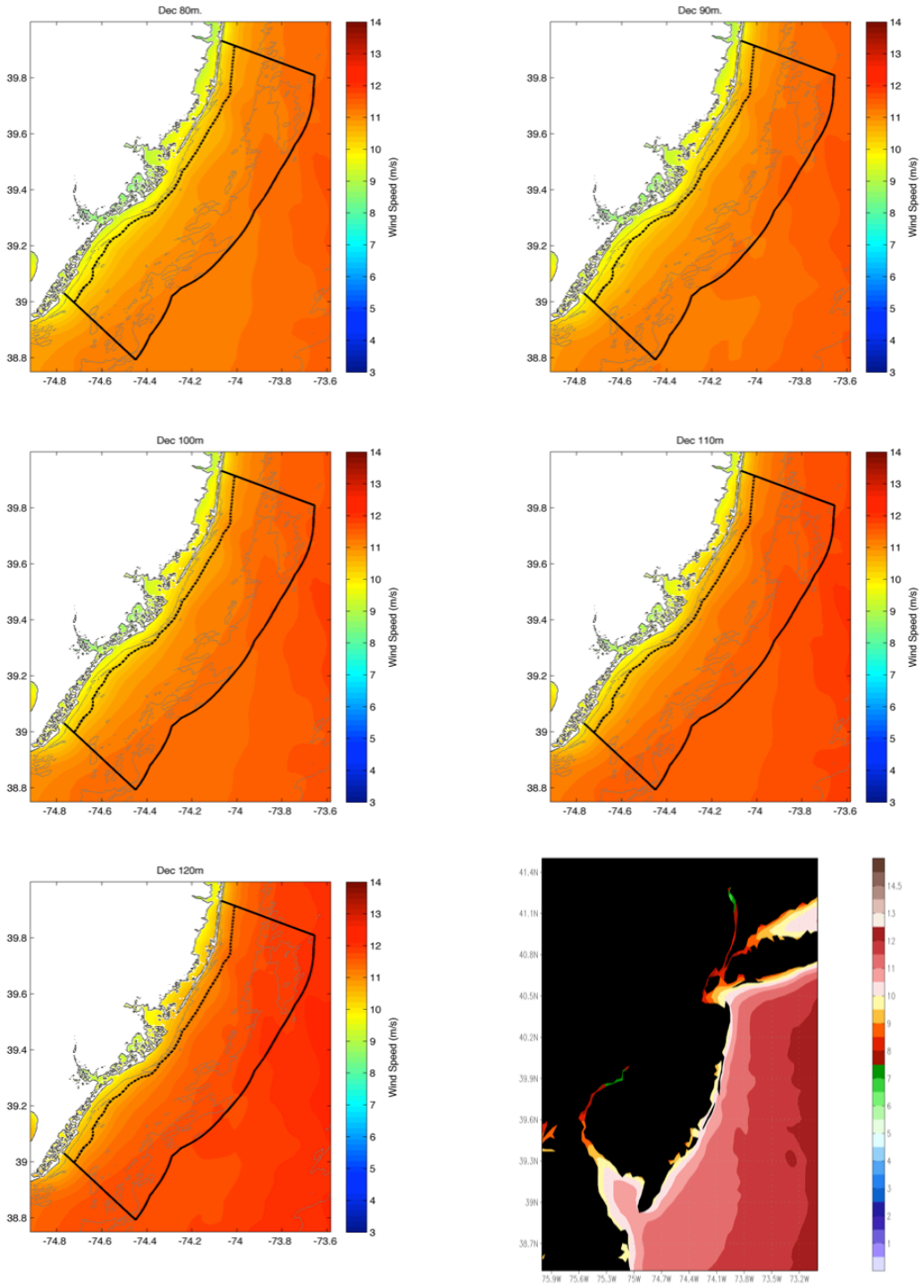

Figure 44: December average wind speed at (a) 80m, (b) 90m, (c) 100m, (d) 110m, (e) 120m, and (f) 100m (zoomed out).

4.5 Offshore Wind Energy Potential

A vital piece of information needed for a wind power project is to determine the frequency of potential energy produced by the wind when the wind is coming from a specific direction. The resultant wind energy rose is a combination of the wind power density (wind speed cubed) and the wind direction/speed frequency that occurs from the various compass sectors. Therefore, the wind energy rose provides a measure of the percentage of potential energy production produced from each wind direction sector.

Based on the wind energy rose analyses along with other siting factors (e.g., turbulence, wind shear, and wind speed variability), WTGs should be placed an adequate distance apart to reduce wake losses, as well as to protect upwind turbines from aerodynamic interference resulting in suboptimal performance and fatigue loading. Protracted extreme loading can degrade the efficiency of the turbine, result in more frequent and costly repairs, and shorten the turbine's lifespan.

The development of an offshore WTG array configuration is a delicate balance of optimizing total energy capacity/power production, turbine efficiency, and installing as many turbines that are determined to be cost-effective for the project design. Onshore wind turbines are typically spaced between 3.5-5 rotor diameters (RD) apart in low wind energy sectors, and 8-10 RD in the predominant wind sectors. Wake from upwind turbines results in wind speed deficits that persist in the downwind direction to at least 8-10 RD as being dependent on ambient turbulence. Turbulence acts to entrain non-perturbated air from outside of the wake-impacted region, thus allowing for a more rapid wind speed recovery. In low turbulence conditions, the wake impact will continue farther downwind than it would be in a more turbulent environment.

The offshore environment is generally found to have very low turbulence due to the lack of surface roughness that would perturb the wind flow. Turbulence is likely to increase in the early stage of sea breeze development, as well as during periods of offshore winds closer to the shoreline. This discussion assumes somewhat higher turbulence downwind from the coastline (W to E) and during the formative stages of sea breeze development (E to W). To minimize wake losses, fatigue loading, and extend the turbine lifespan, a spacing of at least 5 RD is recommended in low energy directions, and 20 RD in predominant wind energy directions.

The offshore wind energy roses produced for NJ's coastal and offshore areas show a bimodal energy distribution. The predominant wind direction is from the SSW along with a significant wind energy contribution from the WNW sector. The ideal turbine layout orientation associated with NJ's offshore wind energy rose distribution would be either WSW to ENE (especially, southern NJ) or NNW to SSE (especially, central NJ). These orientations provide the least wake impact on downwind WTG arrays. NJ's offshore wind energy roses are presented on the proceeding page.

A realistic wind energy capacity/wind power production estimate is needed to determine the wind power production density for both a specific WTG site along with an entire area (e.g., NJ's coastal/offshore waters) to decide whether or not the site (area) is viable for cost-effective wind energy development. An annual wind power production density analysis for NJ's offshore wind energy development, which is based on the annual wind resource analysis for each offshore virtual meteorological tower, is presented on the page following the wind energy rose diagrams.

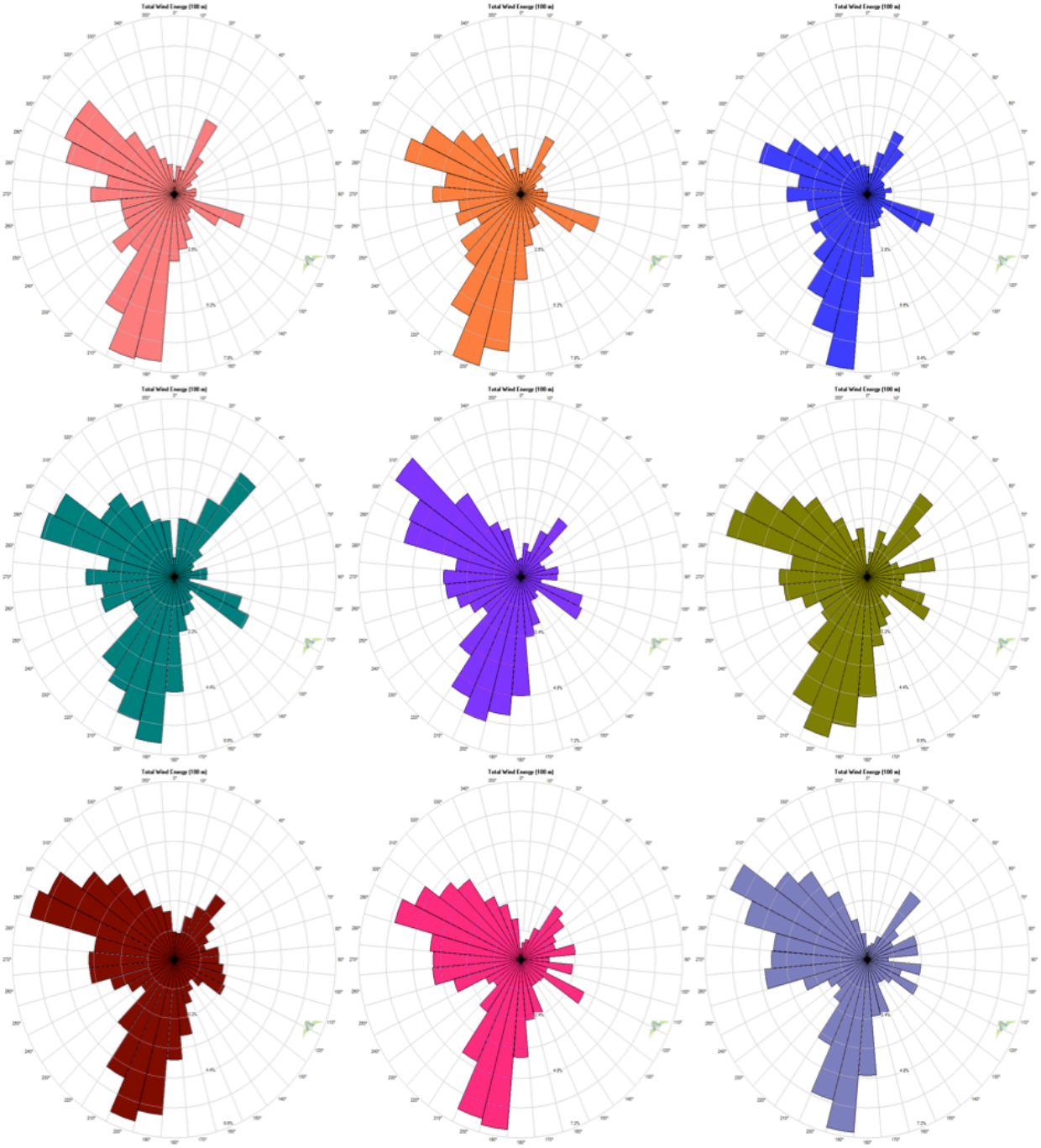

Figure 45: Wind energy rose at Virtual Met Tower (a) A3, (b) B3, (c) C3, (d) D3, (e) E3, (f) F3, (g) G3, (h) H3, and (i) I3.

4.5.1 Annual Average Maps: 90m Wind Speed and 100m Wind Power Density. Objective 4 of the proposal states that optimum offshore wind resource areas will be determined. While monthly and seasonal wind resource maps have been created and presented above, the annual mean wind resource map at 90m is presented in Figure 46.

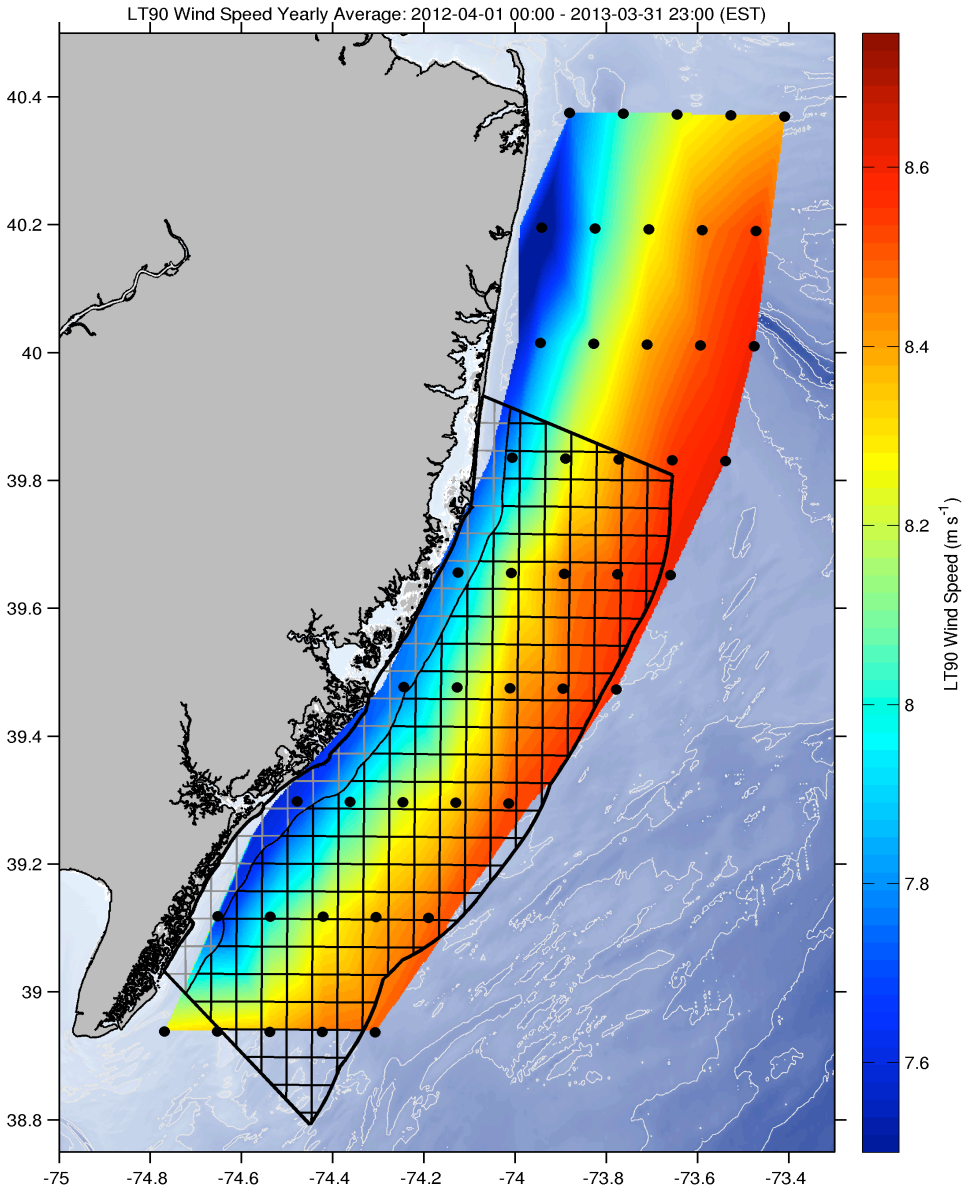

Figure 46. Annual average wind speed (m/s) at 90m.

This compares well to the National Renewable Energy Laboratory (NREL) annual wind resource map produced by AWS TruePower. Inshore locations have an annual average wind speed at 90m of about 7.5 m/s, which is near NREL's inshore values of 7.5-8.5 m/s near shore of NJ. Farther offshore, values increase to about 8.5 m/s, matching well with NREL's values of 8.5-9.0 m/s farther offshore (about 12-50 nm offshore).

Objective 6 of the project proposal states that locations will be determined which can support an additional 2000 MW above the currently proposed 1000 MW wind energy generating capacity. Figure 47 below shows a map of annual average wind power density (W m^{-2}). Values range from about 550 W m^{-2} along the coast to about 750-800 W m^{-2} farther offshore. If a mean wind power density of 700 W m^{-2} is used as a basis for calculations of potential generating capacity, then it would take only 4.29 km^2 of offshore water to produce 3000 MW. This area is less than 0.1% of the entire 2010 NJ DEP EBS study area (outlined in black in Figure 47). Furthermore, 4.29 km^2 is equal to about 55% of the area of one U.S. Outer Continental Shelf (OCS) Lease Block (black grid cell in Figure 47). Of course, this does not take into account necessary spacing of each wind turbine across the study area, to avoid turbulent wake effects. This would significantly expand the area needed to produce 3000 MW of generating capacity.

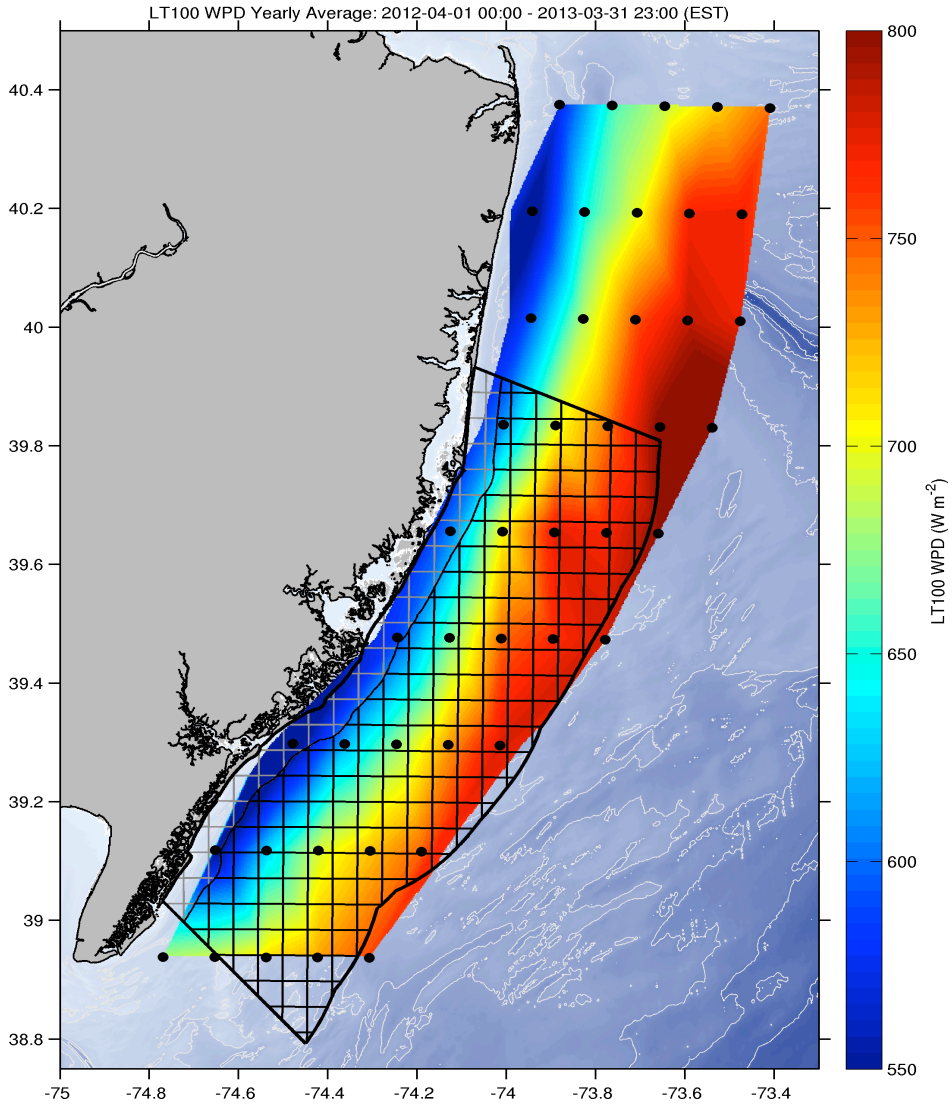

Figure 47. Annual average wind power density (W m^{-2}) at 100m.

4.6 Site Suitability

The determination of site suitability is a crucial step in the development of a wind power project. The turbine manufacturer must run an aerodynamic load model with which to determine whether the turbine design specifications are a suitable fit for the site-specific wind climate of the proposed location. The various wind characteristic studied include *wind shear, extreme winds, turbulence,* and *inflow angle*. The extreme wind analysis includes a discussion of two important storms that occurred in the recent past, Irene (2011) and Sandy (2012), and how these storms fit into the historical record and the implications for the survivability and operation of wind plants offshore of New Jersey.

4.6.1 Offshore Wind Shear Analysis. Wind shear is an important variable in determining the long-term hub height wind speed. Wind shear **(α)** is determined by the equation:

$$\alpha = \{\ln(V_2/V_1)\}/\{\ln(Z_2/Z_1)\}$$

Where,

$\mathbf{V_2}$ and $\mathbf{Z_2}$ are the respective higher elevation estimated wind speed (m/s); selected upper level height (m).

$\mathbf{V_1}$ and $\mathbf{Z_1}$ are the respective lower elevation monitored wind speed (m/s); measurement height (m).

Wind shear is generally used to estimate winds at heights higher than those measured using a traditional 10m meteorological tower. However, since data are extracted at the model elevation levels of interest, the wind shear can be directly calculated between potential hub heights and heights associated with WTG blade dimensions. The following images portray estimated annual average wind shear above NJ's coastal/offshore waters.

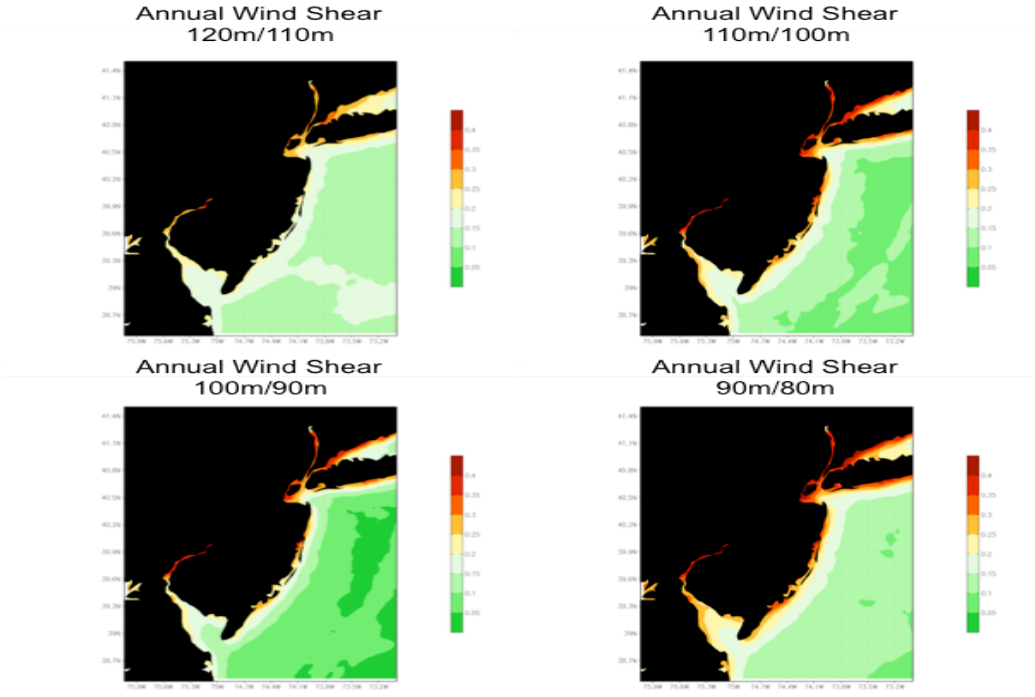

Figure 48: Annual average wind shear between (a) Upper left, 120m and 110m (b) upper right, 110m and 100m (c) lower left, 100m and 90m (d) lower right, 90m and 80m.

The wind shear values determined in this analysis are higher off the coast of NJ than the lower offshore wind shear values seen in most offshore wind energy studies. Wind shear values derived for NJ's offshore wind resource reach a maximum value of approximately 0.2 immediately offshore. This high shear value is probably due to the transition in surface roughness from the relatively smooth ocean surface to the varying terrestrial features over associated inland areas. Shear values are generally highest during the summer months due to sea breeze development and convective activity as is shown in Figure 49 (a) that shows monthly wind shear values for virtual meteorological tower C3, which is approximately 15km east of Atlantic City. Figure 49 (b) shows the diurnal wind shear profile at C3 averaged over an annual period. Figure 49 (c) shows the wind shear value by wind direction at C3. Wind shear is highest when winds are coming from the west-southwest sector, which is the direction of a concave and sheltered portion of the coastline from Avalon to Atlantic City.

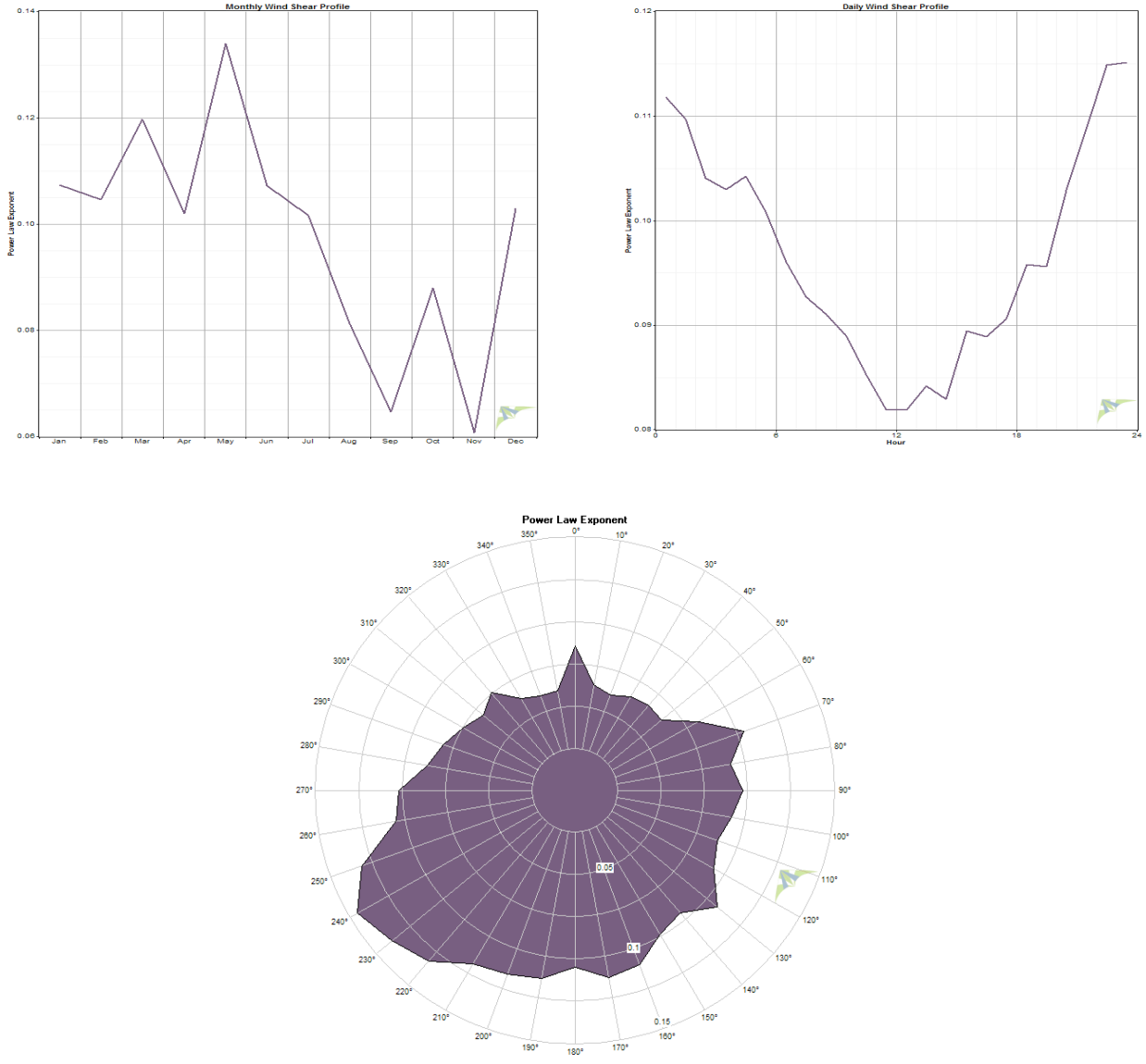

Figure 49: Virtual meteorological tower C3: (a) upper left, monthly wind shear; (b) upper right, diurnal wind shear; (c) lower left, wind shear by direction (winds coming from the designated direction).

4.6.2 Offshore Extreme Wind Analysis and Turbulence Intensity Evaluation. An important aspect in the determination of the suitability of a wind park to be located within the marine environment is an extreme wind analysis along with an evaluation of the turbulence intensity that can be expected at the designated site. The International Electrotechnical Commission (IEC) has established design standards (61400-1) that can be used to determine if a specific WTG is suitable for the selected site. The IEC standards provide criteria that determine the structural integrity of the WTG during extreme wind loading conditions and associated turbulence intensity. The IEC established a classification scale for WTGs that ranges from Class I (high wind speed) to Class III (low wind speed). This classification scheme is further subdivided into three distinct wind speed categories: average wind speed, extreme 50-year reference wind speed (V_{ref}), and extreme wind gust (V_{gust50}) (Manwell et al., 2009). These wind classifications are also dependent on the average annual turbulence intensity (TI) values at the established (reference) wind speed value. Turbulence intensity is used in wind load models for most WTG applications. Turbulence intensity is derived using the following equation:

$$\mathbf{TI = \sigma u / U}$$

Where,

TI is turbulence intensity (%).
σu is the 10 minute standard deviation of the horizontal wind speed (m/s).
U is the average 10 minute wind speed (m/s).

The IEC wind/turbulence classification criteria are presented in **Table 6.**

Table 6. IEC wind turbine class and subclass specifications.

Class		I	II	III	S
Vavg	m/s	10	8.5	7.5	
V_{ref}	m/s	50	42.5	37.5	Specific
V_{gust50}	m/s	70	59.5	52.5	Design
A	TI	0.16			Criteria
B	TI	0.14			
C	TI	0.12			

The vast majority of offshore wind projects utilize Class I turbines, as these allow an average annual wind speed of 10 m/s, a V_{ref} of 50 m/s, and V_{gust50} of 70 m/s. A Class II turbine is rated for an average wind speed of 8.5 m/s, V_{ref} of 42.5 m/s and V_{gust50} of 59.5 m/s.

Offshore Extreme Wind Analysis: The East Coast of the United States is susceptible to Tropical Cyclones during the summer and autumn months. The State of New Jersey is relatively protected from a direct strike from a hurricane due to its position within the concave coast of the

New York Bight, and due to the natural tendency of tropical systems to accelerate to the north and east as they enter the mid-latitudes. The eastern side of a hurricane generally contains the strongest and sustained high winds, thus the coastal areas are rarely impacted by true hurricane conditions. Studies conducted by the National Hurricane Center have shown that the return period for any hurricane (> 33 m/s, 74 mph) passing within 65 nautical miles of the New Jersey coast (considered a hurricane strike) is 18 years (Figure 50a, and the return period of a major hurricane (> 50 m/s, 111 mph) is 76 years (Figure 50b).

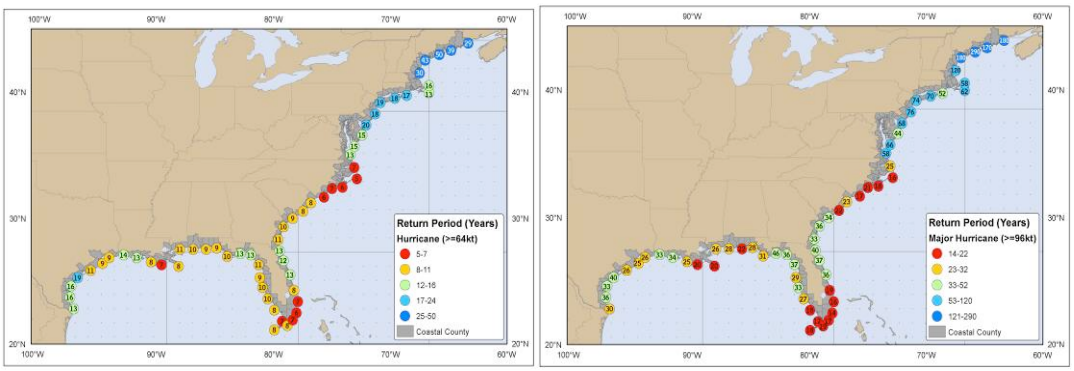

Figure 50: (a) Hurricane and (b) Major Hurricane Return Period (years) from the National Hurricane Center.

The period from 1900-2010 has been determined by the National Hurricane Center to have 5 hurricanes (Gloria 1984, Belle 1976, Donna 1960, 1944, and 1903) passing within 65 nm of the New Jersey coast. Only the 1903 storm directly struck the NJ coast; however, this storm's intensity rapidly decreased to a tropical storm.

In 2011 and 2012, Hurricanes Irene and Sandy respectively made a direct landfall along the NJ shoreline. While these storms have been determined not to be an official hurricane at the time of landfall, the damage that occurred on land, and the wind conditions offshore, were consistent with that of a hurricane. While it is unusual to have consecutive years with nearby hurricanes, 1893 and 1894 had hurricanes passing close to shore.

The hurricane of record occurred in 1821, when a hurricane estimated to have an intensity of 55-65 m/s made a direct landfall at Cape May (Ludlam, 1963). A study of sediment along the New Jersey shoreline distinctly shows the intensity of the storm surge from the 1821 hurricane, as well as indicating a storm of similar (or greater) intensity occurring between 1278 and 1438 (Donnelly, et al., 2001).

The lack of tall tower data presents a challenge in both the estimation of the wind resource, as well as estimation of extreme winds at hub height. The standard in the wind energy industry is to determine an extreme wind speed for a return period of 50 years. This analysis is done through the use of a best-fit Gumbel distribution. A Gumbel distribution is most reliable when utilizing several years of data. As this study focused on a one-year period, this dataset alone is not sufficient to properly determine the extreme wind risk for an offshore wind project. To remedy this problem, a Gumbel distribution using ten years of data from the Delaware Bay Buoy (44009) was used, which was then scaled to 100 m hub height using the wind shear calculated during the current study.

During the period of Jan 2003 to Dec 2012, the average wind speed at the 5 m measurement height at the buoy was 6.31 m/s. For observed conditions at the buoy, V_{ref} = 25.2 m/s, and V_{gust5} = 33.2 m/s.

Table 7. Extreme wind analysis at Delaware Bay Buoy (44009) at 5 m.

Return Period (yr)	V_{ref} (m/s)	V_{gust50} (m/s)
20	23.8	31.1
25	24.1	31.6
50	25.2	33.2
100	26.3	34.7

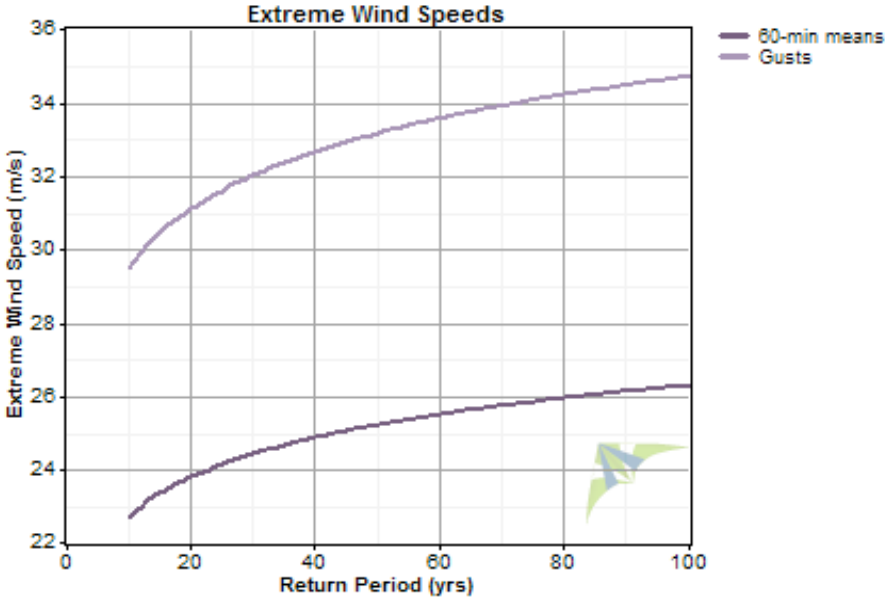

Figure 51: Extreme wind analysis at Delaware Bay Buoy (44009) at 5 m.

The RU-WRF model calculated wind shear at the Delaware Bay Buoy location was 0.10. The 100 m hub height wind speed at the buoy using the power law is 8.51 m/s. When the 5 m wind speed at the Delaware Bay Buoy is adjusted to hub height, V_{ref} = 34.0 m/s and V_{gust5} = 44.7 m/s.

Table 8. Extreme Wind Analysis at Delaware Bay Buoy (44009) at 100 m using modeled wind shear of 0.10.

Return Period (yr)	V_{ref} (m/s)	V_{gust50} (m/s)
20	32.1	42
25	32.6	42.6
50	34	44.7
100	35.5	46.8

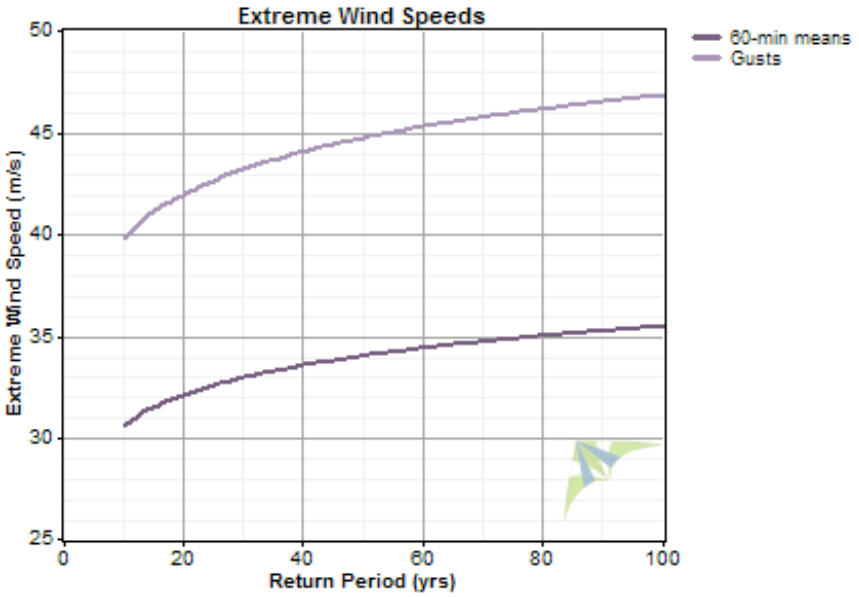

Figure 52: Extreme wind analysis at Delaware Bay Buoy (44009) at 100 m using modeled wind shear of 0.10.

While this assumption for wind speed is adequate, the assumption for wind gust is likely conservative as the ratio of wind gust to wind speed decreases with height as the wind becomes less turbulent above the surface. Given the lack of measured conditions above the surface, this conservative analysis for V_{gust50} is justifiable.

The time period studied for this extreme wind analysis includes Irene and Sandy. While neither storm was technically a hurricane at landfall, Sandy should be considered to be a representative hurricane event along the NJ coastline.

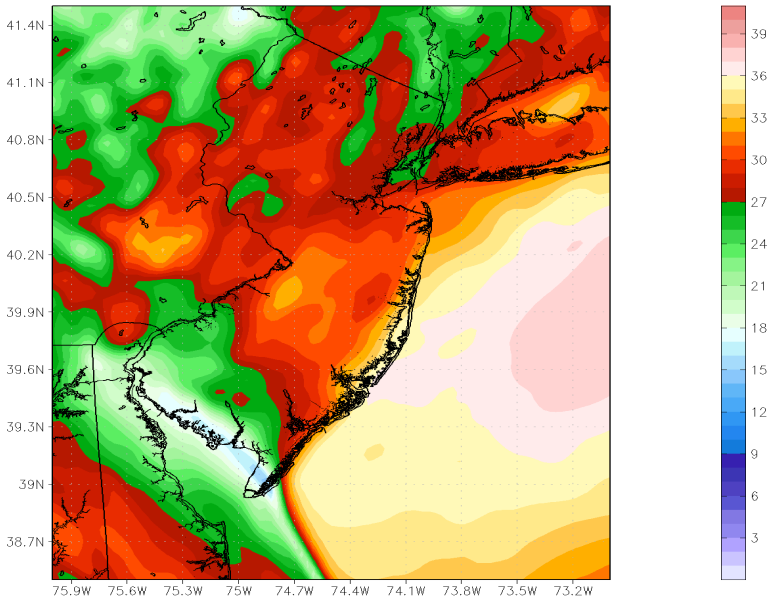

Figure 53: "Superstorm" Sandy 100 m wind speed (m/s) valid October 29, 2012 1800 GMT (operational forecast run 20121028 – 42 hour forecast).

Virtual meteorological tower F5 was modeled to have a 100 m wind speed of 34.69 m/s during the peak of Sandy. Given the similar extreme wind speed estimate at the DE Bay Buoy, coupled with the historical perspective that Sandy was the most destructive storm to strike the area since 1821, the analysis is considered valid for a storm with a 50 to 100 year return period.

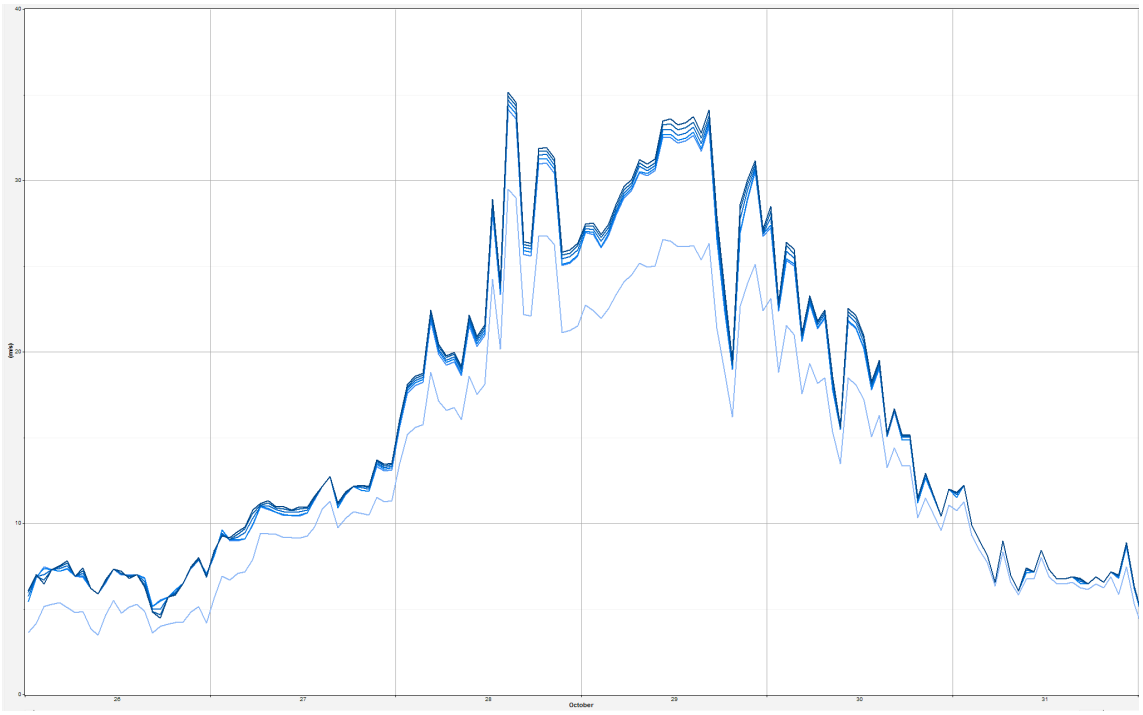

Figure 54: Virtual meteorological tower F5 wind speeds during "Superstorm" Sandy.

Offshore Turbulence Evaluation. Regarding offshore turbulence, classic boundary layer meteorology would suggest that TI values would be quite low over the ocean, as surface roughness is at a minimum except in the instance of high seas. This is likely to be the case offshore of the New Jersey coast, except during sea breeze occurrences. The sea breeze is a mesoscale phenomenon that has significant turbulence along the sea breeze front, the boundary at which the onshore flowing marine air converges with the offshore flowing larger scale wind. This convergence results in rising motion and the development of small-scale turbulent eddies that advect onshore with the propagating sea breeze front. While the sea breeze front and adjacent areas are highly turbulent, the region embedded within the sea breeze circulation will generally have low turbulence due to highly stable marine air (Briere, 1987).

The sea breeze along the NJ coast has been shown to develop offshore, and then penetrate inland against the larger-scale synoptic wind (Bowers, 2004). This onshore flow will subject the study area to a one to two hour period of high wind shear and intense turbulence, which will be followed by low wind shear and minimal turbulence during sea breeze events. These periods of high turbulence are not expected to be of significant concern because they generally occur over a short time period and are accompanied by winds either below or just above threshold wind speeds for most utility scale turbines.

Offshore wind speed and turbulence data detected from remote-sensing systems (e.g., LIDAR) could not be obtained during the time frame of this study. Consequently, we were not able to make a realistic conclusion regarding representative turbulence within the study area.
It is therefore highly recommended that this topic be revisited when the acquisition of robust LIDAR data from the wind developers becomes available.

4.6.3 Offshore Wind Inflow Angle Analysis. Inflow angle, or the vertical variation from the horizon of the wind flow, is an additional parameter that should be taken into account when designing utility scale WTG arrays to be constructed in complex terrain. Vertical wind speeds are generally minimal in the offshore environment, except during brief periods associated with synoptic scale air mass exchange convection, sea breeze frontal propagation, and thunderstorm activity. Therefore, inflow angle is not anticipated to be a primary concern for offshore wind energy development.

4.7 Sea Breeze / Non-Sea Breeze Analysis

4.7.1 Sea Breeze. Local wind perturbations, such as the sea breeze circulation, have a significant influence on the offshore wind resource at temporal and spatial scales compatible to the size of a "typical" offshore wind turbine array. Furthermore, there appears to be much more variability in the offshore wind resource during sea breeze occurrences when compared to "normal" synoptic flow situations. The sea breeze is driven by the thermal difference between the warm land and relatively cooler ocean and, under weak atmospheric boundary layer wind conditions, can affect much of the state along with a relatively large area offshore that can extend well beyond the area selected for wind energy development. It should be noted that there is minimal information associated with the offshore component of the sea breeze circulation. Therefore, RU-COOL's innovative monitoring and modeling endeavors are focused on investigating the details of the offshore dynamics of the sea breeze circulation and its influence on the offshore wind resource during both coastal upwelling and non-upwelling events.

Since a primary objective of our study is to determine the variability of the offshore wind resource adjacent to NJ's coast, data acquired from recent sea breeze occurrences were used to ascertain the significant variability in the offshore wind resource caused by the sea breeze

circulation when compared to non-sea breeze occurrences. Sea breeze occurrences were identified by analyzing CODAR (Coastal Radar) surface current and wavelet energy transformation data, infrared (IR) satellite SSTs, NOAA Doppler RADAR, and meteorological tower data. These data sets along with RU-WRF model simulations were used to analyze the sea breeze circulation, which frequently occurs during peak energy demand periods associated with "hot" summer days.

An understanding of the temporal and spatial properties of the sea breeze circulation is essential for evaluating offshore wind power production when and where energy is needed. Therefore, sea breeze analyses and predictions will provide the information necessary to effectively evaluate the coincidence associated with offshore wind energy generation, peak electrical power demand, and the potential penetration of offshore wind energy into the power grid.

Examples of high-resolution (0.75 km horizontal grid spacing) model simulations for a sea breeze event affected by coastal upwelling are shown in the simulations presented below for 10 m and 90 m heights above mean sea level.

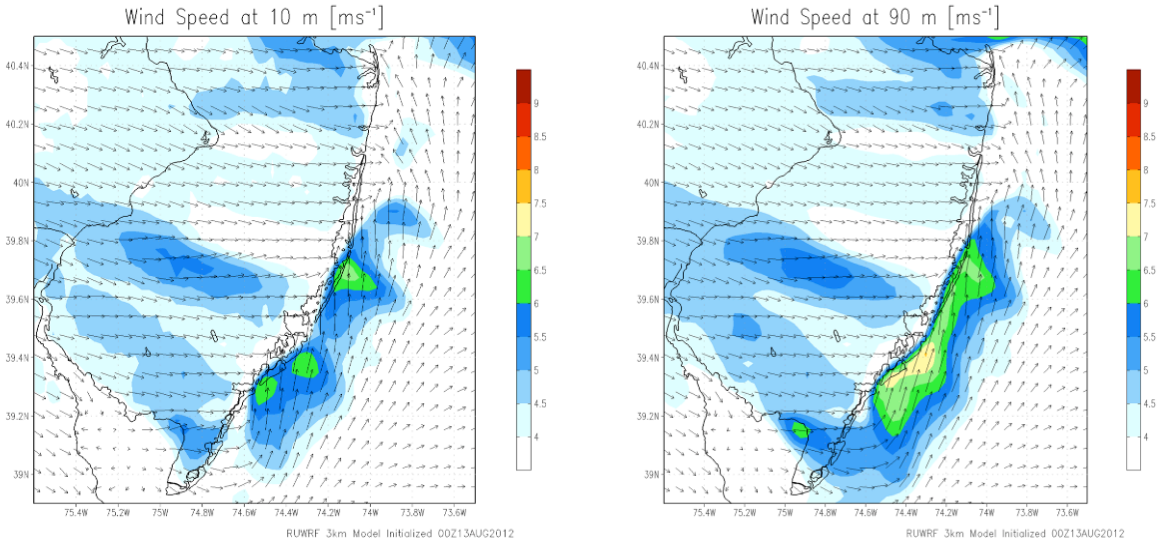

Figure 55: NJ Sea Breeze Circulation Simulations.

The following vertical cross-sectional simulation of the sea breeze circulation and associated sea breeze "front" along with RADAR images that detected the sea breeze front are associated with the same sea breeze/upwelling event presented in the preceding 10 m and 90 m wind resource simulations.

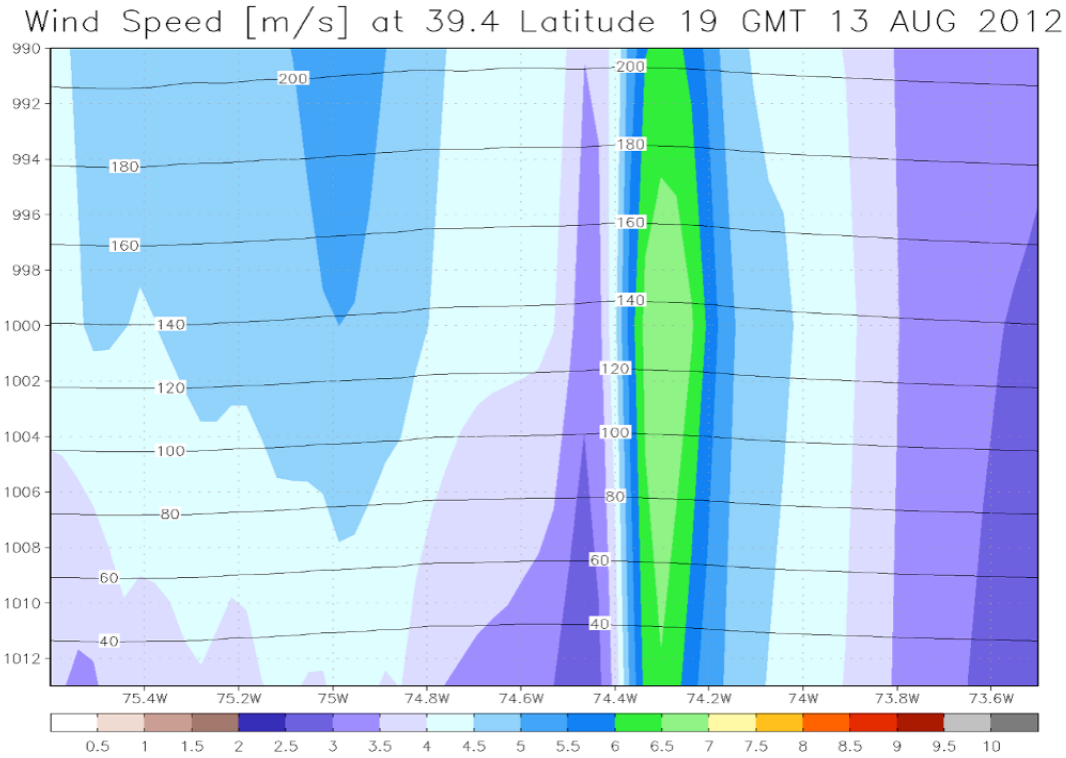

Sea Breeze Front

<Onshore/COASTLINE/Offshore>

Figure 56: Vertical Cross-Section of Onshore and Offshore Components of the Sea Breeze Circulation.

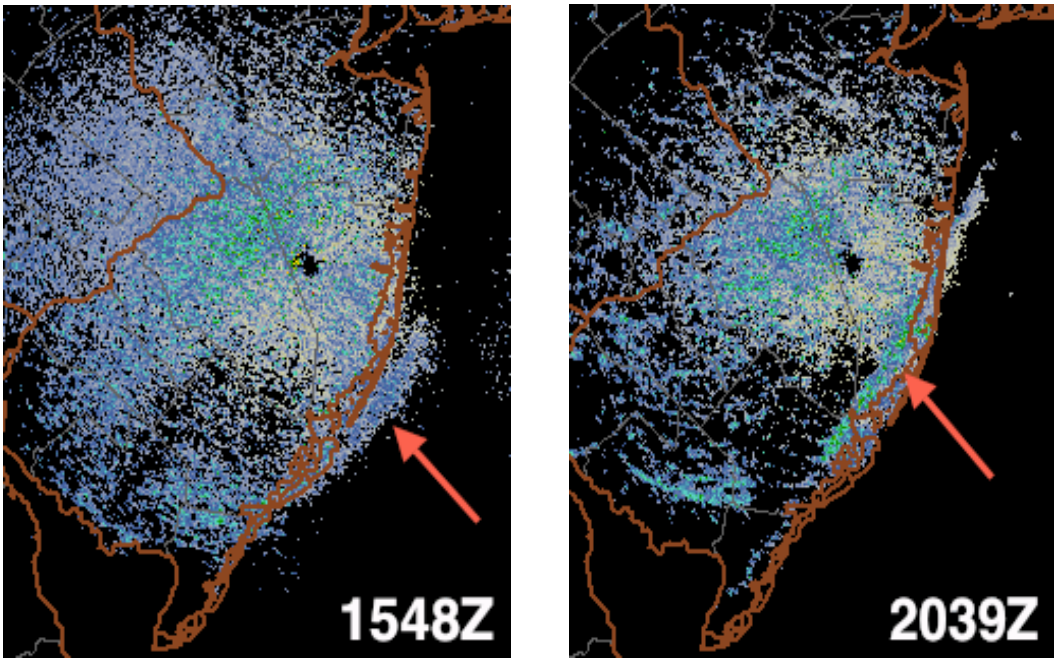

Figure 57: RADAR Detection of the Sea Breeze "Front" and its Propagation Onshore.

The preceding images (i.e., horizontal simulations @ 10m, 90 m heights and a vertical cross-sectional simulation associated with sea breeze development) indicate that the most intense wind speeds occurred immediately behind the sea breeze front that formed along the mid-central to southern NJ coast with wind speeds becoming minimal farther offshore where wind energy parks are proposed to be located. It appears that sea breeze development during this particular occurrence was minimal or non-existent along the north Jersey coast/Raritan Bay area south to the mid-central Jersey coast. The sea breeze was also not well defined along the most southern NJ coast/DE Bay area.

The RADAR images show the sea breeze front formed offshore close to the coast with minimal inland propagation, which was the result of a relatively strong opposing synoptic flow. This synoptic flow pattern is shown in the 10 m and 90 m sea breeze simulations shown on the previous page. When analyzing the referenced sea breeze simulations, it appears that maximum wind speeds at the 10 m height ranged from ~5.0 to 6.5 m/s (light blue to green areas) and ranged from ~6.0 to 7.5 m/s (green to yellow areas) at the 90 m height. The vertical cross-sectional simulation indicates that maximum wind intensities were ~7.0 m/s (green to light green areas) occurred at heights between 60 m and 160 m, which coincide with "typical" offshore wind turbine generator (WTG) hub and blade tip heights.

The following cross-sectional diagram of the sea breeze circulation shows that the offshore area where proposed wind energy systems are to be implemented exhibits minimal wind speeds from the sea surface up to heights greater than 100 meters.

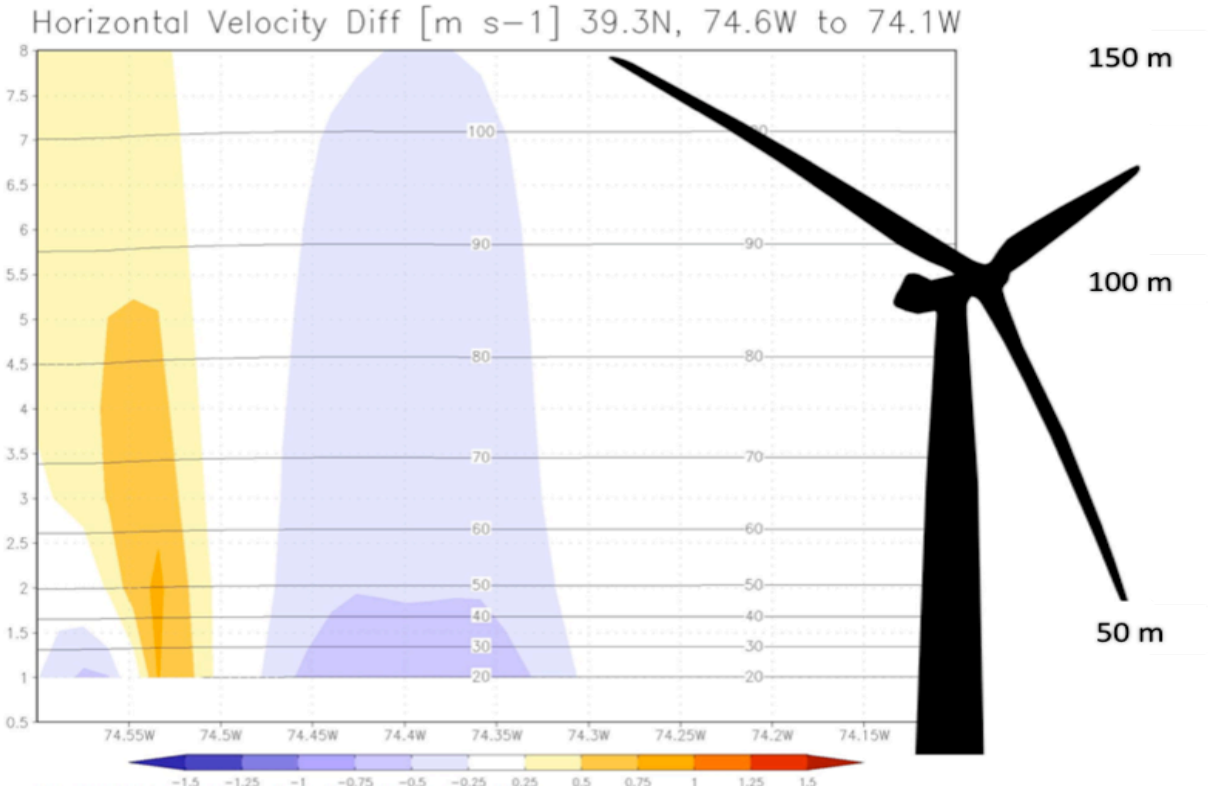

Figure 58: Offshore Wind Speeds associated with the Sea Breeze Circulation for areas defined for NJ's Offshore Wind Energy Development Endeavors normalized to 4.0 m/s from the sea surface to heights >100m, which correspond to Offshore WTG Dimensions.

Referring to the preceding diagram, maximum wind speeds appear to occur near the coast near the sea breeze "front". Additionally, the locations of these maximum wind speeds associated with the sea breeze circulation coincide with most pronounced upwelling centers.

Prior studies (Bowers, 2004; Dunk, 2007) have indicated that intense sea breeze circulations with minimal inland penetration generally occur during upwelling conditions. These studies also indicated that sea breeze intensities are less during non-upwelling occurrences. However, during these non-upwelling events, inland penetrations and the vertical extent of the sea breeze circulation appear to be greater. Consequently, it is imperative that the impact of the sea breeze on the offshore wind resource and resultant wind energy power production, especially during periods of peak energy demand, need to be extensively analyzed when determining the proper location of offshore wind parks and associated WTG array arrangements.

RU-WRF model simulation results, using the unique de-clouded IR satellite SST data, were compared to inshore weather RADAR and offshore coastal ocean high-frequency (HF) RADAR (CODAR). Small-scale offshore wind variability is resolved and simulated in the model. These results will be critical for producing forthcoming accurate and reliable offshore wind resource assessments and precise operational forecasts. The variability in the offshore wind resource is well defined when comparing model simulations at heights representative of offshore wind turbine dimensions for the 12 Sep 2012 sea breeze event and a non-sea breeze event (25 Sep 2012). These simulations show that maximum wind speeds occur along the coast and farther offshore past the influence of the sea breeze circulation. Winds offshore areas adjacent to NJ appear to be light and variable at heights ranging from the sea surface to heights above the 100m level.

If similar sea breeze events occur when proposed WTG arrays become operational, there will be minimal offshore wind power production during these occurrences. As stated in previous reports, sea breeze events have a high probability of occurring during periods of peak energy demand during the summer months. Our analysis indicates that a large zone of subsidence over the coastal ocean and subsequent divergence is shown to occur in unison with the inland-propagating sea breeze front. Therefore, the correct placement of offshore WTG arrays could be a critical factor in determining the availability of supplemental energy supply during periods of "peak" demand. The non-sea breeze simulation indicates that offshore wind vectors exhibit higher wind speeds and are relatively consistent.

The sea breeze and non-sea breeze occurrences used for our analysis are shown in the following simulations:

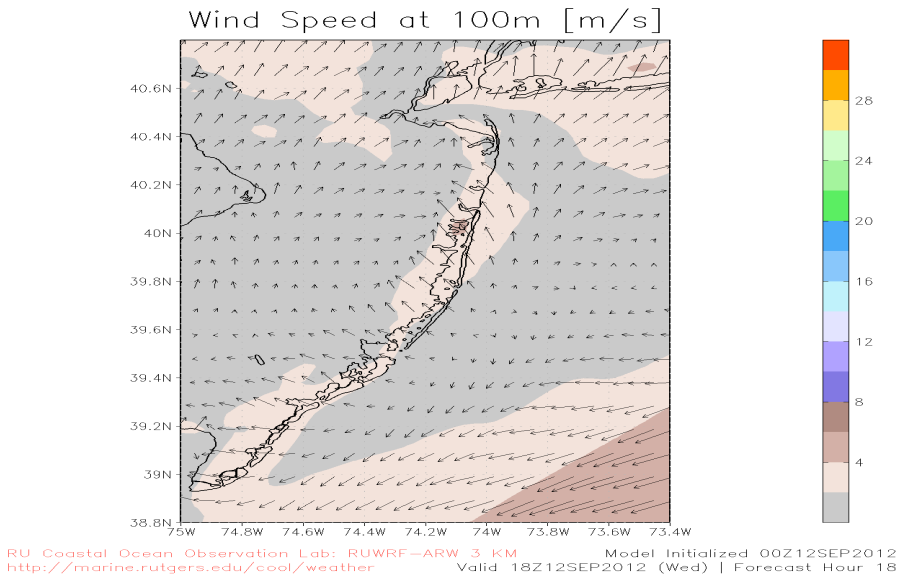

Figure 59: 12 Sep 2012 Sea Breeze Simulation

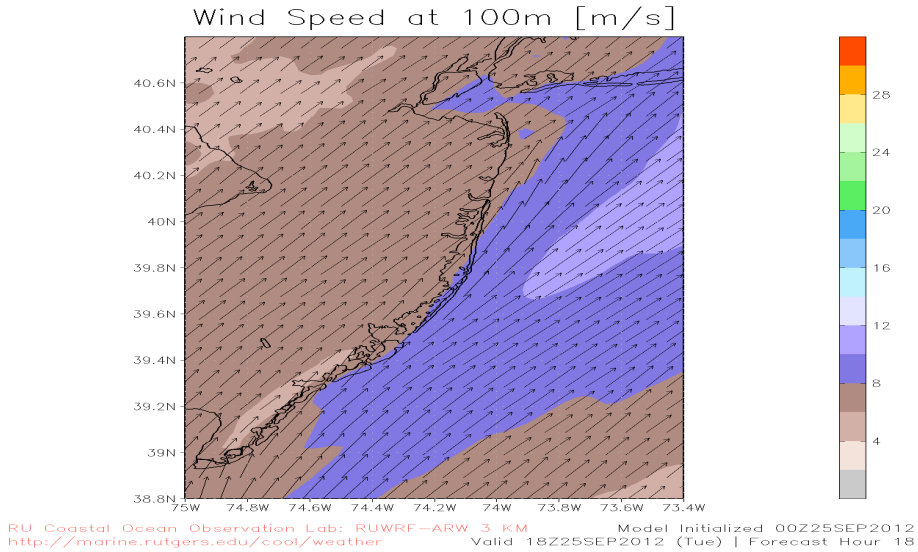

Figure 60: 25 Sep 2012 Non-Sea Breeze Simulation

Sea breeze and non-sea breeze simulations indicate that there is substantially more temporal and spatial variability in the offshore wind resource during sea breeze events when compared to non-sea breeze occurrences. Variability in the offshore wind resource tends to be more evident in northern portions of the study region when compared to central and southern areas adjacent to the NJ coast. Based on this analysis, it appears that the offshore area with the best wind resource would range from the central to the southern areas adjacent to NJ's coast, which is the region designated for offshore wind development.

4.7.2 Non-Sea Breeze Analysis.

It should be noted that winds generally increase in intensity from the coast to areas farther offshore. Furthermore, during non-sea breeze occurrences, offshore winds tend to be

more consistent with less variability. However, these conditions are dependent on the timing and duration of air mass exchanges (i.e., frontal passages), coastal storm occurrences, and other meso to synoptic scale flow phenomena. Example wind flow patterns during a non-sea breeze day (2 Feb 2012) are shown in the following simulations. Wind speeds at both the 10m and 90m heights increase from the coast to offshore areas (~6.5 m/s to 8.5 m/s @10m; ~7.0 m/s to >9.0 m/s @90m). Offshore wind flow vectors appear to be relatively "smooth" with minimal deviations from the wind flow streamlines.

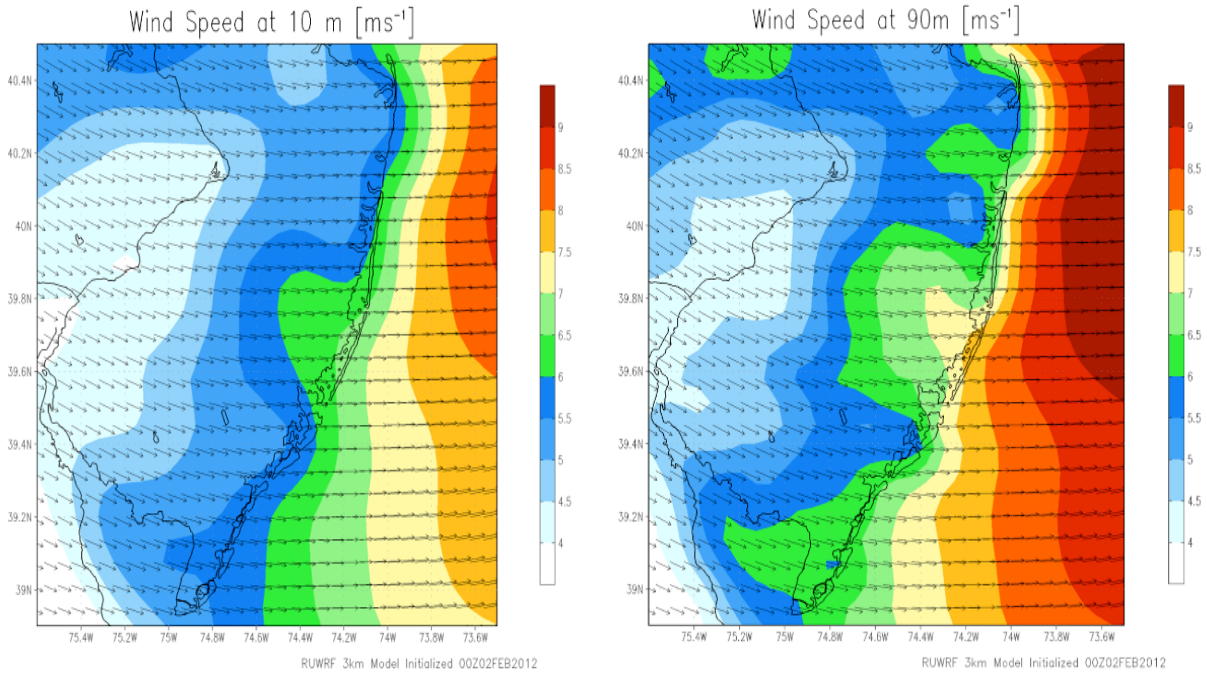

Figure 61: Non-Sea Breeze Wind Flow Vectors @10m and 90m Heights (2 Feb 2012).

4.7.3 NJ Sea Breeze Climatology. An overview of the number of New Jersey sea breeze days by month from Jan 2012 to Apr 2013 is presented in Figure 62. A day was labeled as a sea breeze day when a clear front in the KDIX weather RADAR data was observed to propagate inland or at least develop along the NJ coastline. Most sea breeze days occurred in the warmer months of March through September, which is consistent with Bowers (2004), who observed most NJ sea breezes occur between the months of May and October.

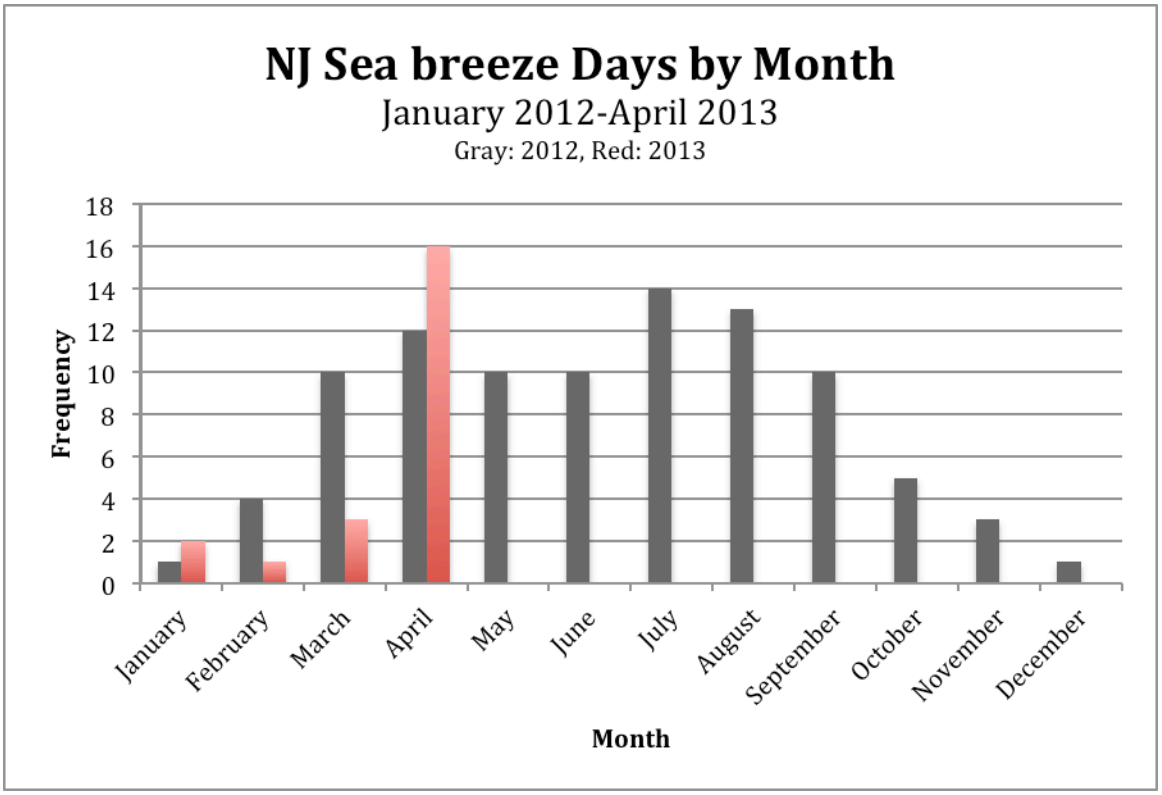

Figure 62: New Jersey sea breeze days by month, as determined using KDIX weather radar. Several more sea breezes occurred in February/March 2012 vs. February/March 2013 (14 vs. four), possibly due to a warmer than average late winter and early spring in 2012 and an average to colder than average late winter and early spring in 2013.

Wind power density (W m^{-2}) at the 100m height was determined for sea breeze events that occurred from 1 Apr 2012 to 31 Mar 2013. This analysis estimated that the overall average wind power density over the offshore study area would be approximately 300-400 W m^{-2}. Wind power density values appear to increase from inshore (~ 300 W m^{-2}) to farther offshore (~ 400 W m^{-2}). Lower values also occur near shore farther north along the NJ coastline, just offshore of Asbury Park but outside of the existing study domain. These estimations are shown in the wind power density contour plot that was produced over the offshore virtual meteorological towers displayed in Figure 63.

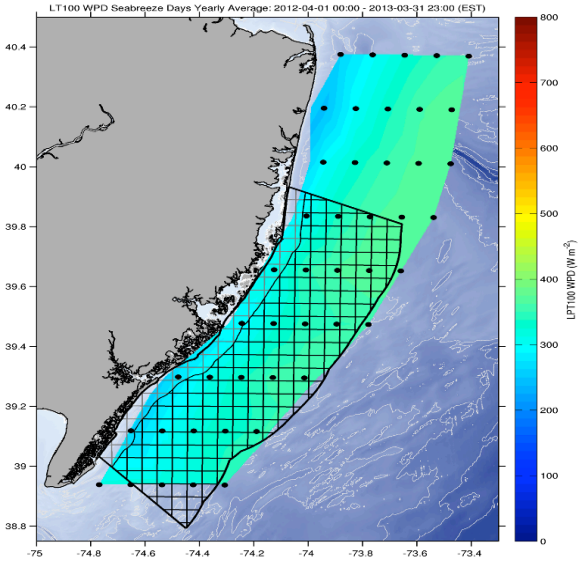

Figure 63: Average wind power density at the 100m height for sea breeze events that occurred from 1 Apr 2012 to 31 Mar 2013. Black dots: virtual meteorological towers; Black outline: 2010 NJDEP OSWEBS area extending 20 nm offshore; Thin Black line: federal-state waters boundary line at 3 nm offshore; Black and Gray grid: federal and state offshore lease blocks.

To put Figure 63 in context, Figure 64 shows the annual average wind power density (W m^{-2}) at 100m across all days from 1 Apr 2012 to 31 Mar 2012. Values range from about 600 to 800 W m^{-2}, double that of the wind power density found only on sea breeze days. A similar pattern of increasing wind power density from inshore to offshore is apparent. A possible reason why wind power density is half that of the annual average on sea breeze days could be because sea breezes most commonly occur on days with high temperatures observed on land and low westerly synoptic flow, which enables the inland propagation of the sea breeze front from low temperatures offshore to higher temperatures onshore.

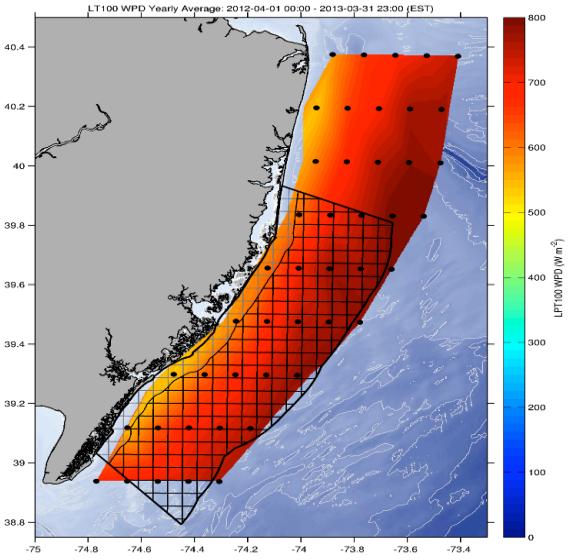

Figure 64: Similar to Figure 63, but for annual average wind power density at the 100m height for all days from 1 Apr 2012 to 31 Mar 2013.

4.7.4 Hourly Spatial Anomaly. A key question still remains: what is the spatial variability of the sea breeze, and how does that variability positively and negatively affect areas for offshore wind power production? With the overall wind power density on a sea breeze day lower than that on an average day, it is critical to determine when and where wind power generation will occur and not occur on those sea breeze days. In order to answer this question, a series of hourly 100m wind power density anomaly plots were produced across all sea breeze days between 1 Apr 2012 and 31 Mar 2013. First, the mean wind power density (W m^{-2}) at the virtual meteorological towers was calculated across all sea breeze days (Figure 63). Then, the mean wind power density was calculated at each hour of the day (EST) across all sea breeze days. Finally, the difference between the mean wind power density at each hour and the daily mean was calculated, which resulted in the "hourly anomaly". With these plots (see series of plots below), we can investigate how the sea breeze spatially evolves offshore of NJ across a day, and how this evolution impacts subsequent wind power production.

The first mode of variability is the negative anomalies across the whole domain from 10:00 to 15:00 EST, and positive anomalies from 19:00 to about 02:00 EST. This aligns with the general diurnal variability in wind speeds, with lower wind speeds in the morning and mid-day, and high wind speeds occurring in the late afternoon and evening hours. Furthermore, the peak in anomalies at hours 19:00 to 02:00 EST matches well with peak demand, which occurs in the late afternoon and early evening when consumers of electricity arrive home after the common workday. It seems that the extension of higher anomalies in wind power density into the late evening and nighttime hours would additionally supply energy into the grid when peak demand lingers later on some days.

The transition hours from lower to higher anomalies (i.e. 16:00 to 18:00 EST) show an interesting pattern. Higher wind power density anomalies develop first near shore (within about 3 nm) at 16:00 EST, from Atlantic City north up along Long Beach Island. Over the next couple hours, those higher anomalies extend offshore until at 19:00 EST most of the study area is covered in positive anomalies. From 19:00 to 21:00 EST, those positive anomalies remain consistent across the domain, and begin to fade at 22:00 to 24:00 EST. Then, interestingly, the positive anomalies appear again at 01:00 EST. At 02:00 EST, negative anomalies develop first nearshore. Over the next couple hours, those negative anomalies spread from north to south and from nearshore to offshore, creating a bi-modal pattern of mainly negative anomalies in the north and positive anomalies in the south. That bi-modal pattern persists until about 10:00 EST, when negative anomalies develop across most of NJ's offshore waters.

The more rapid change over near shore to positive anomalies in the late afternoon (17:00 EST), and the more rapid change over to negative anomalies in the early morning (e.g. 03:00 EST), could be due to the greater influence of continental air masses nearshore as compared to offshore. Because land heats up and cools down more quickly than water, this increase and decrease develops first at inshore locations. The greater positive anomalies at 16:00 to 19:00 EST nearshore would likely benefit wind farms developed closer to shore during the earlier parts of the evening peak demand period as compared to those developed farther offshore. This pattern is evident over the sea breeze days, often during hot summer days when energy demand is at its peak.

The diurnal variation in the offshore wind resource caused by the sea breeze circulation is best described using hourly simulations that capture the daily development, intensity, propagation, and duration of the sea breeze and its impact on wind power density values.

Representative offshore wind resource variations resulting from the average across all sea breeze events are depicted in the following simulations.

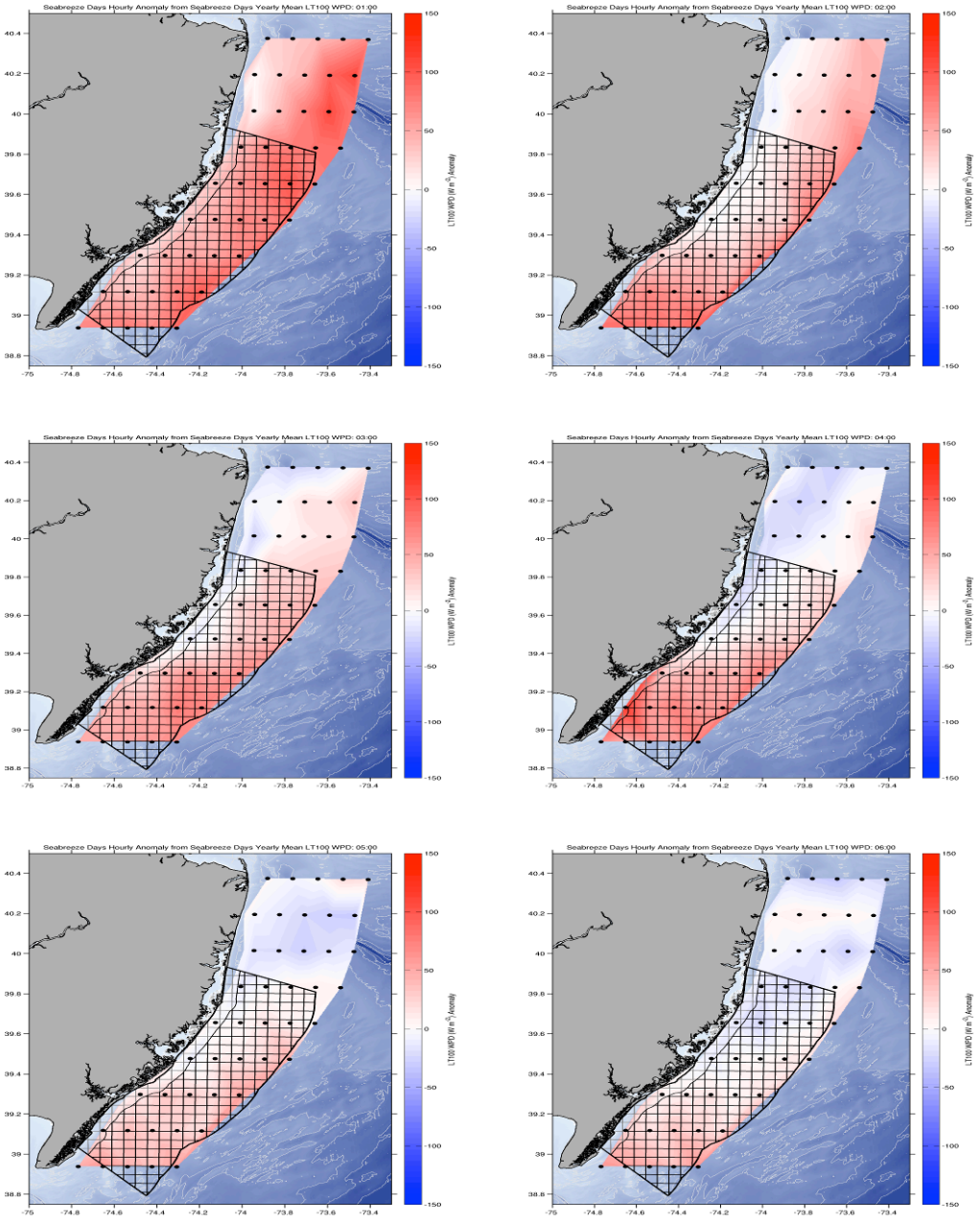

Figure 65a: Hourly offshore wind resource simulations derived across the average sea breeze day that show the variation in the offshore wind resource and associated wind power density function for hours 0100 to 0600.

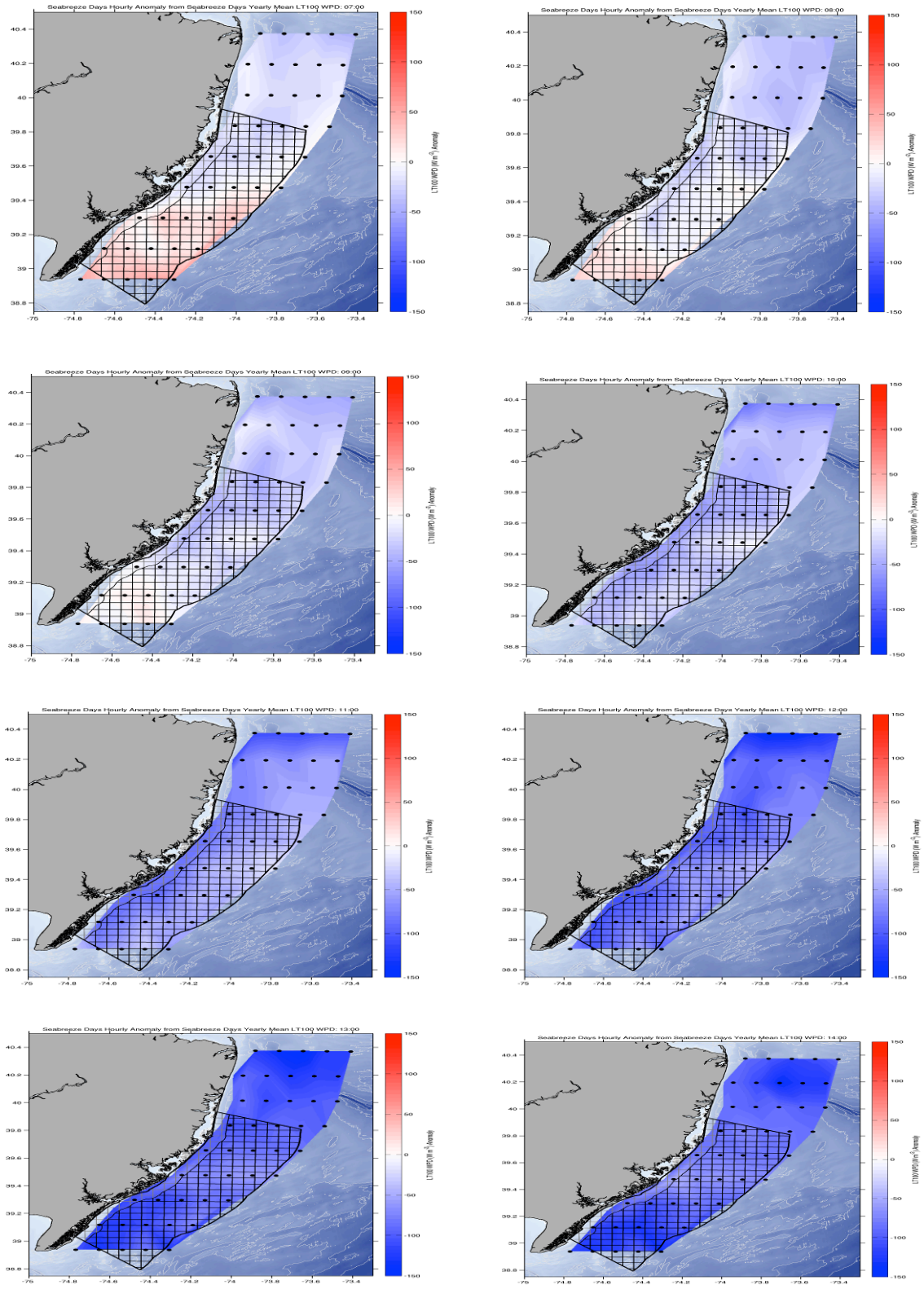

Figure 65b: Same as Figure 65a, except the simulations are for hours 0700 to 1400.

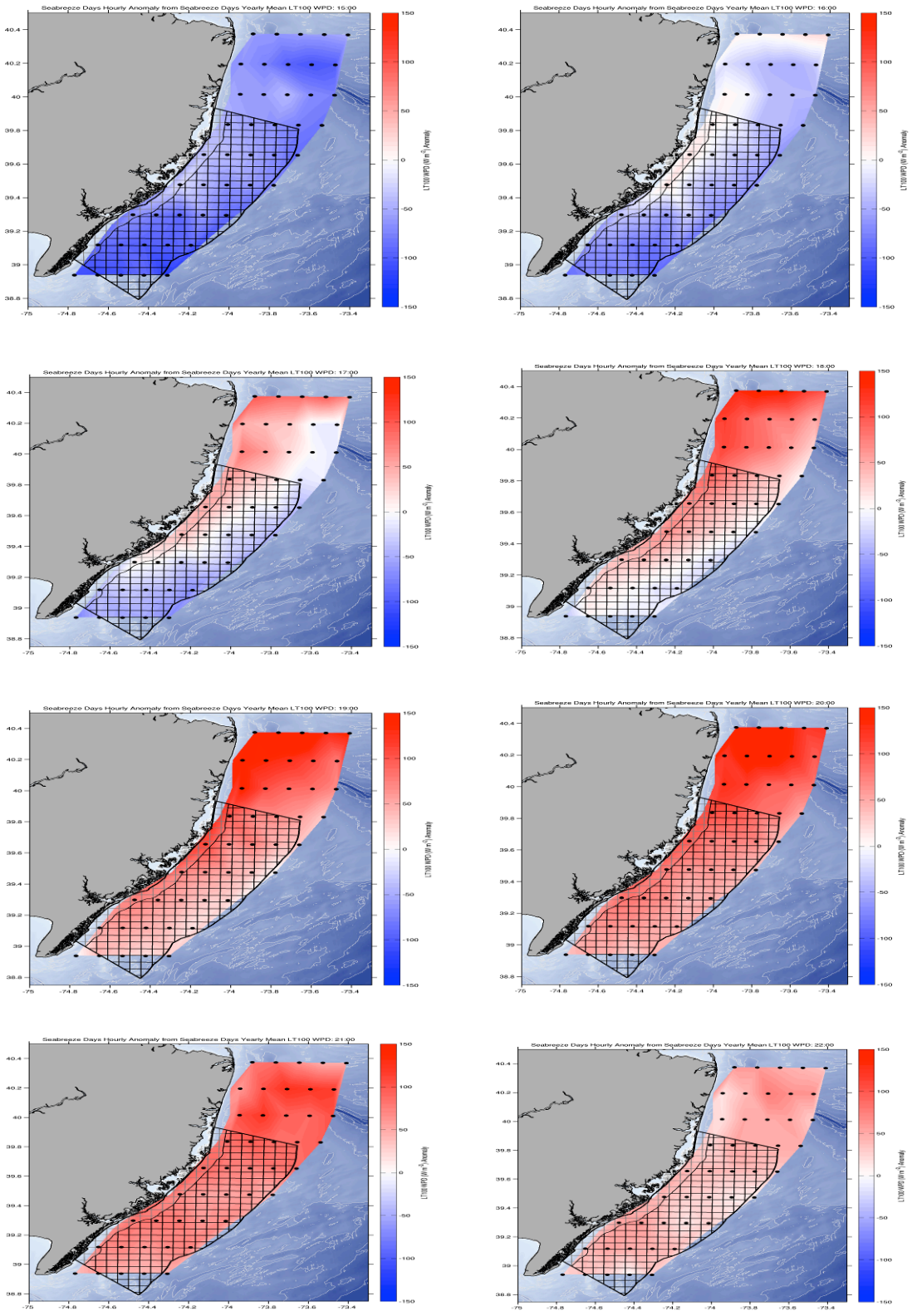

Figure 65c: Same as Figure 65a, except the simulations are for the hours 1500 to 2200.

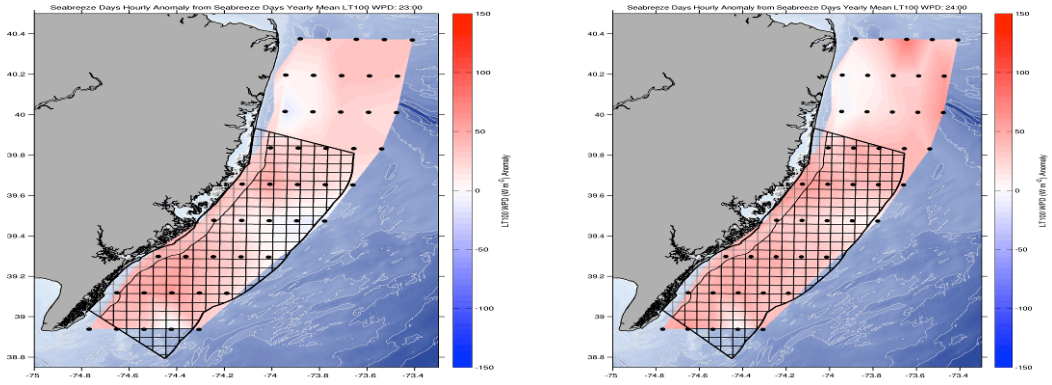

Figure 65d: Same as Figure 65a, except the simulations are for the hours 2300 to 2400.

The vertical structure of the sea breeze circulation, and how coastal upwelling influenced a sea breeze case study in both Aug 2012 and Sep 2012, were analyzed in both an extended abstract and presentation for the Oceans 2012 MTS/IEEE Conference in Virginia Beach, VA (Seroka et al., 2012).

4.8 Extreme Weather Analysis

Although "extreme" weather events occur much less frequently than sea breeze occurrences, severe coastal storms (e.g., Hurricanes, Nor'easters, and other coastal storms) have a significant impact on the offshore wind resource. Tropical Storm "Irene" and Hurricane "Sandy" are excellent examples of extreme wind events that result in potential wind turbine generation "cut-out" periods for planned offshore wind parks. With funding from USEPA, RU-COOL had an underwater autonomous underwater gliding vehicle (AUV) deployed along the NJ coast during both severe storm events. The RU-COOL glider that monitored ocean parameters (e.g., SSTs) during "Irene" along with the glider track and resultant ocean temperatures are respectively shown in the following picture, visible satellite image, and graphic:

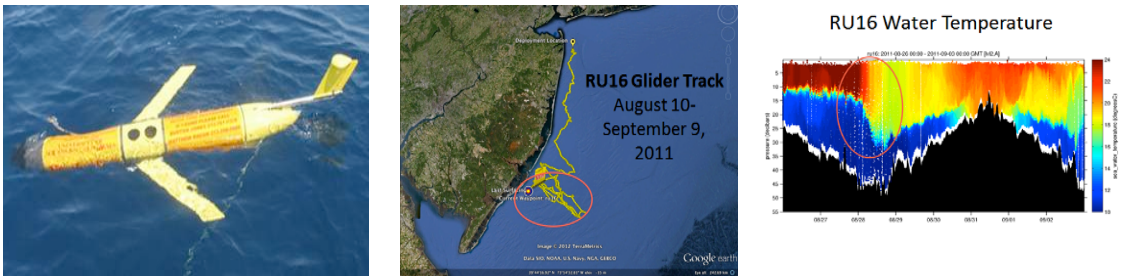

Figure 66: RU-16 Glider Deployed During Hurricane Irene, Glider Track, and Monitored Ocean Temps

Case Studies of Hurricanes Irene and Sandy. Hurricanes Irene and Sandy both occurred during the time frame of this study and are considered excellent examples of extreme weather conditions that severely impact offshore, coastal, and inland areas. These severe storms also significantly alter the offshore wind resource during their movement over ocean waters.

Although not conclusive, warmer-than-average sea surface temperatures in the Atlantic may have helped to keep Hurricane Sandy at hurricane strength just before it made landfall in NJ

(Gillis, 2012). Increased Arctic ice melt may have also weakened the gradient between the cold northern Canadian zones and the warmer mid-latitudes, weakening the usually strong westerly flow of the Jet Stream (Francis and Vavrus, 2012). This weaker westerly flow may have helped Hurricane Sandy to make its unusual left turn toward the Mid-Atlantic coast. In a warming planet, both warmer sea surface temperatures and increased ice melt will occur. Therefore, it is possible that storms similar to Hurricane Sandy may be increasingly likely to make landfall in more northern sections of the U.S. East Coast, including NJ. It is thus critical to accurately forecast these storms well in advance, in order to aid in planning for periods of unavailability due to hazardous conditions and high wind hysteresis periods for NJ offshore wind parks.

While hurricane track forecast errors have decreased by a factor of 2-3 over the last two decades, the predictive skill for hurricane intensity forecasts has remained "flat" over the last twenty years (Pasch & Blake, 2012). Although track forecasts for both storms were accurate several days in advance, intensity forecasts were less accurate. Irene's intensity was overpredicted by many operational hurricane models and over forecasted by the National Hurricane Center, and for Sandy, the rapid acceleration and intensification just before landfall were underpredicted (Glenn et al., 2013).

By operating a regional component of the Integrated Ocean Observing System (IOOS) along with the BPU funded CODAR network, RU-COOL observed each hurricane's impact on the ocean in real-time, and analyzed the impacted ocean's influence on each hurricane's intensity. One key component to the Mid-Atlantic regional IOOS network is the fleet of autonomous underwater gliders (Schofield et al., 2010). At least one glider was deployed in each of the two storms, collecting critical sub-surface ocean data that acted as both validation to ocean models and input into atmospheric model (i.e. RU-WRF model) sensitivity studies.

In this final report, we detail ocean observations attained for and during Hurricane Irene, and their evident direct impact on atmospheric forecasts of the storm. Similar ocean observations were gathered for Hurricane Sandy, and the authors encourage the reader to refer to Glenn et al. (2013) for additional information.

Figure 67 depicts the rapid mixing that occurred hours ahead of Hurricane Irene's landfall at Tuckerton, NJ, cooling the SSTs and available energy to fuel the storm.

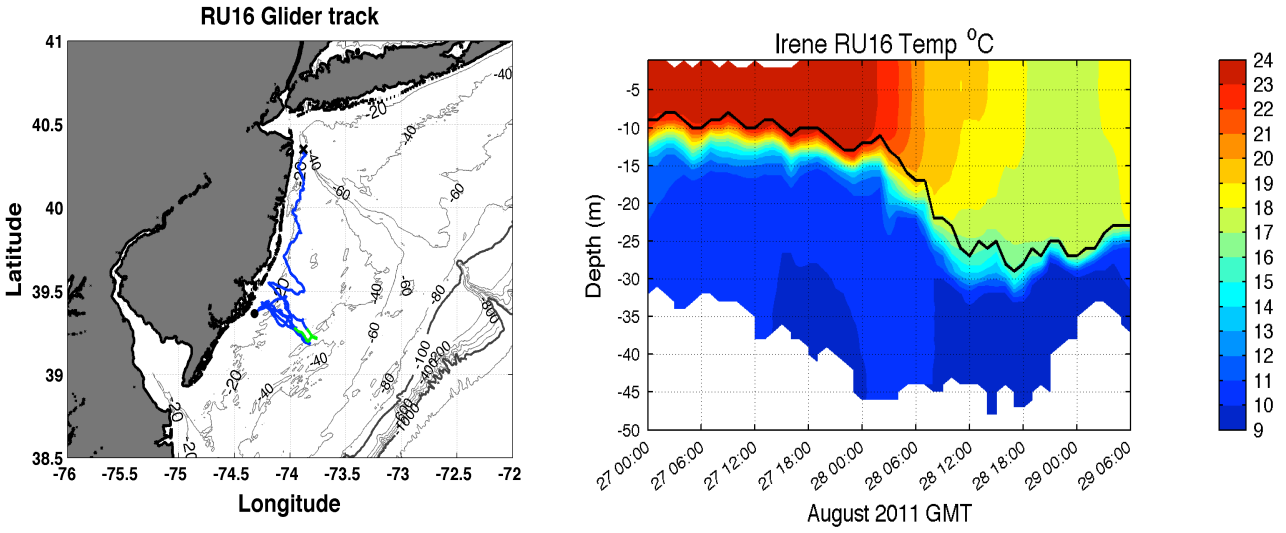

Figure 67: (a) Glider track in Hurricane Irene. (b) Glider temperature section for the portion of the glider track marked in green. Black line is the depth of the surface mixed layer.

These sub-surface glider temperature data can not only inform ocean models, but can be used as a cross-check of satellite SST products and their capability to capture storm mixing and cold wakes from tropical storms like Hurricanes Irene and Sandy.

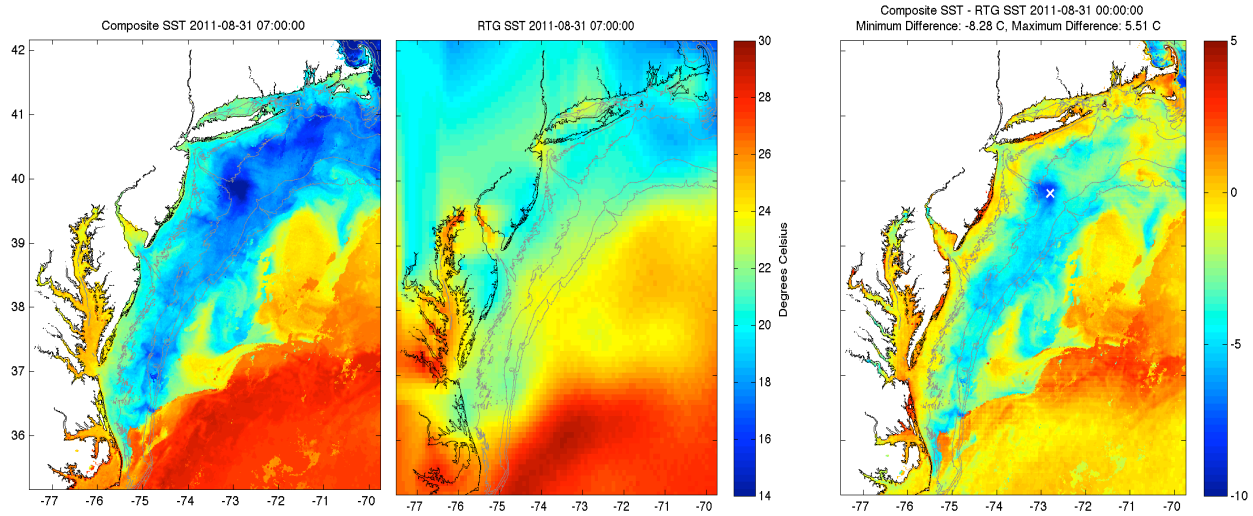

Figure 68: Post-Hurricane Irene Satellite-derived Sea Surface Temperature (SST) products for August 31, 2011. (a) Locally composited SST showing the surface cooling. (b) Operational global SST product with the cool pixels incorrectly identified as clouds. (c) Difference.

Post-Hurricane Irene satellite-derived SSTs that are depicted in Figure 68, which show a large difference in the cooling observed between our declouded, coldest-pixel SST composite developed during this study and an operational global SST product. Our SST product captures the significant surface cooling (8-10°C) which occurred during Hurricane Irene's passage through the Mid-Atlantic coastal waters.

These SST products were used in a simple hindcast sensitivity study using a version of the WRF model, which is similar to the RU-WRF model configuration. This sensitivity study illustrates the significant impact of the cooler water on Hurricane Irene's projected intensity. The glider data informs us that the cooling occurred ahead of the storm's eye as the high winds of the outer wind bands approached. Therefore, the eye of the hurricane passed over cooler water as it propagated northward. A "fixed" warm SST run was performed using the Real-Time Global (RTG) SST product available a day in advance of Hurricane Irene's arrival. This served as our base case or control run.

Because available ocean models did not cool early enough and sufficiently, the declouded coldest-pixel SST composite developed during this study was used to simulate the change in SST as the storm passed. Starting with the warm pre-storm SST, the cold post-storm SST was applied everywhere at the time of the peak mixing observed in the glider data. The resulting WRF forecast was lower by 5-10 knots. These results are shown in the simulations presented on the following page.

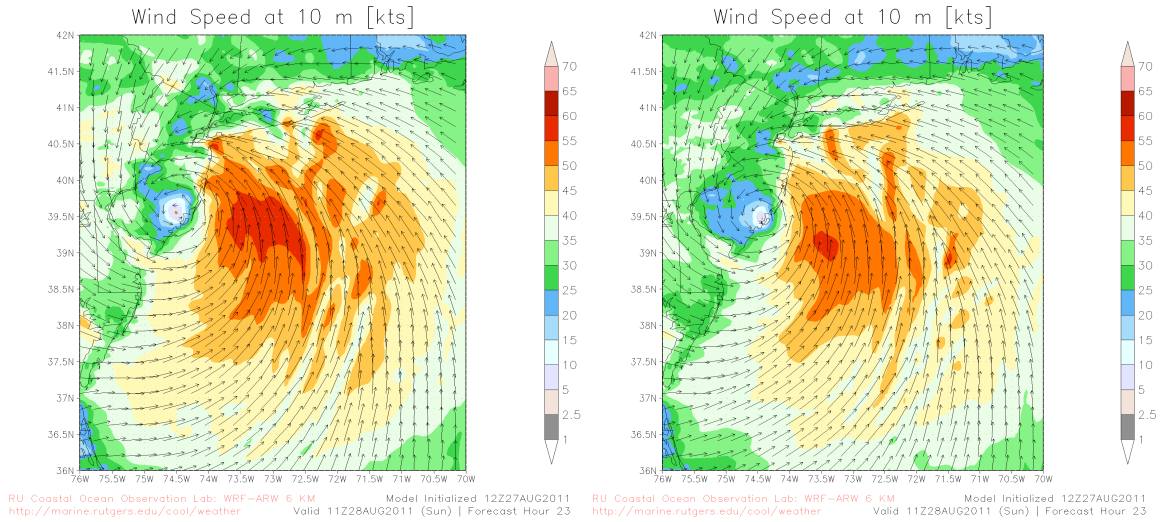

Figure 69: WRF model atmospheric hindcasts of Hurricane Irene with different ocean boundary conditions. Simulation using the warm SST throughout the run (left). Simulation switching to the cold SST when the cooling is observed in the glider data.

The ocean observations including CODAR detected surface currents, IR satellite coldest-pixel composites of SSTs, and sub-surface glider measurements that were available during Hurricanes Irene and Sandy provided never-before seen 3-dimensional views of the dynamic ocean response as two major storms made landfall in New Jersey. The atmospheric sensitivity studies performed show that the evolving surface temperature of the ocean can have a major impact on hurricane intensity. Therefore, better forecasts of the rapidly changing coastal ocean underneath hurricanes are essential in the quest for improvements in hurricane intensity forecasts. Also, improvements in tropical storm forecasting result in improvements in the prediction and subsequent planning for periods when proposed offshore wind parks may be impacted by extreme winds.

5. Summary

Through this work we were able to integrate high-resolution ocean observations into an annual atmospheric simulation of winds in support of developing offshore wind assessments. The model was validated against in situ point measurements in the vertical and with CODAR estimated offshore wind fields in the horizontal. With this model we were able to map the wind resource over the year averaged into hourly, monthly and seasonal time scales at high spatial resolution. These maps were then used to estimate the power density from these wind fields across the offshore study region. Sea breeze and non-sea breeze simulations indicate that there is substantially more temporal and spatial variability in the offshore wind resource during sea breeze events when compared to non-sea breeze occurrences. Variability in the offshore wind resource tends to be more evident in northern portions of the study area when compared to central and southern areas adjacent to the NJ coast. Based on this analysis, it appears that the offshore area with the best wind resource would range from the central to the southern areas adjacent to NJ's coast. Furthermore, the peak in hourly afternoon anomalies matches well with peak demand, which occurs in the late afternoon and early evening when consumers of electricity arrive home after the common workday.

6. Implications

The advanced diagnostic applications and resultant adaptive procedures developed during this offshore wind study could be used to provide a significant basis for proposed atmospheric, ocean, and wave model coupling routines. The "coupled" model can then be applied as a viable "tool" for operational forecasting procedures that will support offshore wind energy construction activities and operational procedures. The components of the "coupled" model system are shown in the following schematic:

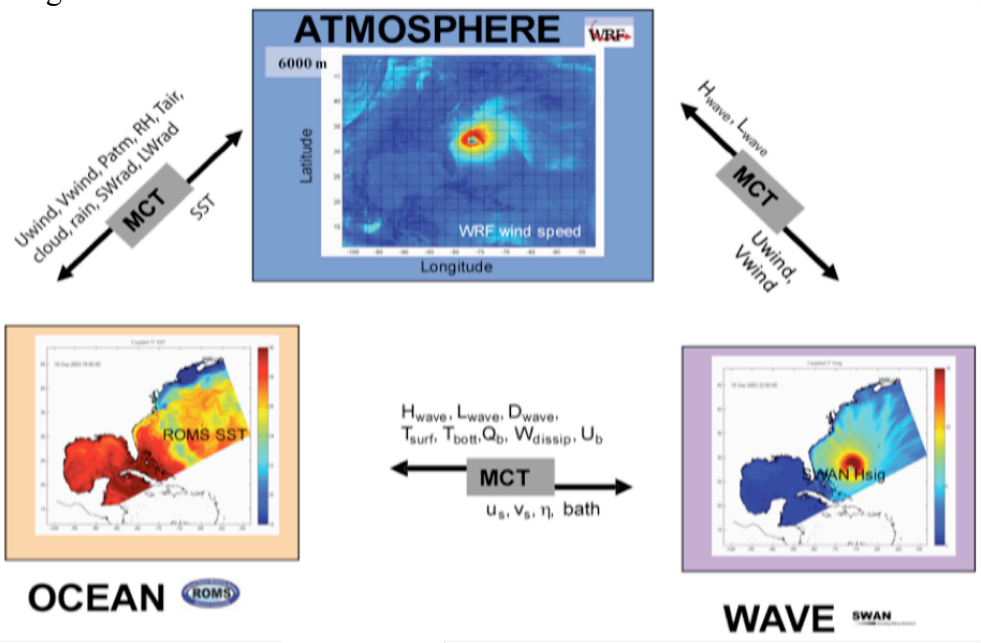

Figure 70: Schematic of the "coupled" ocean/atmosphere/wave model.

Wind resource analytical/predictive information will also substantially support NJ's associated energy, environmental, economic, and educational programs that are pertinent for cost-effective offshore wind energy development and implementation. For example, the resultant data can be provided to the Rutgers Center for Economic, Energy, and Environmental Policy (RU-CEEEP) for input into their energy and economic models to determine the "baseline" for cost-effective offshore wind energy incorporation into the electrical power grid controlled by the PJM Interconnection.

The preceding information can be made available to the Rutgers Business School (RBS) to evaluate supply chain management and job creation issues that are associated with the offshore wind energy industry. Additionally, the results of CEEEP's analysis could be incorporated into the Rutgers Department of Environmental Sciences (DES) air quality model that will convert offshore wind energy production into pollutants that would be emitted by equivalent fossil fuel generating plants. Therefore, there will be a "total picture" of the cost-effectiveness of offshore wind energy installations and subsequent operations. The resultant studies will resolve a substantial portion of the "uncertainty" associated with the reliability and economic benefits relevant to NJ's offshore wind energy endeavors.

References

Beardsley, R. C., and D. B. Haidvogel (1981): *Model studies of wind driven transient circulation in the Middle Atlantic Bight, part 1: Adiabatic boundary conditions*, *J. Phys. Oceanogr*., 11, 355 – 375.

Beardsley, R. C., W. C. Boicourt, and D. V. Hansen (1976): *Physical oceanography of the Middle Atlantic Bight*, *Limnol. Oceanogr*. Spec. Symp., 2, 20 – 34.

Bowers, L. (2004): *The Effect of Sea Surface Temperature on Sea Breeze Dynamics Along the Coast of New Jersey*, Master of Science Thesis, Institute of Marine and Coastal Sciences, Rutgers University, New Brunswick, NJ.

Briere, S. (1987): *Energetics of Daytime Sea Breeze Circulation from a Two-Dimensional*, *Third-Order Turbulence Closure Model*, Journal of the Atmospheric Sciences, 44, 1455-1474.

Chant, R. J., S. M. Glenn, and J. T. Kohut (2004): *Flow reversals during upwelling conditions on the New Jersey inner shelf J. Geophys. Res.,* Vol. 109, No. C12, C12S03. 10.1029/2003JC001941

Chao, Y., Z. Li, J. Kindle, J. Paduan, and F. Chavez (2003): *A high-resolution surface vector wind product for coastal oceans: Blending satellite scatterometer measurements with regional mesoscale atmospheric model simulations, Geophys. Res. Lett*., 30(1), 1013, doi:10.1029/2002GL015729.

Donnelly, J. P, S. Roll, M. Wengren, J. Butler, R. Lederer, and T. Webb III (2001): *Sedimentary Evidence of Intense Hurricane Strikes From New Jersey*, Geology, 29, 615-618.

Dunk, R. (2007): *NJ Offshore & Coastal Wind Energy Analysis, Phase 4,* Rutgers IMCS Coastal Laboratory for Applied Meteorology (CLAM), New Brunswick, NJ, Study funded by NJBPU Office of Clean Energy, Trenton, NJ, Rutgers Contract No. 4-25290.

Dvorak, M. et al. (2012): *US East Coast offshore wind energy resources and their relationship to peak-time electricity demand*, published online in the Wiley Online Library (wileyonlinelibrary.com), DOI:10.1002/we.1524, Wind Energy.

Francis, J. A., and S. J. Vavrus (2012): *Evidence linking Arctic amplification to extreme weather in mid-latitudes*, Geophys. Res. Lett., 39, L06801, doi:10.1029/2012GL051000.

Glenn, S. M. and R. Dunk (2010): *An Advanced Atmospheric/Ocean Assessment Program Designed to Reduce the Risks Associated with Offshore Wind Energy Development Defined by the NJ Energy Master Plan and the NJ Offshore Wind Economic Development Act,* Rutgers IMCS Coastal Ocean Observation Laboratory (RU-COOL), New Brunswick, NJ, $1.8 million grant funded by NJBPU Office of Clean Energy, Trenton, NJ, Rutgers Grant No. BPU-069G.

Gillis, J. (2012): *Did Global Warming Contribute to Hurricane Sandy's Devastation?* In New York Times Green Blog, October 30, 2012, Available: http://green.blogs.nytimes.com/2012/10/30/did-global-warming-contribute-to-hurricane-sandys-devastation/

Glenn, S. M. et al. (2013): *Process-Driven Improvements to Hurricane Intensity and Storm Surge Forecasts in the Mid-Atlantic Bight: Lessons Learned from Hurricanes Irene and Sandy*. Proc. Oceans '13 MTS/IEEE Bergen.

Houghton, R. W., R. Schlitz, R. C. Beardsley, B. Butman and J. L. Chamberlin (1982): *The Middle Atlantic Bight cold pool: Evolution of the temperature structure during summer 1979*. J. Phys. Oceanogr., 12, 1019-1029

Kohut, J. T., S. M. Glenn, and R. J. Chant (2004): Seasonal current variability on the New Jersey inner shelf, J. Geophys. Res., 109, C07S07, doi:10.1029/2003JC001963.

Ludlum, D. M. (1963): *Early American hurricanes*: Boston, American Meteorological Society, 198 p.

Manwell, J F., J. McGowan, and A. Rodgers (2009): Wind Energy Explained: Theory, Design and Application, Wiley, 688 p.

NJDEP (2010): *Ocean Wind Power Ecological Baseline Study Final Report*, NJDEP. http://www.nj.gov/dep/dsr/ocean-wind/report.htm accessed April 25, 2013.

Pasch, R. and E. Blake (2012): *2012 Review of the NCEP Production Suite*: Report from NHC, National Centers for Environmental Predictions, Maryland.

Schofield, O., J. Kohut, S. Glenn, J. Morell, J. Capella, J. Corredor, J. Orcutt, M. Arrott, I. Krueger, M. Meisinger, C. Peach, F. Vernon, A. Chave, Y. Chao, S. Chien, D. Thompson, W. Brown, M. Oliver, W. Boicourt (2010): *A regional Slocum glider network in the Mid-Atlantic coastal waters leverages broad community engagement.* Marine Technology Society 44(6): 64-74.

Seroka, G. N., R. Dunk, S. M. Glenn, L. Bowers, J. Kerfoot, M. Crowley, H. Roarty, L. Palamara (2012): *Rutgers University Coastal Ocean Observation Laboratory (RU-COOL) advanced modeling system developed to cost-effectively support offshore wind energy development and operational* applications, *Proc. Oceans 2012 MTS/IEEE*, pp.1-4, Oct 2012.

Shirtliffe, G. M. (1999): *QuikSCAT science data product user's manual, overview, and geophysical data products.* Version 1.0. JPL D-18053, Jet Propulsion Laboratory, Pasadena, CA.